CONTRACTOR REPORT

SAND98–0627
Unlimited Release
UC–705

Calculation of Electron Emission from a Tantalum Foil Irradiated by 100-kV and 50-kV X Rays

Martin J. Berger
5011 Elm Street
Bethesda, MD 20814

Prepared by
Sandia National Laboratories
Albuquerque, New Mexico 87185 and Livermore, California 94550

Sandia is a multiprogram laboratory operated by Sandia Corporation, a Lockheed Martin Company, for the United States Department of Energy under Contract DE-AC04-94AL85000.

Printed March 1998

Sandia National Laboratories

Issued by Sandia National Laboratories, operated for the United States Department of Energy by Sandia Corporation.

Available to DOE and DOE contractors from
Office of Scientific and Technical Information
P.O. Box 62
Oak Ridge, TN 37831

Prices available from (615) 576-8401, FTS 626-8401

Available to the public from
National Technical Information Service
U.S. Department of Commerce
5285 Port Royal Rd
Springfield, VA 22161

NTIS price codes
Printed copy: A05
Microfiche copy: A01

DISCLAIMER

Portions of this document may be illegible electronic image products. Images are produced from the best available original document.

SAND98-0627
Unlimited Release
Printed March 1998

Distribution
Category UC-705

Calculation of Electron Emission from a Tantalum Foil Irradiated by 100-kV and 50-kV X Rays*

Martin J. Berger

5011 Elm Street
Bethesda, MD 20814

Abstract

Two Monte Carlo programs, XITRAN and XMTRAN, were developed for calculating the emission of electrons from high-Z foils irradiated with x rays. XITRAN follows all individual elastic collisions of electrons with atoms, whereas XMTRAN uses the condensed-random-walk model. Both codes take into account photo-electrons, fluorescence radiation, and Auger electrons. Comparisons are made with an experiment by Dolan at Sandia Laboratories involving the backward and forward emission of electrons from a tantalum foil irradiated by 100-kV and 50-kV x-ray beams. There is good agreement between results from the XITRAN and XMTRAN codes. There is also good agreement between calculation and experiment in regard to the number of electrons emitted per incident x-ray photon, and in regard to the angular distribution of the emerging electrons. In regard to the electron energy spectra, there is fair agreement down to a spectral energy of 20 keV, whereas below 20 keV the calculated spectra lie considerably below the measurements.

---

* The work described in this report was performed for Sandia National Laboratories under Contract No. AK-1998.

Introduction

This report describes two new Monte Carlo codes, XITRAN and XMTRAN which were developed to calculate the emission of electrons from a high-Z target irradiated by x rays. XITRAN simulates all individual elastic collisions of electrons with atoms, whereas XMTRAN uses the condensed random-walk model and samples elastic multiple-scattering deflections at the end of successive short track segments. The two codes are identical in respect to the transport of photons and the production of photoelectrons and Auger electrons. They use the continuous-slowing-down approximation (csda), with the electron energy assumed to decrease along the track at a rate given by the stopping power.

The objective of this investigation was to obtain answers to two questions:

1) Is there good agreement between the results obtained with the single-scattering code XITRAN and the condensed-random-walk code XMTRAN?

2) Do the Monte Carlo predictions agree with the experimental results of Dolan[1] regarding the emission of electrons from a tantalum target irradiated by 100-keV and 50-keV x rays?

As will be shown in this report, the answer to the first question is yes. The answer to the second question is a qualified yes. There is good agreement in regard to the average number of electrons emitted per incident photon, and in regard to the angular distribution of the electrons, but less close agreement in regard to energy spectra.

Preliminary studies were carried out with two simpler Monte Carlo codes ITRAN and MTRAN, which deal with the transmission and reflection of electrons by foils. ITRAN takes into account all individual elastic collisions, whereas MTRAN is based on the condensed-random-walk.model. Another Monte Carlo code applicable to reflection and transmission problems is ETRAN[24], which takes into account energy-loss straggling, but can also be run in the csda mode. Numerical experiments with ETRAN indicate that for high-Z materials such as tantalum or gold the effect of energy-loss straggling is small, not only for reflection and transmission coefficients, but also for angular distributions and even for energy spectra of reflected or transmitted electrons. Straggling effects are expected to be even smaller in problems involving electrons set in motion by x rays, because the electron source then has a broad energy spectrum, and is spatially as well as directionally diffuse.

The production of secondary electrons in inelastic collisions, and their transport through the target, is treated in ETRAN but not in XITRAN, XMTRAN, ITRAN or MTRAN. However, for the comparisons with Dolan's measurements one needs to consider only electrons with energies greater than 5 keV, so that the omitted contribution from secondary electrons is insignificant.

Stopping Powers

Electron stopping powers at energies below 10 keV were obtained from Ashley[3] and from Fernandez-Varea, Mayol, Liljequist and Salvat[4]. These authors treat soft collisions with the use of experimental optical data, and hard collisions by extending the optical oscillator strength distribu-

tion into the region of large momentum transfer, using a free-electron-gas model. Special attention is given to energy transfers to tightly-bound inner-shell electrons, and exchange effects are taken into account.

Stopping powers for gold were obtained from tabulated stopping powers based on Bethe's theory[2] above 20 keV, from Ashley[3] below 10 keV, and by interpolation at intermediate energies. Stopping powers for gold from Fernandez-Varea[4] agree within 2% with those from Ashley[3]. The adopted curve of stopping power vs. energy is compared in Fig. 1 with the Bethe theory.

Fernandez-Varea et al [4] fitted their stopping powers for Al, Si, Cu and Au, between 1 keV and 10 keV, by an empirical expression similar to Bethe's formula, with two disposable parameters that depend only on the atomic number Z. Plots of these parameters against *log(Z)* are nearly straight lines. This facilitated interpolation with respect to *log(Z)* to obtain stopping powers for tantalum up to 10 keV, which were again combined with Bethe's values above 20 keV. Tables 1 and 2 give the stopping powers for gold and tantalum used in the present work.

Elastic Scattering Cross Sections

Cross sections for the elastic scattering of electrons by atoms were obtained from a database ELAST[5], calculated with a computer code of Riley[6,7]. This code treats scattering by a static, screened Coulomb potential, via a phase-shift analysis involving the numerical solution of the Dirac equation. In the preparation of ELAST, the screened Coulomb potential was obtained from electron density distributions calculated with a relativistic Hartree-Fock code of Desclaux[8].

Monte Carlo Code ITRAN

Let $\sigma(T)$ be the total elastic scattering cross section at energy T, and let $\mu(T) = (N_A/A)(1 + 1/Z)\sigma(T)$ be the elastic-scattering coefficient, where N_A is Avogadro's constant, A is the atomic weight, and Z is the atomic number. The factor $(1 + 1/Z)$ is included to take into account, approximately, the inelastic scattering by atomic electrons. Let $L(T)$ denote the stopping power. In the continuous-slowing-down approximation the average number of collisions which an electron makes while slowing down from initial energy T_0 to energy T is given by

$$Q(T, T_0) = \int_T^{T_0} [\mu(T')/L(T')]dT', \tag{1}$$

and the residual range is

$$r_0(T) = \int_0^T [1/L(T')]dT'. \tag{2}$$

Suppose an electron has made an elastic collision at energy T'. The probability that the next collision will occur when the energy is between T and $T + dT$ is given by

$$\exp\left(-\int_T^{T'} [\mu(T'')/L(T'')]dT''\right)[\mu(T)/L(T)]dT. \quad (3)$$

The variable

$$q(T, T') = \int_T^{T'} [\mu(T'')/L(T'')]dT'' \quad (4)$$

is therefore distributed exponentially, as exp(-q). In order to sample the value of T one sets $q = \log(\rho)$, where ρ is a random number, and then solves for T as a function of q and T'. This can be easily done by interpolation in a table of three columns (energy T, collision number Q and residual range r_0). The beginning part of such a table (for tantalum) might look as follows:

Partial T-Q-r_0 Table

T	$Q(T)$	$r_0(T)$
(keV)		(g/cm^2)
512.000	0.00000	0.33554
509.051	83.06068	0.33300
506.119	165.71702	0.33047
503.204	247.97091	0.32796
500.306	329.82424	0.32546
497.424	411.26990	0.32298
*	*	*
*	*	*

One selects *an initial energy T',* and interpolates in the T-Q-r_0 table to obtain an initial collision number $Q(T')$ and residual range $r_0(T')$. Then one samples a value of q from an exponential distribution. The new collision number is $Q = Q' + q$. By interpolation in the table the new energy T and range $r_0(T)$ are obtained. The path length traveled (in a straight line) to the collision point is equal to the difference of residual ranges, $r_0(T') - r_0(T)$. An angular deflection is sampled from the elastic-scattering cross-section at energy T. This procedure is continued until the electron energy falls below a pre-assigned value.

Elastic scattering cross sections from database EIAST were used to prepare angular cross-section histograms evaluated at the midpoint energies of successive grid intervals of the T-Q-r_0 table. The energy grid was very fine, so that it was permissible to sample angular deflections from the pre-

computed histogram at an energy closest to the actual electron energy T. The set of histograms, and the T-Q-r_0 table, were incorporated into an file ELPREP.079 for gold (or ELPREP.073 for tantalum). Further details about the preparation of these files can be found in Appendix 1.

The random sampling of deflection angles from the histograms is done with the aliasing method of Kronmal and Peterson[9] which requires only one random number and one comparison per selection, regardless of the number of bins in the histogram. Pseudo-random numbers are generated with the fast random-number generator MZRAN of Marsaglia and Zaman[10], which has a period approximately equal to 10^{28} and passes very stringent tests of randomness.

Monte Carlo Code MTRAN

For comparing the condensed-random-walk model with ITRAN, it would in principle have been sufficient to rely on ETRAN[24] or the series of TIGER codes[25]. It was considered preferable to develop a new code MTRAN such that the differences between MTRAN and ITRAN are confined to the treatment of elastic collisions, with all other procedure and cross sections identical. Moreover MTRAN is a simpler code than the general-purpose codes ETRAN and TIGER, uses more up-to-date sampling techniques, and runs faster. All required angular multiple-scattering distributions, together with step sizes of the condensed random walk, are incorporated into a file GSHE.079 for gold (or GSHE.073 for tantalum). The preparation of such input files is further discussed in Appendix 2. The sampling of multiple-scattering deflections in MTRAN is done with the same aliasing technique and random-number generator as those used for single scattering in ITRAN.

Comparison of Results from ITRAN and MTRAN

Table 3 compares number albedos and energy albedos from ITRAN and MTRAN, for electrons incident normally on a gold foil, At ten different energies between 100 keV to 10 keV. The results at each energy are based on a sample of 100,000 Monte Carlo histories which were followed until the electron energy fell below 1 keV. The agreement between the predictions of the two codes is good, but there are small differences. The reflection coefficients from MTRAN at all energies are about 2% smaller than those from ITRAN. These differences are largely due to the fact that multiple-scattering deflections are allowed in MTRAN to occur only at the end of each short track segment. Thus the electrons are pushed a little too deep into the target, which lowers the albedo.

Table 4 presents comparisons of for number transmission coefficients and energy transmission coefficients from the same runs of ITRAN and MTRAN. These results are tabulated as functions of the thickness of the gold foil in units of the range. The differences between ITRAN and MTRAN now are reversed, and the transmission coefficients from MTRAN are somewhat larger than those from ITRAN, by 2-3%. Even larger differences occur for foil thicknesses such that the transmission is less than about 5%. However, for such deep penetrations energy-loss straggling can no longer be disregarded, and neither ITRAN nor MTRAN is adequate. However, in the context of the problem of x-ray-induced electron emission, such rare deep-penetration events are of little importance.

MTRAN runs faster than ITRAN. This advantage can largely be retained, by a hybrid Monte Carlo code IMTRAN that is currently being developed. In IMTRAN all individual elastic collisions are sampled until the electron energy falls below a specified switching energy, whereupon the Monte Carlo calculation is continued according the condensed-random-walk model. Thus IMTRAN contains MTRAN and ITRAN as limiting cases. In trial calculations for the transmission and reflection of 64-keV and 16-keV electrons by gold foils it was found that with a switching energy approximately equal to 90% of the initial electron energy, the systematic differences relative to ITRAN are removed.

Comparison of Results from ITRAN, ETRAN and a Sandia Experiment

Fig. 2 shows comparisons of number transmission coefficients for electrons incident normally on gold foils, obtained with ITRAN and with ETRAN (run in the csda mode and without secondary electrons). The differences are quite small.

Table 5 compares number and energy albedos for electrons with energies of 32, 59, 109 and 314 keV incident at 0° (normally) and at 60° on a thick tantalum target. Results from ITRAN and from ETRAN (with straggling and secondaries, and in the continuous-slowing-down approximation without secondaries), are compared with experimental results of Lockwood, Ruggles, Miller and Halbleib[11]. The agreement between the experiment and the calculations is generally good, except for the number reflection coefficient at 32 keV (60° incidence). In regard to ITRAN, the agreement with experiment is improved if the results are multiplied by the (straggling/csda) reflection-coefficient ratio from ETRAN.

Comparison of Transmission Results from ITRAN and from Experiments

Fig. 3 compares number transmission coefficients from ITRAN with measurements of Neubert and Rogaschewski[12] for electrons incident normally on gold foils, for various electron energies from 15 keV to 60 keV. Another comparison with measurements by these authors is made in Fig. 4, which shows the transmission as a function of the angle of incidence (between 0° and 80°), for foil thicknesses from 98 to 1110 $\mu g/cm^2$. In Figs.3 and 4 the agreement between calculation and experiment is close.

Fig. 5 shows comparisons with transmission coefficients measured by Reimer and Drescher[13] for electrons incident normally on a gold foil, at many energies from 9.3 keV to 102 keV. The agreement is poorer in this case, particularly at the lower energies up to 17.3 keV, where the measured transmission significantly exceeds the calculated transmission. Because electron histories in ETRAN are terminated at 1 keV, and because of the neglect of energy-loss straggling, one would expect the calculated transmission to be somewhat too low for large foil thicknesses, but not to the extent indicated in Fig. 5.

The experimental results of Neubert and Rogaschewski at 13.4 keV and 17.3 keV are compared directly in Fig. 6 with the results of Reimer and Drescher at 15 keV. The transmission coefficients are plotted as functions of the foil thickness in units of the range, so that one would expect the 15-keV curve to lie between the 13.4-keV and 17.3keV curves. This is not the case, however, indicating an inconsistency between the two experiments.

X-ray Induced Electron Emission: Formulation of the Problem

In the experiment of Dolan[1], x-ray beams were incident normally on thin metallic foils, and measurements were made of the distribution in energy and angle of the electrons emitted in the backward and forward directions. The measurements were confined to electron energy above 5 keV. Here we are concerned only with the measurements with a 0.0025-cm tantalum foil. The efficiency was defined by Dolan as follows:

> Backward Efficiency: Average number of electrons (with energy > 5 keV) leaving through the entrance surface of the foil, divided by the average number of photons entering the foil.
>
> Forward Efficiency: Average number of electrons (with energy > 5 keV) leaving through the exit surface of the foil, divided by the average number of photons leaving the foil.

Dolan used different filtrations for the x-ray beams used for the measurement of electron emission in the backward and forward emission, so that the x-ray spectrum at the entrance surface (for backward emission) was approximately the same as the spectrum at the exit surface (for forward emission). The x-ray spectra used with a tantalum foil are shown in Fig. 7.

Outline of XITRAN and XMTRAN Codes

The transport of electrons through the foil is simulated with the same cross sections and random-sampling procedures in XITRAN as in ITRAN, and in XMTRAN as in MTRAN. The transport of photons is treated in direct analogy to the physical processes, except that Compton-scattered photons are treated as if they left the target without further interaction. For the low-energy x-ray spectra considered here, this omission is unimportant, because the Compton cross section in a high-Z material such as tantalum, at the energies of interest, is extremely small compared to the photoelectric cross section. At the cost of some complication, Compton scattering could readily be included in XITRAN or XMTRAN, if it were required to deal with target foils of intermediate or low atomic number, or with x-ray beams of higher energy.

Photon cross sections were obtained from a database PHOTEX compiled by J. H. Hubbell at the NIST Photon and Charged Particle Data Center. The cross sections for tantalum, calculated with the computer program XCOM[14], are shown in Table 6. The relative probabilities for the ejection of photoelectrons from various shells are shown in Table 7. XITRAN expects these data in the form of two input files, XAR.073 and XSHELL.073, in which the cross sections are arranged so as to facilitate interpolation with respect to photon energy, taking into account the presence of absorption edges.

The interaction of the x-ray photons with atoms results in an internal and external cascade. The internal cascade consists of the fluorescence photons and Auger electrons that are emitted from a single atom during the relaxation process following the absorption of a photon. The intensities and spectra of these radiations were obtained from the Livermore Evaluated Atomic Data Library[15], and their angular distributions were assumed to be isotropic. The fluorescence data are organized into an input file FLUOR.073, and the Auger-electron data into an input file AUGER.073.

The external cascade involves emission of successive generations of fluorescence photons and their photoelectric absorption in different atoms. In order to distinguish the contributions to the emitted electron current from different processes, XITRAN was actually separated into three programs, XITRANI, XITRAN2, and XITRAN3, and XMTRAN into XMTRAN1, XMTRAN2, and XMTRAN3. These codes carry out the following calculations:

XITRAN1 and XMTRAN1 follow the photoelectrons ejected after the absorption of the incident x rays.

XITRAN2 and XMTRAN2 follow the photoelectrons ejected after the absorption of first generation of fluorescence radiation produced within the target.

XITRAN3 and XMTRAN3 follow the Auger electrons emitted after the absorption of the incident x rays.

A fourth program was also written which follows Auger electrons emitted after the absorption of the first generation of fluorescence photons, and a fifth program which follows the photoelectrons produced when the second generation of fluorescence photons is absorbed. However, in exploratory calculations these additional processes were found to make insignificant contributions to the total efficiency, and they were therefore omitted from further consideration. Finally, it should be noted that XITRAN1, XITRAN2, and XITRAN3 (or XMTRAN1, XMTRAN2, and XMTRAN3) have many parts in common, and could be merged into a single code. Running instructions for the codes are given in Appendix 3.

Effect of the Angular Distribution of Photo-Electrons

The available information on the angular dependence of the photoelectric cross section is rather limited. In an older review, Davisson and Evans[16] recommended, at low energies, the use of a non-relativistic formula derived by Fischer[17] for photoelectrons ejected from the K shell. Fischer's cross section was also adopted in the ETRAN code (where only the K shell is treated), and is used for all shells in the Tiger series and in the Sandia discrete-ordinates code CEPXS[20].

The most thorough calculations of the photoelectric cross section differential in the photoelectron angle were made by Tseng, Pratt, Yu and Ron[18], and by Kim, Pratt, Ron and Tseng[19]. Reference 18 also contains a thorough review of the experimental data. These authors carried out numerical calculations in the central-field approximation, and concentrated on exploring relativistic, multipole and screening effects. Even though the computational apparatus appears to be available, comprehensive calculations encompassing all shells of a high-Z atom are not yet available.

Among the results presented by Tseng et al are angular distributions of photoelectrons ejected from the $2S_{1/2}$ and $2P_{1/2}$ shells of uranium, at 40, 60 and 80 keV. In Fig. 8, their distributions at 60 keV are compared with Fischer's formula, and with a simple $\sin^2(\theta)$ law where θ is the emission angle. It can be seen that for the $2S_{1/2}$ shell, the accurate distribution of Tseng is close to the $\sin^2(\theta)$ law but differs considerably from Fischer's formula, whereas the opposite is the case for the $2P_{1/2}$ shell.

In exploratory calculations, the XITRAN1 code was used to calculate the backward and forward efficiencies for electrons released by 60-keV photons from the $2S_{1/2}$ and $2P_{1/2}$ shells, both for a uranium target and a tantalum target with a thickness of 0.0025 cm. This was done three times: with a $\sin^2(\theta)$ law (S); with Fischer's formula (F); and with numerical results of Tseng (TS) et al for uranium read from graphs in reference 18. The ratios of the efficiencies obtained under these three assumptions are shown in Table 8. It can be seen that the efficiency TS is close to efficiency S for the $2S_{1/2}$ shell, but close to efficiency F for the $2P_{1/2}$ shell. This is consistent with the shapes of the angular distributions shown in Fig. 8.

Systematic Calculations with XITRAN and XMTRAN

Calculations for monoenergetic photon beams were made at energies corresponding to the mid-points of the all energy bins of the spectral histograms shown in Fig. 7. This involved 43 photon energies for application to 100-keV spectra, and 35 energies for 50-keV x-ray spectra. For each photon energy, a sample of 10 million photons was followed, and the secondary electron histories were followed with XITRANI, XITRAN2 and XITRAN3, or with XMTRAN1, XMTRAN2 and XMTRAN3. The electrons were followed only until the energy fell below 5 keV, which shortened the calculation and simplified the treatment of fluorescence radiation and Auger spectra.

Each photon has only a small chance to interact in the target, and the electrons released in the target only have a small chance to escape from it. Therefore the number of electrons emerging in the backward and forward directions, per 10 million incident photons, was typically only about 30,000. In preliminary versions of XITRAN and XMTRAN, the photons were forced to have at least one interaction in the target, but this approach was later abandoned because it did not significantly reduce the computing time.

In the absence of better information about the angular distribution of photoelectrons, and in view of the experience described in "Comparison of Transmission Results from ITRAN and from Experiments" on page 9, all Monte Carlo calculations were done twice, with the following two assumptions designated as Case 1 or Case 2.

Case 1: The angular distribution is taken to be proportional to $\sin^2(\theta)$ for ejection from $2S_{1/2}$, $3S_{1/2}$, $4S_{1/2}$, $5S_{1/2}$ and $6S_{1/2}$ shells, and calculated from by Fischer's formula for all other shells.

Case 2: The angular distribution is calculated from Fischer's formula for all shells.

Case 2 corresponds to the assumptions made in the TIGER series[25] and in the CEPXS code[20]. Strictly speaking, Fischer's formula was intended only for the K-shell, and the application to other shells, with appropriate binding energies, is just a convenient assumption which leads to reasonable results. The consideration of Cases 1 and 2 at least provides some indication of the sensitivity of the results to the assumed angular distribution.

The output of the Monte Carlo codes consists of a) efficiencies, b) energy spectra integrated over all directions, c) angular distributions integrated over all spectral energies down, and d) joint

energy-angular distributions. The information in item d) has been stored but not yet analyzed. An annotated partial output file from XITRAN1 is shown in Table 9.

Various codes were developed for processing the output of the large number of Monte Carlo runs. These were developed in pairs, with those indicated by "1" and "2" pertaining to 100-keV and 50-keV x-ray spectra, respectively. Codes called EMIT1 and EMIT2 were used to extract backward and forward efficiencies for monoenergetic photon beams, keeping track separately of contributions from (1) photoelectrons from absorption of x rays, (2) photoelectrons from the absorption of fluorescence radiation produced in the target, and (3) Auger electrons.

The forward efficiency is calculated in XITRAN and XMTRAN as the number of emerging electrons divided by the number of photons incident on the target. In EMIT1 and EMIT2 it is converted to an efficiency according to Dolan's definition (based on the number of photons leaving through the exit surface). This conversion is done assuming exponential absorption of photons in the target. The direct and converted forward efficiencies are indicated in Table 10 as TRANN and TRANC, respectively.

Results such as those shown in Table 10 were processed with codes called EFFIC1 and EFFIC2 to obtain the corresponding efficiencies averaged over the x-ray spectra. Table 11 shows partial backward and forward efficiencies calculated with EMIT1 and EMIT2 for Case 2. It can be seen that the dominant contribution comes from photoelectrons ejected after the absorption of the incident x rays, and that there are only minor contributions from Auger electrons, and from photoelectrons due to the absorption of fluorescence radiation.

Comparison of Efficiencies

Experimental values of backward and forward efficiencies obtained by Dolan[1] are compared in Table 12 with several theoretical results. The comparisons include calculated results from a) XITRAN and XMTRAN for Case 1 and Case 2; b) from the multigroup discrete-ordinates code CEPXS[20]; c) from the condensed-random-walk Monte Carlo code CYLTRAN[26]; d) from the code QUICKE based on the analytical method of MacCallum and Dellin[27].

The experimental errors are stated by Dolan to 15-20%. The statistical uncertainties of the results from XITRAN and XMTRAN are 1-2%, but the overall errors are expected to be larger, perhaps 5 to 10%, particularly in view of the uncertainties regarding the angular distribution of photoelectrons. The differences between measured and calculated efficiencies are well within the combined limits of error, and this appears to be the case not only for XITRAN and XMTRAN, but also for CEPXS, SANDYL and QUICKE.

In Table 13, the differences between efficiencies calculated by various methods are summarized in terms of efficiency ratios. The differences between the XITRAN results for Case 1 and Case 2 vary from 4% to 8%. The backward efficiency is smaller in Case 2 than in Case 1, whereas the opposite holds for the forward efficiency. The differences between the results from XITRAN and XMTRAN are always less than 1%. The results from CEPXS are always higher than those from XITRAN, by amounts ranging from 5% to 11%.

Comparison of Electron Spectra and Angular Distributions

Codes called COMBIN1 and COMBIN2 were used to add the results from XITRAN1, XITRAN2 and XITRAN3, or from XMTRAN1, XMTRAN2 and XMTRAN3, for monoenergetic photon sources. The combined results were in turn processed by codes called XSUM1 and XSUM2 to obtain efficiencies, energy spectra and angular distributions averaged over the x-ray spectra in Dolan's experiment. The efficiencies thus obtained are the same as those already discussed in Section 13. The energy spectra of emitted electrons were plotted with a code SPLOT. and the angular distributions with a code APLOT. Both of these codes use a library of plotting routines by Kahaner and Anderson[21], and must be compiled with the Lahey Fortran F77L compiler and used on an IBM-compatible personal computer.

Figs. 9a-d show comparisons between calculated electron spectra with the measurements of Dolan, four sets of conditions (backward and forward emission, 100-keV and 50 keV x-ray spectra). These are 2 - electron spectra integrated over all directions of emergence in the backward or forward direction. Four calculations are included in each comparisons. For example, Figs. 9a-1, 9a-2, 9a-3 and 9a-4 are for calculations for Cases 1 and 2 with XITRAN and XMTRAN.

There is practically no difference between the spectra calculated with XITRAN and XMTRAN. At 100 keV, the calculated spectra for Case 2 are somewhat closer to the experimental spectra than those calculated for Case 1 in the case of backward emission, whereas the converse holds for forward emission. At 50 keV the differences between Cases 1 and 2 are hardly noticeable.

Both at 100 keV and 50 keV, the agreement between theory and experiment is good down to a spectral energy of 20 keV. Below 20 keV the measured spectra are significantly higher than the calculated spectra. These discrepancies are greater at 100 keV than at 50 keV. The measured spectra at and close to the bottom energy (5 keV) show an upturn and rise, which is absent from the calculated spectra. Similar discrepancies in the low-energy part of the spectra were also found by Dolan when he compared his measurements with the predictions of the Monte Carlo code SANDYL.

It seem unlikely that these low-energy discrepancies are due to the omission of energy-loss straggling in electron transport in XITRAN and XMTRAN. Perhaps more likely are errors in the input data pertaining to fluorescence radiation and Auger electrons, It seems also possible that the actual x-ray spectra in the experiment differed somewhat from the histograms given by Dolan, by having a larger low-energy component. A proper explanation is still lacking.

Fig. 10 compares calculated angular distributions of the emergent electrons (integrated over all spectral energies down to 5 keV) with experimental results of Dolan. These comparisons are made for the same set of conditions as for the spectra in Fig. 9. The results from XITRAN and XMTRAN, for Cases 1 and 2, are all close to each other, and agree well with the measurements, and follow an approximate cosine law. This confirms that the directional distribution of the electrons emerging from the tantalum foil is insensitive to the initial angular distribution of the photoelectrons, and is determined mainly by multiple elastic scattering.

Appendix 1: Preparation of Elastic-Scattering Data for ITRAN and XITRAN

With a code called TLIST a energy grid extending from 512 keV to 1 keV was created, such that successive energies decrease by a factor $2^{-1/120} = 0.994243$. The output from TLIST consists of a file TLIST.512 with 1081 grid energies, and 1080 average (geometric-mean) energies for this grid. TLIST.512 was then separated into two files, THIGH.512 and TLOW.512, with average energies consisting respectively of energies above and below 8 keV.

Elastic scattering cross sections were obtained from the database EIAST[5] in the form of files EIAST1.079 and ELAST2.079 for gold, or EIAST1.073 and ELAST2.073 for tantalum. A code called ELINT was then used to interpolate these cross sections with respect to energy. ELINT was run twice: for the average energies in THIGH.512, to generate an expanded cross section file ELINTH.073 (or ELINTH.079) consisting of cross sections at 65 angles and 720 energies; and for the average energies in TLOW.512, to generate a cross section file ELINTL.073 (or ELINTL.079) consisting of cross sections at 193 angles and 360 energies. Interpolated total cross sections were also obtained.

The interpolated cross sections were used by a code called ELPREP to generate 720 64-bin histograms and 360 192-bin histograms to be used for the sampling of elastic deflections. ELPREP also prepares a table of 1081 energies and corresponding collision numbers and csda ranges (see "Monte Carlo Code ITRAN" on page 6). For this purpose ELPREP uses the interpolated total cross sections from ELINT, and electron stopping powers from files EMOD.079 or EMOD.073. The output from ELPREP is stored in files ELPREP.073 for tantalum (or ELPREP.079 for gold).

Appendix 2. Preparation of Multiple-Scattering Data for MTRAN and XMTRAN

With a code called ENGLIST a energy grid extending from 128 keV to 1 keV was created. The successive grid energies also specify the step sizes in the condensed random walk. On the basis of exploratory numerical studies the energy grid and resulting step sizes were chosen so that the average cosine of the multiple-scattering deflection angle per step is approximately equal to 0.94.

Elastic scattering cross sections for tantalum and gold from the database ELAST were used in a code called ELINT1F to obtain interpolated cross sections at the successive geometric mean energies of the energy grid. These cross sections were used by a code called GSCOF1 which calculates expansion coefficients for the Goudsmit-Saunderson Legendre series[22]. The step sizes were calculated by a code called STEPP which uses stopping powers from files EMOD.073 for tantalum and EMOD.079 for gold, and produces two output files. One is an information file called STEPPETAB.073 or STEPPETAB.079, which lists step sizes, collision frequencies and average multiple-scattering deflection cosines per step. The main output is stored in STEPPE.079 or STEPPE.073 which were used by a code called GSDIS3 to calculate the Goudsmit-Saunderson multiple-scattering distribution in the form of histograms for successive steps of the condensed random walk.

These histograms, together with the step sizes and csda ranges passed through from STEPPE.079 or STEPPE.073, are stored in file GSHE.079 or GSHE.073 to provide input for MTRAN or XMTRAN. The method of evaluating the Goudsmit-Saunderson Legendre series followed the procedure discussed in Berger and Wang[23]. For high-Z materials such as gold or tantalum, the step sizes at low energies must be rather small if the average deflection cosine is to be kept to 0.94, corresponding to an angle of 20°. Therefore the number of collisions per step, at low energies, is quite small, so that there is an appreciable probability that no elastic collision will occur in the step. These probabilities included in the arrays in GSHE.079 or GSCE.073, and are taken into account in MTRAN and XMTRAN.

Appendix 3: Running Instructions for XITRAN and XMTRAN

XITRAN1, XITRAN2 and XITRAN3, as well as XMITRAN1, XMTRAN2 and XMTRAN3, are to be run in the same manner, with a "submit file" supplying the required input data. Each submit file can be used to set up one or more runs with different initial energies. The instructions about the submit file and required input Are given in the prologue of the Fortran source code, and are reproduced below for XITRAN1:

```
c       XITRAN1 calls the following subroutines:
c             INDEX: converts atomic number to file extension
c             SCOF, BSPOL and BSPOLL: cubic-spline interpolation
c             BLIN: linear interpolation
c             ALIAS: setup of alias sampling arrays
c             LOCATE: classification in regard to energy and angle
c             TIMDAT, WATCH and TIMDIF: timing
c
c       The following input data files must be available for a material
c       with atomic number jjj:
c
c       ELPREP.jjj:   electron multiple scattering, stopping powers,
c                     ranges and collision numbers
c       XAR.jjj:      photon scattering and attenuation coefficients
c       XSHELL.jjj:   probabilities of ejection of photoelectrons
c                     from various shells
c       SHMARKi.jjj: Markers indicating shells for which sin2(theta)
c                     angular distribution is used.
c
c       Input is organized by a SUBMIT file which must contain the
c       following information:
c
c       Line 1: OUTPUT
c             Name of output file; termination if name = FIN
c
c       Line 2: IZ,EPHOT,IZ,IHIST,IMONIT,ISEED
c             IZ: atomic number of target
c             EPHOT: energy of incident photons, keV
c             IHIST: number of Monte Carlo histories to be done
c             IMONIT: number of histories after which progress report
c                   appears on monitor
c             ISEED: random number seed
c
c       Line 3: BOUND,TTOP,TBOT,BOUND,JMAX,LMAX,MODE
c             BOUND: target thickness, cm2/g
c             TTOP: top electron energy for classification, keV
```

```
c       TBOT: bottom electron energy for classification, keV
c       JMAX: number of energy bins for classification
c       LMAX: number of angular bins for classification
c       MODE: selects file from which shell markers are taken
c
c           If MODE=1,INPUT4=SHMARK1.jjj ; angular distribution
c                     of photoelectrons is assumed to be given
c                     by sin2(theta) for ejection from shells
c                     2Sl/2,3Sl/2,4Sl/2, 5Sl/2 and 6Sl/2, and
c                     by Fischer's formula for all other shells
c
c           If MODE=2,INPUT4=SHMARK2,jjj; angular distribution
c                     is assumed to be given by Fischer's
c                     formula for all shells.
```

The subroutines called and the input data for XITRAN2 and XITRAN3 are the same, except that a fluorescence data file FLUOR.073 must also be available for XITRAN2, and an Auger data file AUGER.073 for XITRAN3. The subroutines called and the input data for XMTRAN1, XMTRAN2 and XMTRAN3 are also the same, except that a multiple-scattering file GSHE.073 is needed instead of the single-scattering file ELPREP.073.

References

1. K. W. Dolan, *X-ray Induced Electron Emission from Metals*, Sandia National Laboratories Report No. SAND74-8642, October 1974, and "X-ray-induced Electron Emission from Metals," *J. Appl. Phys.*, Vol. 46, p. 2456-2463, June 1975.
2. International Commission on Radiation Units and Measurements, ICRU Report 37, "Stopping Powers for Electrons and Positrons," 1984.
3. J. C. Ashley, "Energy Loss Rate and Inelastic Mean Free Path of Low-Energy Electrons and Positrons in Condensed Matter," *J. of Electron Spectroscopy and Related Phenomena*, Vol. 50, p. 323-334, 1990.
4. J. M. Fernandez-Varea, R. Mayol, D. Liljequist and F. Salvat, "Inelastic Scattering of Electrons in Solids from a Generalized Oscillator Strength Model Using Optical and Photoelectric Data," *J. Phys: Condens. Matter*, Vol. 5, p. 3593-3610, 1993.
5. M. J. Berger, S. M. Seltzer, R. Wang and A. Schechter, *Elastic Scattering of Electrons and Positrons by Atoms*, National Institute of Standards and Technology Report NISTIR-5188, 1993.
6. M. E. Riley, *Relativistic, Elastic Electron Scattering from Atoms at Energies Greater than 1 keV*, Sandia National Laboratories Report SLA-74-0107, 1974.
7. M. E. Riley, C. J. MacCallum, and F. Biggs, "Theoretical Electron-Atom Elastic Scattering Cross Sections. Selected Elements, 1 keV to 256 keV," *Atom. Data and Nucl. Data Tables*, Vol. 15, p. 443-476, 1975.
8. J. P. Desclaux, "A Multiconfiguration Relativistic Dirac-Fock Program," *Computer Phys. Communications*, Vol. 9, p. 31-45, 1975.
9. R. A. Kronmal and A. V. Peterson, Jr., "On the Alias Method for Generating Random Variables from a Discrete Distribution," *The American Statistician*, Vol. 33, 214-218, 1979.
10. G. Marsaglia and A. Zaman, "Some Portable Very-long-period Random Number Generators," *Computers in Physics*, Vol. 8, p. 117-121, 1994.
11. G. J. Lockwood, L. E. Ruggles, G. J. Miller and J. A. Halbleib, *Electron Energy and Charge Albedos - Calorimetric Measurement vs. Monte Carlo*, Sandia National Laboratories Report No. SAND80-1968, November 1981.
12. G. Neubert and S. Rogaschewski, "Measurements of the Back-scattering and Absorption of 15-60 keV Electrons for Transparent Solid Films at Various Angles of Incidence," *J. Phys. D: Appl. Phys.*, Vol. 17, p. 2439-2454, 1984.
13. J. Reimer and H. Drescher, *J. Phys. D: Appl. Phys.*, Vol. 10, p. 805-815, 1977.
14. M. J. Berger and J. H. Hubbell, *XCOM: Photon Cross Sections on a Personal Computer*, National Bureau of Standards Report NBSIR 87-3597, 1987.
15. S. T. Perkins, D. E. Cullen, M. H. Chen, J. H. Hubbell, J. Rathkopf and J. Scofield, Report UCRL-50400, Vol. 30, *Tables and Graphs of Atomic Subshell and Relaxation Data Derived form the LLNL Evaluated Atomic Data Library (EADL), Z=1-100*, Lawrence Livermore National Laboratory, 1991.
16. C. M. Davisson and R. D. Evans, "Gamma-Ray Absorption Coefficients," *Rev. Mod. Phys.* Vol. 24, p. 79-107, 1952.
17. J. Fischer, *Ann. Phys. (Leipzig)*,. Vol. 8, p. 821, 1931.
18. H. K. Tseng, R. H. Pratt, S. Yu and A. Ron, "Photoelectron Angular Distributions," *Phys. Rev. A*, Vol. 17, p. 1061-1079, 1978.

19. Y. S. Kim, R. H. Pratt, A. Ron and H. K.Tseng, "Photoelectron Angular Distributions from the Subshells of High-Z Elements," *Phys. Rev. A*, Vol. 22, p. 567-576, 1980.
20. L. J. Lorence, Jr., J. E. Morel, and G. D. Valdez, *Physics Guide to CEPXS, a Multi-group Coupled Electron-photon Cross-section Code,* Sandia National Laboratories Report No. SAND89-1685, 1989.
21. D. K. Kahaner and W. E. Anderson, *Volksgrapher: a Fortran plotting package user's guide, Version 3.0*, National Institute of Standards Report 90-4238, 1990.
22. S. Goudsmit and J. L. Saunderson, "Multiple Scattering of Electrons," *Phys. Rev.*, Vol. 57, p. 24-29, 1940.
23. M. J. Berger and R. Wang, "Multiple-Scattering Angular Deflections and Energy-Loss Straggling", Chapter 2 of *Monte Carlo Transport of Electrons and Photons*, T. M. Jenkins, W. R. Nelson and A. Rindi (Eds.), Plenum Press, New York, 1988.
24. S. Seltzer, "Electron-Photon Monte Carlo Calculations: The ETRAN Code", *Int. J. Radiat. Appl. Inst. Part A: Appl. Radiat. Isot.*, Vol. 42, p. 917-941, 1991.
25. J. A. Halbleib, R. P. Kensek, T. A. Mehlhorn, G. D. Valdez, S. M. Seltzer and M. J. Berger, *ITS Version 3.0: The Integrated TIGER Series of Coupled Electron/Photon Monte Carlo Transport Codes,* Sandia National Laboratories Report No. SAND91-1634, March 1992.
26. H. M. Colbert, Sandia Laboratories Report SLL-74-0012, 1974.
27. C. J. MacCallum, and T. A. Dellin, "Photo-Compton Currents in Unbounded Media", *J. Appl. Phys.*, Vol. 44, p. 1878-1884, 1973; Sandia Laboratories Report SLL-74-0218, 1974.

Figure Captions

Fig.1. Stopping powers of gold. The dotted curve is calculated from Bethe's theory. The solid curve represents the stopping powers adopted in the present work, and was obtained by merging the Bethe curve above 20 keV with the values from the theory of Ashley[3] below 10 keV.

Fig.2. Comparisons of results from the ETRAN and ITRAN codes, pertaining to the transmission of electrons through gold foils (normal incidence). The solid curves, from ITRAN, and the dotted curves from ETRAN (run in the csda mode) are plotted as functions of the foil thickness in units of the range.

a. Electron energies of 10, 15, 20 and 25 keV
b. Electron energies of 30, 40, 60 and 60 keV

Fig.3. Comparison of calculated and experimental transmission curves for electrons incident normally on gold foils. The solid curves were calculated with the ITRAN code. The dotted curves represent measurements by Neubert and Rogaschewski[12].

a. Electron energies of 15, 20, 25 and 30 keV
b. Electron energies of 30, 40, 50 and 60 keV

Fig.4. Comparison of calculated and measured transmission curves for 30-keV electrons incident at various angles on a gold foil. The experimental results (represented by circles, squares, etc.) are from Neubert and Rogaschewski[12]. The curves were calculated with the ITRAN code, and are plotted, for various foil thicknesses, as functions of the angle of incidence. (Note that α=0 corresponds to normal incidence).

Fig.5. Comparison of calculated and experimental transmission curves for electrons incident normally on gold foils. The solid curves were calculated with the ITRAN code. The dotted curves represent measurements by Reimer and Drescher[13].

a. Electron energies of 9.3, 11, 13.4 and 17.3 keV
b. Electron energies of 25.2, 32.4, 41.5 and 62.1 keV
c. Electron energies of 81.8 and 102 keV

Fig.6. Comparison of measured transmission curves of Neubert and Rogaschewski[12] and of Reimer and Drescher[13], for electrons incident normally on gold foils.

Fig.7. Spectra of the x-ray beams used in Dolan's experiment. These are plots of histograms given in the Appendix of Reference1. Spectra #3 and #12 were used to measure the induced electron emission in the backward direction, and Spectra #7 and #8 in the forward direction.

a. Spectra #3 and #7 (endpoint energy 100 keV)
b. Spectra #12 and #8 (endpoint energy 50 keV)

Fig. 8. Comparison of the angular distributions of photoelectrons from various theories, for electrons ejected from the 2Sl/2 and 2Pl/2 shells of uranium atoms. The solid curves are from the numerical calculations of Tseng et al[18] and the dotted curves are from the formula of Fischer[17]. The dashed curves were calculated assuming a cross section proportional to $\sin^2(\theta)$. All distributions are normalized to unity.

a. For electrons ejected from the 2 S 1/2 shell of uranium
b. For electrons ejected from the 2 P 1/2 shell of uranium

Fig.9. Comparison of measured and calculated energy spectra of electrons emitted from a 0.0025-cm tantalum foil irradiated by x rays. The spectra were obtained by integrating the joint energy-angle distributions over all directions of emergence. The points (o) are from the experiment of Dolan[1]. The histograms were calculated with XITRAN or XMTRAN, as indicated. In the calculations marked as Case 2, the angular distributions of photoelectrons from all shells were calculated from the formula of Fischer[17]. For Case 1, a $\sin^2(\theta)$ distribution was assumed for ejection from shells 2 Sl/2, 2 S 3/2,...,6 S 1/2, and Fischer's formula for all other shells. Fig.9 includes 16 plots for the following conditions:

a. 100-keV source, backward emission
b. 100-keV source, forward emission
c. 50-keV source, backward emission
d. 50-keV source, forward emission

Items a, b, c and d each include four plots, marked 1, 2, 3 and 4:

1. Calculated with XITRAN, Case 1
2. Calculated with XITRAN, Case 2
3. Calculated with XMTRAN, Case 1
4. Calculated with XMTRAN, Case 2

Fig.10 Comparison of measured and calculated angular distributions of electrons emitted from a 0.0025-cm tantalum foil irradiated by x rays. The angular distributions were obtained by integrating the joint energy-angle distributions over all spectral energies above 5 keV. Fig.10 includes 16 plots for the same set of conditions indicated for Fig. 9.

Table 1. Electron stopping powers and ranges in gold, calculated from Bethe's theory above 20 keV, from theory of Ashley [3] below 10 keV, and by interpolation at intermediate energies.

T = electron energy, keV
SC = collision stopping power, MeV cm2/g
SR = radiative stopping power, MeV cm2/g
ST = total stopping power, MeV cm2/g
RG = csda range, mg/cm2

T	SC	SR	ST	RG
1.00	29.96890	0.00438	29.97328	0.03436
1.25	27.50200	0.00508	27.50708	0.04308
1.50	25.51760	0.00586	25.52346	0.05252
1.75	23.92190	0.00665	23.92855	0.06265
2.00	22.56730	0.00743	22.57473	0.07341
2.50	20.30110	0.00887	20.30997	0.09680
3.00	18.47830	0.01018	18.48848	0.12263
3.50	16.98340	0.01136	16.99476	0.15087
4.00	15.73500	0.01241	15.74741	0.18146
4.50	14.67870	0.01338	14.69208	0.21435
5.00	13.78280	0.01426	13.79706	0.24950
5.50	13.02090	0.01508	13.03598	0.28680
6.00	12.37060	0.01583	12.38643	0.32617
7.00	11.31600	0.01718	11.33318	0.41070
8.00	10.45550	0.01836	10.47386	0.50256
9.00	9.70939	0.01941	9.72880	0.60168
10.00	9.05797	0.02036	9.07833	0.70815
12.50	7.76582	0.02237	7.78819	1.00644
15.00	6.82747	0.02402	6.85149	1.34956
17.50	6.12839	0.02543	6.15382	1.73536
20.00	5.59487	0.02666	5.62153	2.16110
25.00	4.83221	0.02872	4.86093	3.12129
30.00	4.28440	0.03043	4.31483	4.21560
35.00	3.87029	0.03190	3.90219	5.43627
40.00	3.54541	0.03321	3.57862	6.77605
45.00	3.28323	0.03439	3.31762	8.22866
50.00	3.06691	0.03547	3.10238	9.78847
55.00	2.88519	0.03647	2.92166	11.45040
60.00	2.73028	0.03741	2.76769	13.20970
70.00	2.47996	0.03914	2.51910	17.00360
80.00	2.28624	0.04070	2.32694	21.13950
90.00	2.13177	0.04214	2.17391	25.59020
100.00	2.00567	0.04348	2.04915	30.33200

Table 2. Electron stopping powers and ranges in tantalum, calculated from Bethe's theory above 20 keV, from the theory of Fernandez-Varea et al [4] below 10 keV, and by interpolation at intermediate energies.

T = electron energy, keV
SC = collision stopping power, MeV cm2/g
SR = radiative stopping power, MeV cm2/g
ST = total stopping power, MeV cm2/g
RG = csda range, mg/cm2

T	SC	SR	ST	RG
1.00	32.30230	0.00448	32.30678	0.03071
1.25	29.30030	0.00517	29.30547	0.03885
1.50	27.00050	0.00593	27.00643	0.04775
1.75	25.10120	0.00670	25.10790	0.05736
2.00	23.50530	0.00745	23.51275	0.06766
2.50	20.98140	0.00884	20.99024	0.09022
3.00	19.05160	0.01009	19.06169	0.11525
3.50	17.51050	0.01121	17.52171	0.14264
4.00	16.24420	0.01222	16.25642	0.17230
4.50	15.18130	0.01313	15.19443	0.20413
5.00	14.27380	0.01397	14.28777	0.23809
5.50	13.48800	0.01474	13.50274	0.27411
6.00	12.79900	0.01545	12.81445	0.31213
7.00	11.64440	0.01671	11.66111	0.39406
8.00	10.71550	0.01782	10.73332	0.48354
9.00	9.94987	0.01880	9.96867	0.58030
10.00	9.29791	0.01967	9.31758	0.68413
12.50	8.00302	0.02153	8.02456	0.97414
15.00	7.05362	0.02306	7.07667	1.30670
17.50	6.33877	0.02434	6.36311	1.67998
20.00	5.78710	0.02545	5.81255	2.09168
25.00	4.98973	0.02732	5.01705	3.02113
30.00	4.41856	0.02885	4.44741	4.08216
35.00	3.98763	0.03017	4.01780	5.26711
40.00	3.65006	0.03132	3.68138	6.56894
45.00	3.37796	0.03237	3.41033	7.98156
50.00	3.15367	0.03332	3.18699	9.49948
55.00	2.96543	0.03420	2.99963	11.11770
60.00	2.80506	0.03503	2.84009	12.83180
70.00	2.54617	0.03655	2.58272	16.53070
80.00	2.34604	0.03793	2.38397	20.56620
90.00	2.18663	0.03919	2.22582	24.91190
100.00	2.05662	0.04037	2.09699	29.54430

Table 3. Comparison of reflection coefficients calculated with Monte Carlo codes ITRAN and MTRAN. The results pertain to reflection from a gold foil of saturation thickness (thicker than 1/2 the csda range). The reflection coefficients include only electrons backscattered with energies greater than 1 keV.

RN and RE: number and energy reflection coefficient calculated with ITRAN

DIFF: percentage amounts by which the reflection coefficients calculated with MTRAN differ from those calculated with ITRAN.

(a) Electrons incident on a gold foil normally (at 0 deg)

Energy (keV)	RN	DIFF(%)	RE	DIFF(%)
100.0	0.5116	-1.6	0.40281	-2.3
80.0	0.5102	-2.2	0.40114	-2.6
60.0	0.5050	-2.1	0.39642	-2.7
50.0	0.4993	-1.8	0.39272	-2.6
40.0	0.4964	-1.8	0.39004	-2.7
30.0	0.4907	-2.7	0.38381	-3.2
25.0	0.4835	-1.5	0.37749	-2.4
20.0	0.4764	-1.9	0.37062	-2.7
15.0	0.4695	-2.0	0.36309	-2.9
10.0	0.4581	-2.5	0.35236	-3.6

(b) Electrons incident on a gold foil at 60 deg

Energy (keV)	RN	DIFF(%)	RE	DIFF(%)
100.0	0.6658	-1.3	0.56824	-1.8
80.0	0.6588	-1.0	0.56219	-1.6
60.0	0.6571	-1.1	0.55903	-1.6
50.0	0.6527	-1.1	0.55451	-1.6
40.0	0.6493	-0.9	0.54984	-1.4
30.0	0.6440	-1.3	0.54334	-2.0
25.0	0.6395	-0.5	0.53735	-1.1
20.0	0.6358	-1.4	0.53199	-2.1
15.0	0.6292	-1.4	0.52246	-2.1
10.0	0.6159	-1.2	0.50543	-2.0

Table 4. Comparison of transmission coefficients calculated with Monte Carlo codes ITRAN and MTRAN. The results pertain to transmission through a gold foil whose thickness is expressed in terms of the ratio x/r , where x is the actual thickness and r the csda range. The transmission coefficients include only electrons transmitted with energies greater than 1 keV.

TRN and TRE: number and energy transmission coefficients calculated with ITRAN

DIFF: percentage amount by which the coefficients calculated with MTRAN differ from those calculated with ITRAN.

(a) Electrons incident on a gold foil normally (at 0 deg)

Number Transmission Coefficients

	100 keV		80 keV		60 keV		50 keV		40 keV	
x/r	TRN	DIFF(%)	TRN	DIFF(%)	TRN	DIFF(%)	TRN	DIFF(%)	TRN	DIFF(%)
0.05	0.7943	1.8	0.7978	1.7	0.8036	1.8	0.8056	1.8	0.8091	1.8
0.10	0.5950	2.0	0.6018	2.1	0.6112	2.1	0.6179	2.1	0.6232	2.2
0.15	0.4352	2.5	0.4416	2.3	0.4551	2.4	0.4620	2.6	0.4711	2.4
0.20	0.2894	3.7	0.2967	2.4	0.3097	2.8	0.3178	2.8	0.3286	2.3
0.25	0.1729	3.0	0.1777	2.8	0.1892	3.2	0.1970	3.8	0.2071	2.8
0.30	0.0888	3.8	0.0939	3.8	0.1028	2.8	0.1086	3.4	0.1173	2.1
0.35	0.0394	6.6	0.0424	6.1	0.0482	2.7	0.0516	3.5	0.0578	5.1
0.40	0.0144	9.7	0.0160	11.3	0.0189	8.3	0.0210	3.0	0.0253	3.9

	30 keV		25 keV		20 keV		15 keV		10 keV	
x/r	TRN	DIFF(%)	TRN	DIFF(%)	TRN	DIFF(%)	TRN	DIFF(%)	TRN	DIFF(%)
0.05	0.7943	1.8	0.7978	1.7	0.8036	1.8	0.8056	1.8	0.8091	1.8
0.10	0.5950	2.0	0.6018	2.1	0.6112	2.1	0.6179	2.1	0.6232	2.2
0.15	0.4352	2.5	0.4416	2.3	0.4551	2.4	0.4620	2.6	0.4711	2.4
0.20	0.2894	3.7	0.2967	2.4	0.3097	2.8	0.3178	2.8	0.3286	2.3
0.25	0.1729	3.0	0.1777	2.8	0.1892	3.2	0.1970	3.8	0.2071	2.8
0.30	0.0888	3.8	0.0939	3.8	0.1028	2.8	0.1086	3.4	0.1173	2.1
0.35	0.0394	6.6	0.0424	6.1	0.0482	2.7	0.0516	3.5	0.0578	5.1
0.40	0.0144	9.7	0.0160	11.3	0.0189	8.3	0.0210	3.0	0.0253	3.9

Energy Transmission Coefficients

	100 keV		80 keV		60 keV		50 keV		40 keV	
x/r	TRE	DIFF(%)	TRE	DIFF(%)	TRE	DIFF(%)	TRE	DIFF(%)	TRE	DIFF(%)
0.05	0.7550	1.9	0.7591	1.9	0.7659	2.0	0.7682	2.0	0.7722	1.9
0.10	0.5137	2.3	0.5214	2.4	0.5325	2.2	0.5391	2.3	0.5454	2.5
0.15	0.3331	2.8	0.3396	2.7	0.3527	2.5	0.3586	3.0	0.3681	2.7
0.20	0.1970	3.8	0.2032	2.9	0.2141	2.7	0.2202	3.1	0.2294	2.6
0.25	0.1047	3.4	0.1088	3.0	0.1170	3.2	0.1224	4.1	0.1295	3.4
0.30	0.0481	4.0	0.0515	3.8	0.0569	3.2	0.0604	3.7	0.0657	3.1
0.35	0.0191	6.9	0.0207	6.3	0.0239	4.3	0.0258	3.7	0.0291	5.8
0.40	0.0062	7.7	0.0070	11.7	0.0084	9.2	0.0094	2.9	0.0114	4.5

	30 keV		25 keV		20 keV		15 keV		10 keV	
x/r	TRE	DIFF(%)	TRE	DIFF(%)	TRE	DIFF(%)	TRE	DIFF(%)	TRE	DIFF(%)
0.05	0.7782	1.9	0.7832	2.0	0.7902	1.5	0.7937	2.0	0.7988	1.7
0.10	0.5590	2.4	0.5682	2.1	0.5799	2.1	0.5900	2.5	0.6039	2.4
0.15	0.3807	3.1	0.3913	2.2	0.4047	1.8	0.4161	2.8	0.4339	2.4
0.20	0.2400	3.4	0.2501	2.6	0.2606	2.3	0.2723	3.7	0.2919	2.4
0.25	0.1375	4.2	0.1461	2.9	0.1550	2.9	0.1641	4.4	0.1821	2.3
0.30	0.0713	4.4	0.0770	4.1	0.0839	2.7	0.0936	1.0	0.1047	1.8
0.35	0.0324	5.9	0.0362	3.7	0.0424	-1.3	0.0459	2.4	0.0546	1.4
0.40	0.0131	5.4	0.0148	4.8	0.0167	9.6	0.0234	-10.2	0.0257	1.2

Table 5. Comparison of calculated and experimental backscattering coefficients for electrons. The calculated results are based on samples of 100,000 Monte Carlo electron histories, and include only electrons backscattered with energies greater than 1 keV.

FRACTION OF ENERGY REFLECTED (0-deg incidence)

		32 keV	58 keV	109 keV	314 keV
1	ETRAN (strag)	0.3809	0.3850	0.4026	0.3961
2	ETRAN (csda)	0.3664	0.3733	0.3906	0.3819
3	ITRAN	0.3712	0.3818	0.3861	0.3756
4	ITRAN (adj)	0.3859	0.3938	0.3980	0.3896
5	Expt (Sandia)	0.398	0.395	0.403	0.377

FRACTION OF ENERGY REFLECTED (60-deg incidence)

		32 keV	58 keV	109 keV	314 keV
1	ETRAN (strag)	0.5437	0.5499	0.5686	0.5612
2	ETRAN (csda)	0.5321	0.5405	0.5572	0.5409
3	ITRAN	0.5365	0.5498	0.5574	0.5472
4	ITRAN (adj)	0.5471	0.5593	0.5688	0.5682
5	Expt (Sandia)	0.535	0.553	0.559	0.557

FRACTION OF NUMBER REFLECTED (0-deg incidence)

		32 keV	58 keV	109 keV	314 keV
1	ETRAN (strag)	0.4912	0.4957	0.5165	0.5176
2	ETRAN (csda)	0.4764	0.4814	0.5017	0.5006
3	ITRAN	0.4792	0.4898	0.4956	0.4925
4	ITRAN (Adj)	0.4941	0.5043	0.5102	0.5042
5	Expt (Sandia)	0.494	0.497	0.506	0.497

FRACTION OF NUMBER REFLECTED (60-deg incidence)

		32 keV	58 keV	109 keV	314 keV
1	ETRAN (strag)	0.6547	0.6586	0.6775	0.6758
2	ETRAN (csda)	0.6360	0.6413	0.6575	0.6413
3	ITRAN	0.6398	0.6487	0.6553	0.6509
4	ITRAN (adj)	0.6586	0.6662	0.6752	0.6859
5	Expt (Sandia)	0.576	0.662	0.662	0.668

1. ETRAN (strag): Version ETR21I. Complete treatment including straggling and secondary electrons.

2. ETRAN (csda): Version ETR21I, run with continuous-slowing-down approximation, omitting secondary electrons or photons.

3. ITRAN: follows all individual elastic collisions, uses continuous-slowing-down approximation and disregards seconday electrons.

4. ITRAN (adj): Results from ITRAN multiplied by the (straggling/csda) coefficient ratio from ETRAN.

5. Experimental results reported by Lockwood, Ruggles, Miller and Halbleib [11].

Table 6. Cross sections for the interaction of photons with tantalum.
Calculated with program XCOM [14].

	PHOTON ENERGY	SCATTERING COHERENT	SCATTERING INCOHER.	PHOTO-ELECTRIC ABSORPTION	PAIR PRODUCTION IN NUCLEAR FIELD	PAIR PRODUCTION IN ELECTRON FIELD	TOTAL ATTENUATION WITH COHERENT SCATT.	TOTAL ATTENUATION WITHOUT COHERENT SCATT.
	(MeV)	(b/atom)	(b/atom)	(b/atom)	(b/atom)	(b/atom)	(cm2/g)	(cm2/g)
	1.000E-03	3.40E+03	1.35E+00	1.05E+06	0.00E-01	0.00E-01	3.51E+03	3.50E+03
	1.500E-03	3.25E+03	2.31E+00	4.67E+05	0.00E-01	0.00E-01	1.57E+03	1.56E+03
	1.735E-03	3.18E+03	2.75E+00	3.44E+05	0.00E-01	0.00E-01	1.15E+03	1.14E+03
M5	1.735E-03	3.18E+03	2.75E+00	4.18E+05	0.00E-01	0.00E-01	1.40E+03	1.39E+03
	1.764E-03	3.17E+03	2.80E+00	6.18E+05	0.00E-01	0.00E-01	2.07E+03	2.06E+03
	1.793E-03	3.16E+03	2.85E+00	9.12E+05	0.00E-01	0.00E-01	3.04E+03	3.03E+03
M4	1.793E-03	3.16E+03	2.85E+00	1.01E+06	0.00E-01	0.00E-01	3.38E+03	3.37E+03
	2.000E-03	3.09E+03	3.23E+00	1.13E+06	0.00E-01	0.00E-01	3.77E+03	3.76E+03
	2.194E-03	3.03E+03	3.58E+00	8.94E+05	0.00E-01	0.00E-01	2.99E+03	2.98E+03
M3	2.194E-03	3.03E+03	3.58E+00	1.04E+06	0.00E-01	0.00E-01	3.46E+03	3.45E+03
	2.327E-03	2.99E+03	3.82E+00	8.99E+05	0.00E-01	0.00E-01	3.00E+03	2.99E+03
	2.469E-03	2.95E+03	4.07E+00	7.80E+05	0.00E-01	0.00E-01	2.60E+03	2.59E+03
M2	2.469E-03	2.95E+03	4.07E+00	8.29E+05	0.00E-01	0.00E-01	2.77E+03	2.76E+03
	2.586E-03	2.91E+03	4.28E+00	7.44E+05	0.00E-01	0.00E-01	2.49E+03	2.48E+03
	2.708E-03	2.87E+03	4.49E+00	6.68E+05	0.00E-01	0.00E-01	2.23E+03	2.22E+03
M1	2.708E-03	2.87E+03	4.49E+00	6.97E+05	0.00E-01	0.00E-01	2.33E+03	2.32E+03
	3.000E-03	2.78E+03	5.01E+00	5.49E+05	0.00E-01	0.00E-01	1.84E+03	1.83E+03
	4.000E-03	2.49E+03	6.69E+00	2.75E+05	0.00E-01	0.00E-01	9.22E+02	9.14E+02
	5.000E-03	2.22E+03	8.28E+00	1.58E+05	0.00E-01	0.00E-01	5.33E+02	5.26E+02
	6.000E-03	1.99E+03	9.75E+00	9.96E+04	0.00E-01	0.00E-01	3.38E+02	3.32E+02
	8.000E-03	1.60E+03	1.23E+01	4.76E+04	0.00E-01	0.00E-01	1.64E+02	1.59E+02
	9.881E-03	1.33E+03	1.44E+01	2.75E+04	0.00E-01	0.00E-01	9.60E+01	9.16E+01
L3	9.881E-03	1.33E+03	1.44E+01	7.19E+04	0.00E-01	0.00E-01	2.44E+02	2.39E+02
	1.000E-02	1.31E+03	1.45E+01	7.01E+04	0.00E-01	0.00E-01	2.38E+02	2.34E+02
	1.114E-02	1.18E+03	1.56E+01	5.26E+04	0.00E-01	0.00E-01	1.79E+02	1.75E+02
L2	1.114E-02	1.18E+03	1.56E+01	7.24E+04	0.00E-01	0.00E-01	2.45E+02	2.41E+02
	1.141E-02	1.15E+03	1.58E+01	6.83E+04	0.00E-01	0.00E-01	2.31E+02	2.27E+02
	1.168E-02	1.12E+03	1.61E+01	6.44E+04	0.00E-01	0.00E-01	2.18E+02	2.15E+02
L1	1.168E-02	1.12E+03	1.61E+01	7.45E+04	0.00E-01	0.00E-01	2.52E+02	2.48E+02
	1.500E-02	8.51E+02	1.87E+01	3.94E+04	0.00E-01	0.00E-01	1.34E+02	1.31E+02
	2.000E-02	6.01E+02	2.19E+01	1.84E+04	0.00E-01	0.00E-01	6.33E+01	6.13E+01
	3.000E-02	3.55E+02	2.62E+01	6.19E+03	0.00E-01	0.00E-01	2.19E+01	2.07E+01
	4.000E-02	2.34E+02	2.85E+01	2.82E+03	0.00E-01	0.00E-01	1.03E+01	9.48E+00
	5.000E-02	1.65E+02	2.98E+01	1.52E+03	0.00E-01	0.00E-01	5.72E+00	5.17E+00
	6.000E-02	1.24E+02	3.05E+01	9.18E+02	0.00E-01	0.00E-01	3.57E+00	3.16E+00
	6.742E-02	1.03E+02	3.08E+01	6.63E+02	0.00E-01	0.00E-01	2.65E+00	2.31E+00
K	6.742E-02	1.03E+02	3.08E+01	3.41E+03	0.00E-01	0.00E-01	1.18E+01	1.15E+01
	8.000E-02	7.78E+01	3.10E+01	2.17E+03	0.00E-01	0.00E-01	7.59E+00	7.33E+00
	1.000E-01	5.34E+01	3.08E+01	1.21E+03	0.00E-01	0.00E-01	4.30E+00	4.12E+00
	1.500E-01	2.61E+01	2.94E+01	4.04E+02	0.00E-01	0.00E-01	1.53E+00	1.44E+00
	2.000E-01	1.56E+01	2.77E+01	1.85E+02	0.00E-01	0.00E-01	7.60E-01	7.08E-01
	3.000E-01	7.38E+00	2.47E+01	6.25E+01	0.00E-01	0.00E-01	3.15E-01	2.90E-01
	4.000E-01	4.29E+00	2.25E+01	2.97E+01	0.00E-01	0.00E-01	1.88E-01	1.74E-01
	5.000E-01	2.80E+00	2.07E+01	1.71E+01	0.00E-01	0.00E-01	1.35E-01	1.26E-01
	6.000E-01	1.97E+00	1.92E+01	1.11E+01	0.00E-01	0.00E-01	1.08E-01	1.01E-01
	8.000E-01	1.12E+00	1.70E+01	5.87E+00	0.00E-01	0.00E-01	7.98E-02	7.61E-02
	1.000E+00	7.26E-01	1.53E+01	3.68E+00	0.00E-01	0.00E-01	6.57E-02	6.32E-02

Table 7. Probabilities for the ejection of photo-electrons from the atomic shells of tantalum, as functions of the photon energy. The probabilities are expressed in terms of percentages.

Energy (eV)	1 S 1/2 1	2 S 1/2 2	2 P 1/2 3	2 P 3/2 4	3 S 1/2 5	3 P 1/2 6	3 P 3/2 7	3 D 3/2 8	3 D 5/2 9	4 S 1/2 10	4 P 1/2 11
1000.0	0.000	0.000	0.000	0.000	0.000	0.000	0.000	0.000	0.000	3.855	4.025
1500.0	0.000	0.000	0.000	0.000	0.000	0.000	0.000	0.000	0.000	5.147	6.001
1735.1	0.000	0.000	0.000	0.000	0.000	0.000	0.000	0.000	0.000	5.685	6.790
1735.1	0.000	0.000	0.000	0.000	0.000	0.000	0.000	0.000	17.874	4.669	5.575
1793.2	0.000	0.000	0.000	0.000	0.000	0.000	0.000	0.000	64.863	2.041	2.451
1793.2	0.000	0.000	0.000	0.000	0.000	0.000	0.000	9.985	58.413	1.836	2.204
2000.0	0.000	0.000	0.000	0.000	0.000	0.000	0.000	31.973	45.662	1.397	1.699
2194.0	0.000	0.000	0.000	0.000	0.000	0.000	0.000	31.793	45.150	1.531	1.878
2194.0	0.000	0.000	0.000	0.000	0.000	0.000	13.869	27.381	38.888	1.319	1.618
2468.7	0.000	0.000	0.000	0.000	0.000	0.000	15.238	26.718	37.737	1.457	1.800
2468.7	0.000	0.000	0.000	0.000	0.000	5.934	14.337	25.137	35.492	1.370	1.692
2708.0	0.000	0.000	0.000	0.000	0.000	6.495	15.282	24.502	34.516	1.463	1.813
2708.0	0.000	0.000	0.000	0.000	4.155	6.226	14.649	23.488	33.072	1.403	1.738
3000.0	0.000	0.000	0.000	0.000	4.707	6.914	15.578	22.659	31.687	1.502	1.862
4000.0	0.000	0.000	0.000	0.000	6.202	9.053	18.730	19.873	27.361	1.835	2.245
5000.0	0.000	0.000	0.000	0.000	7.622	10.739	20.945	17.619	23.993	2.144	2.558
6000.0	0.000	0.000	0.000	0.000	8.915	12.096	22.575	15.780	21.300	2.430	2.817
8000.0	0.000	0.000	0.000	0.000	11.223	14.072	24.730	12.984	17.258	2.952	3.214
9881.1	0.000	0.000	0.000	0.000	13.143	15.355	25.890	11.063	14.533	3.393	3.484
9881.1	0.000	0.000	0.000	61.750	5.027	5.873	9.903	4.232	5.559	1.298	1.332
10000.0	0.000	0.000	0.000	62.010	5.036	5.859	9.855	4.164	5.465	1.299	1.329
11136.1	0.000	0.000	0.000	61.801	5.467	6.112	10.075	3.838	5.003	1.400	1.384
11136.1	0.000	0.000	27.337	44.908	3.973	4.441	7.320	2.788	3.636	1.017	1.006
11681.5	0.000	0.000	27.998	44.511	4.069	4.464	7.294	2.652	3.450	1.039	1.011
11681.5	0.000	13.516	24.214	38.495	3.519	3.860	6.308	2.294	2.984	0.898	0.874
15000.0	0.000	16.670	24.044	36.121	4.059	4.006	6.255	1.796	2.298	1.022	0.907
20000.0	0.000	20.575	23.241	33.268	4.806	4.145	6.148	1.352	1.696	1.197	0.942
30000.0	0.000	26.703	21.776	28.867	5.966	4.181	5.761	0.881	1.071	1.471	0.958
40000.0	0.000	31.213	20.493	25.725	6.853	4.115	5.371	0.642	0.761	1.684	0.950
50000.0	0.000	34.698	19.417	23.351	7.558	4.019	5.025	0.499	0.579	1.852	0.932
60000.0	0.000	37.479	18.522	21.485	8.127	3.920	4.725	0.406	0.463	1.991	0.913
67416.4	0.000	39.207	17.953	20.335	8.485	3.848	4.530	0.356	0.401	2.077	0.898
67416.4	80.554	7.624	3.491	3.954	1.650	0.748	0.881	0.069	0.078	0.404	0.175
80000.0	81.064	7.885	3.243	3.547	1.704	0.707	0.803	0.056	0.061	0.417	0.166
100000.0	81.791	8.125	2.930	3.058	1.754	0.652	0.706	0.042	0.045	0.429	0.153
150000.0	82.529	8.614	2.519	2.408	1.863	0.576	0.571	0.026	0.027	0.456	0.136
200000.0	82.835	8.932	2.302	2.070	1.937	0.535	0.498	0.019	0.020	0.474	0.127
300000.0	83.123	9.298	2.066	1.715	2.022	0.488	0.419	0.013	0.013	0.496	0.116
400000.0	83.284	9.491	1.932	1.532	2.068	0.459	0.376	0.010	0.010	0.507	0.110
500000.0	83.413	9.595	1.841	1.419	2.093	0.440	0.350	0.008	0.009	0.513	0.105
600000.0	83.527	9.655	1.772	1.343	2.106	0.424	0.332	0.007	0.008	0.516	0.101
800000.0	83.707	9.702	1.681	1.249	2.117	0.404	0.309	0.006	0.007	0.519	0.097
1000000.0	83.843	9.714	1.621	1.194	2.120	0.391	0.296	0.005	0.006	0.520	0.093

Table 7, continued

Energy (eV)	4 P 3/2 12	4 D 3/2 13	4 D 5/2 14	4 F 5/2 15	4 F 7/2 16	5 S 1/2 17	5 P 1/2 18	5 P 3/2 19	5 D 3/2 20	5 D 5/2 21	6 S 1/2 22
1000.0	11.187	15.667	23.239	16.599	21.194	0.870	0.758	1.802	0.298	0.419	0.088
1500.0	14.434	18.373	26.506	10.774	13.655	1.046	0.996	2.169	0.334	0.462	0.102
1735.1	15.672	18.863	26.980	9.077	11.474	1.126	1.096	2.318	0.341	0.468	0.109
1735.1	12.870	15.492	22.159	7.455	9.422	0.925	0.901	1.904	0.280	0.384	0.089
1793.2	5.607	6.654	9.501	3.065	3.871	0.403	0.394	0.827	0.120	0.165	0.039
1793.2	5.043	5.984	8.545	2.756	3.482	0.362	0.354	0.744	0.108	0.148	0.035
2000.0	3.783	4.271	6.061	1.704	2.149	0.271	0.269	0.553	0.077	0.105	0.026
2194.0	4.088	4.410	6.227	1.562	1.966	0.294	0.293	0.593	0.079	0.108	0.028
2194.0	3.522	3.798	5.363	1.345	1.693	0.253	0.253	0.511	0.068	0.093	0.024
2468.7	3.813	3.862	5.421	1.179	1.480	0.276	0.278	0.550	0.070	0.094	0.026
2468.7	3.587	3.634	5.100	1.109	1.393	0.260	0.261	0.517	0.065	0.088	0.025
2708.0	3.764	3.619	5.055	0.985	1.235	0.275	0.277	0.540	0.065	0.087	0.026
2708.0	3.609	3.469	4.845	0.944	1.184	0.264	0.266	0.518	0.063	0.083	0.025
3000.0	3.786	3.423	4.758	0.822	1.029	0.280	0.283	0.541	0.062	0.082	0.026
4000.0	4.315	3.246	4.447	0.553	0.688	0.336	0.336	0.611	0.059	0.077	0.032
5000.0	4.726	3.042	4.117	0.400	0.495	0.389	0.379	0.666	0.056	0.072	0.037
6000.0	5.040	2.839	3.806	0.304	0.375	0.438	0.416	0.710	0.052	0.067	0.041
8000.0	5.477	2.475	3.264	0.192	0.235	0.528	0.472	0.770	0.046	0.058	0.050
9881.1	5.732	2.188	2.852	0.135	0.164	0.604	0.510	0.806	0.041	0.051	0.057
9881.1	2.192	0.837	1.091	0.052	0.063	0.231	0.195	0.308	0.016	0.019	0.022
10000.0	2.182	0.825	1.075	0.050	0.061	0.231	0.195	0.307	0.015	0.019	0.022
11136.1	2.232	0.773	1.001	0.042	0.051	0.249	0.203	0.314	0.014	0.018	0.024
11136.1	1.622	0.562	0.727	0.030	0.037	0.181	0.147	0.228	0.011	0.013	0.017
11681.5	1.617	0.539	0.695	0.028	0.034	0.184	0.148	0.227	0.010	0.012	0.017
11681.5	1.399	0.466	0.601	0.024	0.029	0.159	0.128	0.197	0.009	0.011	0.015
15000.0	1.393	0.377	0.479	0.015	0.018	0.181	0.133	0.196	0.007	0.009	0.017
20000.0	1.377	0.293	0.365	0.009	0.010	0.211	0.138	0.194	0.006	0.007	0.020
30000.0	1.304	0.198	0.239	0.004	0.004	0.259	0.142	0.184	0.004	0.004	0.025
40000.0	1.225	0.147	0.173	0.002	0.002	0.297	0.141	0.173	0.003	0.003	0.028
50000.0	1.152	0.116	0.134	0.001	0.002	0.327	0.138	0.163	0.002	0.002	0.031
60000.0	1.088	0.095	0.108	0.001	0.001	0.351	0.135	0.154	0.002	0.002	0.033
67416.4	1.045	0.084	0.094	0.001	0.001	0.367	0.133	0.148	0.002	0.002	0.035
67416.4	0.203	0.016	0.018	0.000	0.000	0.071	0.026	0.029	0.000	0.000	0.007
80000.0	0.186	0.013	0.014	0.000	0.000	0.074	0.025	0.026	0.000	0.000	0.007
100000.0	0.164	0.010	0.011	0.000	0.000	0.076	0.023	0.023	0.000	0.000	0.007
150000.0	0.133	0.006	0.006	0.000	0.000	0.081	0.020	0.019	0.000	0.000	0.008
200000.0	0.116	0.005	0.005	0.000	0.000	0.084	0.019	0.017	0.000	0.000	0.008
300000.0	0.098	0.003	0.003	0.000	0.000	0.087	0.017	0.014	0.000	0.000	0.008
400000.0	0.088	0.002	0.003	0.000	0.000	0.090	0.016	0.013	0.000	0.000	0.008
500000.0	0.082	0.002	0.002	0.000	0.000	0.091	0.016	0.012	0.000	0.000	0.009
600000.0	0.078	0.002	0.002	0.000	0.000	0.091	0.015	0.011	0.000	0.000	0.009
800000.0	0.073	0.001	0.002	0.000	0.000	0.092	0.014	0.010	0.000	0.000	0.009
1000000.0	0.070	0.001	0.002	0.000	0.000	0.092	0.014	0.010	0.000	0.000	0.009

Table 8. Ratios of efficiencies for photon-induced electron emission calculated with XITRAN1 under three different assumptions about the angular distribution of photo-electrons:

TS: obtained with uranium cross section of Tseng et al [18].
F: obtained with cross section of Fischer [17], (a) for uranium, or (b) for tantalum.
S: obtained assuming a cross section sin2( ).

All results are for 60-keV photons, and and pertain to photo-electrons ejected from the 2S1/2 shell or the 2P1/2 shell of (a) uranium or (b) tantalum.

a) 60-keV photons incident on a 0.0025-cm uranium target

	Electrons from 2S 1/2 shell			Electrons from 2P1/2 shell		
Efficiency ratio	Backward Emission	Forward Emission	Total Emission	Backward Emission	Forward Emission	Total Emission
S/F	1.172	0.867	1.018	1.177	0.865	1.018
TS/F	1.145	0.890	1.017	1.005	1.007	0.987
TS/S	0.977	1.006	0.998	0.830	1.164	0.987

b) 60-keV photons incident on a 0.0025-cm tantalum target

	Electrons from 2S 1/2 shell			Electrons from 2P1/2 shell		
Efficiency ratio	Backward Emission	Forward Emission	Total Emission	Backward Emission	Forwaard Emission	Total Emission
S/F	1.210	0.844	1.003	1.210	0.844	1.003
TS/F	1.180	0.865	1.002	1.016	0.993	1.003
TS/S	0.975	1.025	0.999	0.840	1.176	0.999

Table 9. Typical output file from XITRAN1

Page 1

```
Program XITRAN1, output file XTR1.960
Submit file SUB1.1
Input file ELPREP.073
Input file XAR.073
Input file XSHELL.073
Input file SHELMARK.073
Photo-electrons produced by incident x-rays

     ISEED     IHIST     ISCOR     JSCOR
     11996  10000000     29982     31434

      EPHOT      TBEGAV       TLST      BOUND
  96.000000   39.272927   5.000000   0.041635

       ALBN       TRANN
   0.002998    0.003143

       TTOP       TBOT  JMAX  LMAX
      100.0        5.0    95    36
```

The first seven lines indicate the name of the code that was run, the name of the output file, and the names of the input files. The other quantities listed have the following meaning:

ISEED: random number seed

IHIST: number of photon histories

ISCOR and JSCOR: number of electrons that emerged from target in backward and forward directions, respectively

EPHOT: photon energy, keV

TBEGAV: average initial energy of electrons, keV

TLST: lowest energy to which electrons were followed, keV

BOUND: mass thickness of foil, in g/cm2

ALBN and TRANN: number of electrons emerging from foil in backward and forward directions, per incident photon

TTOP and TBOT: top and bottom energies for the purpose of classifying the emerging electrons with respect to energy, keV

JMAX: number of equal energy intervals in spectrum between TTOP and TBOT

LMAX: number of equal angular intervals (in deg) between 90 and 180 deg in the backward direction, or between 0 and 90 deg in the forward direction

Table 9, continued.

Page 2

T1	T2	ISPEC-Ref	SPEC-Ref	ISPEC-Tra	SPEC-Tra
100.0	99.0	0	0.0000E+00	0	0.0000E+00
99.0	98.0	0	0.0000E+00	0	0.0000E+00
98.0	97.0	0	0.0000E+00	0	0.0000E+00
97.0	96.0	0	0.0000E+00	0	0.0000E+00
96.0	95.0	12	1.2000E-06	24	2.4000E-06
95.0	94.0	31	3.1000E-06	32	3.2000E-06
94.0	93.0	52	5.2000E-06	123	1.2300E-05
93.0	92.0	145	1.4500E-05	169	1.6900E-05
92.0	91.0	115	1.1500E-05	182	1.8200E-05
91.0	90.0	91	9.1000E-06	183	1.8300E-05
90.0	89.0	145	1.4500E-05	168	1.6800E-05
89.0	88.0	127	1.2700E-05	144	1.4400E-05
88.0	87.0	123	1.2300E-05	155	1.5500E-05
87.0	86.0	145	1.4500E-05	175	1.7500E-05
86.0	85.0	192	1.9200E-05	331	3.3100E-05
85.0	84.0	306	3.0600E-05	540	5.4000E-05
84.0	83.0	558	5.5800E-05	780	7.8000E-05
83.0	82.0	566	5.6600E-05	687	6.8700E-05
82.0	81.0	541	5.4100E-05	730	7.3000E-05
81.0	80.0	593	5.9300E-05	618	6.1800E-05
80.0	79.0	538	5.3800E-05	585	5.8500E-05
79.0	78.0	540	5.4000E-05	592	5.9200E-05
78.0	77.0	525	5.2500E-05	509	5.0900E-05
77.0	76.0	518	5.1800E-05	512	5.1200E-05
76.0	75.0	465	4.6500E-05	467	4.6700E-05
75.0	74.0	450	4.5000E-05	418	4.1800E-05
74.0	73.0	494	4.9400E-05	427	4.2700E-05
73.0	72.0	429	4.2900E-05	426	4.2600E-05
72.0	71.0	406	4.0600E-05	427	4.2700E-05
71.0	70.0	438	4.3800E-05	368	3.6800E-05
70.0	69.0	364	3.6400E-05	371	3.7100E-05
69.0	68.0	368	3.6800E-05	364	3.6400E-05
68.0	67.0	390	3.9000E-05	341	3.4100E-05
67.0	66.0	376	3.7600E-05	310	3.1000E-05
66.0	65.0	365	3.6500E-05	314	3.1400E-05
65.0	64.0	288	2.8800E-05	321	3.2100E-05
64.0	63.0	334	3.3400E-05	305	3.0500E-05
63.0	62.0	292	2.9200E-05	294	2.9400E-05
62.0	61.0	312	3.1200E-05	244	2.4400E-05
61.0	60.0	283	2.8300E-05	257	2.5700E-05

Page 2 pertains to the spectrum of the electrons emitted in the backward and forward directions.

T1 and T2: boundaries of energy spectrum histogram, keV

ISPEC-Ref and ISPEC-Tra: number of electrons in various spectral bins emerging in backward and forward directions, respectively

SPEC-Ref and SPEC-Tra: spectra of electrons spectra in backward and forward directions, per keV and normalized to one incident x-ray photon.

Table 9, continued.

Page 2, continued

T1	T2	ISPEC-Ref	SPEC-Ref	ISPEC-Tra	SPEC-Tra
60.0	59.0	269	2.6900E-05	263	2.6300E-05
59.0	58.0	255	2.5500E-05	242	2.4200E-05
58.0	57.0	269	2.6900E-05	214	2.1400E-05
57.0	56.0	261	2.6100E-05	220	2.2000E-05
56.0	55.0	227	2.2700E-05	204	2.0400E-05
55.0	54.0	221	2.2100E-05	195	1.9500E-05
54.0	53.0	204	2.0400E-05	175	1.7500E-05
53.0	52.0	184	1.8400E-05	173	1.7300E-05
52.0	51.0	191	1.9100E-05	176	1.7600E-05
51.0	50.0	193	1.9300E-05	186	1.8600E-05
50.0	49.0	165	1.6500E-05	156	1.5600E-05
49.0	48.0	166	1.6600E-05	193	1.9300E-05
48.0	47.0	183	1.8300E-05	156	1.5600E-05
47.0	46.0	152	1.5200E-05	141	1.4100E-05
46.0	45.0	172	1.7200E-05	151	1.5100E-05
45.0	44.0	137	1.3700E-05	125	1.2500E-05
44.0	43.0	141	1.4100E-05	129	1.2900E-05
43.0	42.0	154	1.5400E-05	117	1.1700E-05
42.0	41.0	117	1.1700E-05	122	1.2200E-05
41.0	40.0	119	1.1900E-05	103	1.0300E-05
40.0	39.0	123	1.2300E-05	99	9.9000E-06
39.0	38.0	120	1.2000E-05	102	1.0200E-05
38.0	37.0	106	1.0600E-05	103	1.0300E-05
37.0	36.0	114	1.1400E-05	99	9.9000E-06
36.0	35.0	101	1.0100E-05	80	8.0000E-06
35.0	34.0	96	9.6000E-06	78	7.8000E-06
34.0	33.0	68	6.8000E-06	74	7.4000E-06
33.0	32.0	82	8.2000E-06	77	7.7000E-06
32.0	31.0	81	8.1000E-06	56	5.6000E-06
31.0	30.0	82	8.2000E-06	53	5.3000E-06
30.0	29.0	66	6.6000E-06	50	5.0000E-06
29.0	28.0	580	5.8000E-05	1190	1.1900E-04
28.0	27.0	1253	1.2530E-04	1819	1.8190E-04
27.0	26.0	1172	1.1720E-04	1438	1.4380E-04
26.0	25.0	1157	1.1570E-04	1255	1.2550E-04
25.0	24.0	1044	1.0440E-04	1145	1.1450E-04
24.0	23.0	944	9.4400E-05	973	9.7300E-05
23.0	22.0	862	8.6200E-05	848	8.4800E-05
22.0	21.0	799	7.9900E-05	764	7.6400E-05
21.0	20.0	753	7.5300E-05	669	6.6900E-05
20.0	19.0	658	6.5800E-05	584	5.8400E-05
19.0	18.0	590	5.9000E-05	517	5.1700E-05
18.0	17.0	527	5.2700E-05	459	4.5900E-05
17.0	16.0	480	4.8000E-05	401	4.0100E-05
16.0	15.0	402	4.0200E-05	353	3.5300E-05
15.0	14.0	366	3.6600E-05	328	3.2800E-05
14.0	13.0	323	3.2300E-05	291	2.9100E-05
13.0	12.0	288	2.8800E-05	267	2.6700E-05
12.0	11.0	258	2.5800E-05	232	2.3200E-05
11.0	10.0	206	2.0600E-05	168	1.6800E-05
10.0	9.0	173	1.7300E-05	137	1.3700E-05
9.0	8.0	114	1.1400E-05	121	1.2100E-05
8.0	7.0	122	1.2200E-05	118	1.1800E-05
7.0	6.0	103	1.0300E-05	91	9.1000E-06
6.0	5.0	72	7.2000E-06	61	6.1000E-06

Table 9, continued.

Page 3

TH1	TH2	IANGDIS-Ref	ANGDIS-Ref	TH1	TH2	IANGDIS-Tra	ANGDIS-Tra
90.0	92.5	27	9.8515E-06	0.0	2.5	67	1.1204E-03
92.5	95.0	87	3.1804E-05	2.5	5.0	202	1.1267E-03
95.0	97.5	151	5.5412E-05	5.0	7.5	347	1.1627E-03
97.5	100.0	250	9.2270E-05	7.5	10.0	438	1.0503E-03
100.0	102.5	345	1.2832E-04	10.0	12.5	618	1.1556E-03
102.5	105.0	432	1.6224E-04	12.5	15.0	691	1.0605E-03
105.0	107.5	593	2.2532E-04	15.0	17.5	826	1.0768E-03
107.5	110.0	605	2.3306E-04	17.5	20.0	998	1.1326E-03
110.0	112.5	784	3.0686E-04	20.0	22.5	1051	1.0578E-03
112.5	115.0	876	3.4912E-04	22.5	25.0	1153	1.0443E-03
115.0	117.5	955	3.8843E-04	25.0	27.5	1167	9.6250E-04
117.5	120.0	1085	4.5144E-04	27.5	30.0	1235	9.3663E-04
120.0	122.5	1055	4.5016E-04	30.0	32.5	1365	9.5982E-04
122.5	125.0	1142	5.0102E-04	32.5	35.0	1352	8.8772E-04
125.0	127.5	1217	5.5049E-04	35.0	37.5	1423	8.7786E-04
127.5	130.0	1254	5.8655E-04	37.5	40.0	1458	8.4972E-04
130.0	132.5	1354	6.5695E-04	40.0	42.5	1457	8.0609E-04
132.5	135.0	1356	6.8476E-04	42.5	45.0	1504	7.9339E-04
135.0	137.5	1375	7.2534E-04	45.0	47.5	1403	7.0850E-04
137.5	140.0	1339	7.4081E-04	47.5	50.0	1464	7.1032E-04
140.0	142.5	1378	8.0309E-04	50.0	52.5	1323	6.1882E-04
142.5	145.0	1341	8.2728E-04	52.5	55.0	1333	6.0297E-04
145.0	147.5	1278	8.3913E-04	55.0	57.5	1247	5.4709E-04
147.5	150.0	1250	8.7896E-04	57.5	60.0	1106	4.7192E-04
150.0	152.5	1202	9.1161E-04	60.0	62.5	1061	4.4146E-04
152.5	155.0	1174	9.6828E-04	62.5	65.0	1018	4.1405E-04
155.0	157.5	1038	9.4016E-04	65.0	67.5	847	3.3756E-04
157.5	160.0	1050	1.0568E-03	67.5	70.0	749	2.9316E-04
160.0	162.5	865	9.8165E-04	70.0	72.5	645	2.4847E-04
162.5	165.0	775	1.0103E-03	72.5	75.0	569	2.1620E-04
165.0	167.5	737	1.1311E-03	75.0	77.5	439	1.6487E-04
167.5	170.0	569	1.0639E-03	77.5	80.0	340	1.2646E-04
170.0	172.5	444	1.0647E-03	80.0	82.5	271	1.0002E-04
172.5	175.0	329	1.1024E-03	82.5	85.0	147	5.3944E-05
175.0	177.5	203	1.1322E-03	85.0	87.5	96	3.5095E-05
177.5	180.0	67	1.1204E-03	87.5	90.0	24	8.7569E-06

Page 3 pertains to the angular distribution of the emitted electrons integrated over spectral energies down to 5 keV.

TH1 and TH2: limits of the angular histogram bins, deg

IANGDIS-Ref and IANGDIS-Tra: number of electrons in various histogram bins emitted in the backward and forward directions

ANGDIS-Ref and ANGDIS-Tra: angular distributions of electrons emitted in backward and forward directions, per stereadian, normalized to one incident x-ray photon

The remainder of the output file pertains to the joint energy-angular distributions of the electrons emitted in the backward and forward directions.

Table 10. Backward and forward efficiencies for incident monoenergetic photon beams, calculated with Fischer's photo-electron angular distribution for all shells.

EPHOT: photon energy, keV
ALBN: number of electrons emitted in backward direction per photon incident on target
TRANN: number of electrons emitted in forward direction per photon incident on target
TRANC: number of electrons emitted in forward direction per photon leaving the target
ATT: photon attenuation coefficient, cm2/g
RATIO: (TRANC/TRANN)*exp(ATT*BOUND), where BOUND is the target thickness, g/cm2

a. Contribution from photo-electrons resulting from the absorption of the incident x rays. Calculated with XITRAN1.

EPHOT	ALBN	TRANN	TRANC	ATT	RATIO
96.000	0.002792	0.003363	0.004070	4.580500	1.210107
94.000	0.002753	0.003267	0.003996	4.835600	1.223029
92.000	0.002691	0.003196	0.003954	5.110800	1.237123
90.000	0.002660	0.003075	0.003852	5.408000	1.252525
88.000	0.002633	0.002975	0.003777	5.730000	1.269431
86.000	0.002552	0.002901	0.003737	6.079400	1.288032
84.000	0.002521	0.002826	0.003698	6.459600	1.308584
82.000	0.002456	0.002721	0.003623	6.874500	1.331385
80.000	0.002372	0.002608	0.003538	7.328400	1.356785
78.000	0.002323	0.002474	0.003427	7.826400	1.385211
76.000	0.002263	0.002394	0.003393	8.374100	1.417161
74.000	0.002153	0.002251	0.003271	8.977700	1.453227
72.000	0.002078	0.002146	0.003206	9.644500	1.494137
70.000	0.002159	0.002130	0.003282	10.383000	1.540791
68.500	0.002164	0.002083	0.003291	10.989000	1.580161
67.500	0.002269	0.002110	0.003395	11.421000	1.608840
66.500	0.002287	0.003058	0.003379	2.396300	1.104917
65.500	0.002327	0.003082	0.003419	2.495400	1.109485
64.000	0.002368	0.003152	0.003520	2.654900	1.116877
62.000	0.002450	0.003166	0.003571	2.890500	1.127887
60.500	0.002513	0.003233	0.003676	3.086800	1.137143
59.500	0.002539	0.003239	0.003705	3.228200	1.143857
58.500	0.002600	0.003303	0.003802	3.378900	1.151057
57.500	0.002636	0.003315	0.003841	3.539700	1.158789
56.000	0.002720	0.003367	0.003944	3.801500	1.171489
54.000	0.002813	0.003396	0.004044	4.194500	1.190815
52.000	0.002908	0.003397	0.004122	4.646200	1.213422
50.000	0.003001	0.003422	0.004244	5.167900	1.240067
48.000	0.003086	0.003454	0.004393	5.773600	1.271737
46.000	0.003227	0.003499	0.004583	6.481100	1.309756
44.000	0.003375	0.003440	0.004664	7.313300	1.355932
42.000	0.003498	0.003451	0.004875	8.299200	1.412749
40.000	0.003615	0.003371	0.005002	9.476800	1.483741
38.000	0.003749	0.003297	0.005190	10.896000	1.574055
36.000	0.003898	0.003170	0.005361	12.621000	1.691263
34.000	0.004056	0.002996	0.005535	14.742000	1.847407
32.000	0.004205	0.002789	0.005750	17.375999	2.061533
30.000	0.004336	0.002453	0.005805	20.691000	2.366637
32.000	0.004167	0.002766	0.005702	17.375999	2.061533
26.000	0.004571	0.001700	0.006031	30.413000	3.547508
24.000	0.004666	0.001264	0.006070	37.688000	4.802516
22.000	0.004680	0.000852	0.006172	47.561001	7.244208
20.000	0.004561	0.000453	0.005825	61.342999	12.858637

Table 10, continued

b. Contribution from photo-electrons resulting from the absorption of secondary fluorescence radiation produced in the target by incident x rays. Calculated with XITRAN2.

EPHOT	ALBN	TRANN	TRANC	ATT	RATIO
EPHOT	ALBN	TRANN	TRANC	ATT	RATIO
96.000	0.000544	0.000520	0.000629	4.580500	1.210107
94.000	0.000561	0.000544	0.000665	4.835600	1.223029
92.000	0.000597	0.000572	0.000708	5.110800	1.237123
90.000	0.000618	0.000586	0.000734	5.408000	1.252526
88.000	0.000663	0.000623	0.000791	5.730000	1.269431
86.000	0.000705	0.000659	0.000849	6.079400	1.288032
84.000	0.000740	0.000700	0.000916	6.459600	1.308584
82.000	0.000777	0.000738	0.000983	6.874500	1.331385
80.000	0.000830	0.000775	0.001052	7.328400	1.356785
78.000	0.000869	0.000809	0.001121	7.826400	1.385211
76.000	0.000932	0.000865	0.001226	8.374100	1.417161
74.000	0.000988	0.000920	0.001337	8.977700	1.453227
72.000	0.001064	0.000951	0.001421	9.644500	1.494137
70.000	0.001112	0.001019	0.001570	10.383000	1.540791
68.500	0.001169	0.001055	0.001667	10.989000	1.580161
67.500	0.001214	0.001079	0.001736	11.421000	1.608840
66.500	0.000005	0.000005	0.000006	2.396300	1.104917
65.500	0.000004	0.000004	0.000004	2.495400	1.109485
64.000	0.000005	0.000005	0.000006	2.654900	1.116877
62.000	0.000005	0.000005	0.000006	2.890500	1.127887
60.500	0.000006	0.000006	0.000007	3.086800	1.137143
59.500	0.000006	0.000005	0.000006	3.228200	1.143857
58.500	0.000008	0.000005	0.000006	3.378900	1.151057
57.500	0.000006	0.000007	0.000008	3.539700	1.158789
56.000	0.000007	0.000005	0.000006	3.801500	1.171489
54.000	0.000007	0.000006	0.000007	4.194500	1.190815
52.000	0.000009	0.000006	0.000007	4.646200	1.213422
50.000	0.000010	0.000008	0.000010	5.167900	1.240067
48.000	0.000012	0.000010	0.000013	5.773600	1.271737
46.000	0.000016	0.000010	0.000013	6.481100	1.309756
44.000	0.000015	0.000010	0.000014	7.313300	1.355932
42.000	0.000015	0.000013	0.000018	8.299200	1.412749
40.000	0.000019	0.000016	0.000024	9.476800	1.483741
38.000	0.000023	0.000015	0.000024	10.896000	1.574055
36.000	0.000027	0.000017	0.000029	12.621000	1.691263
34.000	0.000030	0.000018	0.000033	14.742000	1.847407
32.000	0.000036	0.000021	0.000043	17.375999	2.061533
30.000	0.000043	0.000021	0.000050	20.691000	2.366637
32.000	0.000036	0.000020	0.000041	17.375999	2.061533
26.000	0.000064	0.000024	0.000085	30.413000	3.547508
24.000	0.000073	0.000022	0.000106	37.688000	4.802516
22.000	0.000099	0.000021	0.000152	47.561001	7.244208
20.000	0.000118	0.000015	0.000193	61.342999	12.858637

Table 10, continued.

c. Contribution from Auger electrons emitted after the absorption of the incident x rays. Calculated with XITRAN3.

EPHOT	ALBN	TRANN	TRANC	ATT	RATIO
96.000	0.000172	0.000141	0.000171	4.580500	1.210107
94.000	0.000183	0.000153	0.000187	4.835600	1.223029
92.000	0.000186	0.000150	0.000186	5.110800	1.237123
90.000	0.000203	0.000158	0.000198	5.408000	1.252526
88.000	0.000222	0.000167	0.000212	5.730000	1.269431
86.000	0.000231	0.000175	0.000225	6.079400	1.288032
84.000	0.000234	0.000186	0.000243	6.459600	1.308584
82.000	0.000255	0.000184	0.000245	6.874500	1.331385
80.000	0.000277	0.000195	0.000265	7.328400	1.356785
78.000	0.000295	0.000212	0.000294	7.826400	1.385211
76.000	0.000311	0.000225	0.000319	8.374100	1.417161
74.000	0.000337	0.000241	0.000350	8.977700	1.453227
72.000	0.000363	0.000243	0.000363	9.644500	1.494137
70.000	0.000383	0.000259	0.000399	10.383000	1.540791
68.500	0.000411	0.000256	0.000405	10.989000	1.580161
67.500	0.000416	0.000259	0.000417	11.421000	1.608840
66.500	0.000018	0.000019	0.000021	2.396300	1.104917
65.500	0.000023	0.000020	0.000022	2.495400	1.109485
64.000	0.000020	0.000021	0.000023	2.654900	1.116877
62.000	0.000026	0.000022	0.000025	2.890500	1.127887
60.500	0.000025	0.000024	0.000027	3.086800	1.137143
59.500	0.000028	0.000023	0.000026	3.228200	1.143857
58.500	0.000030	0.000025	0.000029	3.378900	1.151057
57.500	0.000030	0.000028	0.000032	3.539700	1.158789
56.000	0.000034	0.000030	0.000035	3.801500	1.171489
54.000	0.000039	0.000033	0.000039	4.194500	1.190815
52.000	0.000040	0.000034	0.000041	4.646200	1.213422
50.000	0.000048	0.000037	0.000046	5.167900	1.240067
48.000	0.000057	0.000046	0.000058	5.773600	1.271737
46.000	0.000066	0.000042	0.000055	6.481100	1.309756
44.000	0.000066	0.000049	0.000066	7.313300	1.355932
42.000	0.000082	0.000054	0.000076	8.299200	1.412749
40.000	0.000092	0.000062	0.000092	9.476800	1.483741
38.000	0.000108	0.000067	0.000105	10.896000	1.574055
36.000	0.000132	0.000071	0.000120	12.621000	1.691263
34.000	0.000139	0.000080	0.000148	14.742000	1.847407
32.000	0.000168	0.000079	0.000163	17.375999	2.061533
30.000	0.000196	0.000083	0.000196	20.691000	2.366637
32.000	0.000173	0.000084	0.000173	17.375999	2.061533
26.000	0.000309	0.000087	0.000309	30.413000	3.547508
24.000	0.000384	0.000080	0.000384	37.688000	4.802516
22.000	0.000519	0.000067	0.000485	47.561001	7.244208
20.000	0.000652	0.000057	0.000733	61.342999	12.858637

Table 11. Contributions to efficiency from electrons produced by different processes:

1: Photo-electrons from absorption of x rays
2: Photo-electrons from fluorescence radiation
3: Auger electrons from absorption of x rays

THese results were calculated with XITRAN for Case 2.

100-keV x-ray spectrum

	Efficiency	
	Backward	Forward
1:	0.002926	0.004457
2:	0.000126	0.000194
3:	0.000090	0.000126
Total:	0.003142	0.004777

50-keV x-ray spectrum

	Efficiency	
	Backward	Forward
1:	0.004049	0.005525
2:	0.000038	0.000100
3:	0.000202	0.000330
Total:	0.004288	0.006055

Table 12. Comparison of calculated and experimental efficiencies for x-ray induced electron emission, for a 0.0025-cm tantalum foil irradiated with 100-keV or 50-keV x-ray beams incident normally.

Backward Efficiency = number of electrons with energies > 5 keV leaving the foil in the backward direction, divided by the the number of photons entering the foil.

Forward Efficiency = number of electrons with energies > 5 keV leaving the foil in the forward direction, divided by the number of photon leaving the foil.

XITRAN: Single-scattering Monte Carlo code

XMTRAN: Condensed-random-walk Monte Carlo code

The statistical uncertainty of the results from XITRAN and XMTRAN is 1-2%. The systematic error, mainly due to the uncertainty of the photo-electron angular distribution, may be 5 to 10%.

Case 1: Calculated assuming that the photo-electron angular distribution is given by sin2( ) for ejection from 2S1/2, 3S1/2, 4S1/2, 5S1/2 and 6S1/2 shells, and by Fischer's formula for all other shells.

Case 2: Calculated with Fischer's formula for all shells.

CEPXS: Sandia multigroup discrete ordinates code; results from R. Weitz (priv.communication, April 1997)

SANDYL: Condensed-random-walk Monte Carlo code of H.M. Colbert [26]; results quoted by Dolan [1].

QUICKE: Code based on analytical method of MacCallum and Dellin [27]; results quoted by Dolan [1].

Dolan: Experimental results in Report SAND74-8642 [1]; numbers in parenthesis represent Dolan's error estimate.

a) 100-keV X-rays: Dolan's Spectrum # 3 for Backward Emission
Spectrum # 7 for Forward Emission

	Efficiency		Ratio of Calculated to Measured Efficiency	
	Backward	Forward	Backward	Forward
XITRAN, Case 1	0.00339	0.00451	0.94	0.92
XITRAN, Case 2	0.00314	0.00478	0.87	0.98
XMTRAN, Case 1	0.00340	0.00453	0.94	0.92
XMTRAN, Case 2	0.00313	0.00482	0.87	0.98
CEPXS	0.00340	0.00502	0.94	1.02
SANDYL	0.0032(5)	0.0053(4)	0.89	1.08
QUICKE	0.0038	0.0047	1.06	0.96
Dolan, Expt.	0.0036(5)	0.0049(7)		

b) 50-keV X-rays : Dolan's Spectrum # 12 for Backward Emission
Spectrum # 8 for Forward Emission

	Efficiency		Ratio of Calculated to Measured Efficiency	
	Backward	Forward	Backward	Forward
XITRAN, Case 1	0.00452	0.00584	0.85	0.93
XITRAN, Case 2	0.00429	0.00605	0.81	0.96
XMTRAN, Case 1	0.00452	0.00587	0.85	0.93
XMTRAN, Case 2	0.00428	0.00610	0.81	0.97
CEPXS	0.00476	0.00652	0.90	1.03
SANDYL	0.0042(2)	0.0053(4)	0.79	0.84
QUICKE	0.0054	0.0064	1.02	1.02
Dolan, Expt	0.0053(8)	0.0063(9)		

Table 13. Comparisons of x-ray induced electron emission efficiencies obtained with different methods of calculation, for 100-keV and 50-keV x-ray spectra. Comparisons are made in terms of efficiency ratios.

a. Efficiency ratio Case 2/Case 1; indicates dependence on assumed angular distribution of photoelectrons.

	100 keV		50 keV	
	Backward	Forward	Backward	Forward
XITRAN	0.92	1.06	0.95	1.04
XMTRAN	0.92	1.06	0.96	1.04

b. Efficiency ratio XMTRAN/XITRAN; indicates dependence on assumed Monte Carlo model.

	100 keV		50 keV	
	Backward	Forward	Backward	Forward
Case 1	1.003	1.006	1.001	1.004
Case 2	0.997	1.008	0.999	1.008

c. Efficiency ratio CEPXS(Case 2)/XITRAN (Case 2); indicates dependence on method of calculation.

100 keV		50 keV	
Backward	Forward	Backward	Forward
1.08	1.05	1.11	1.08

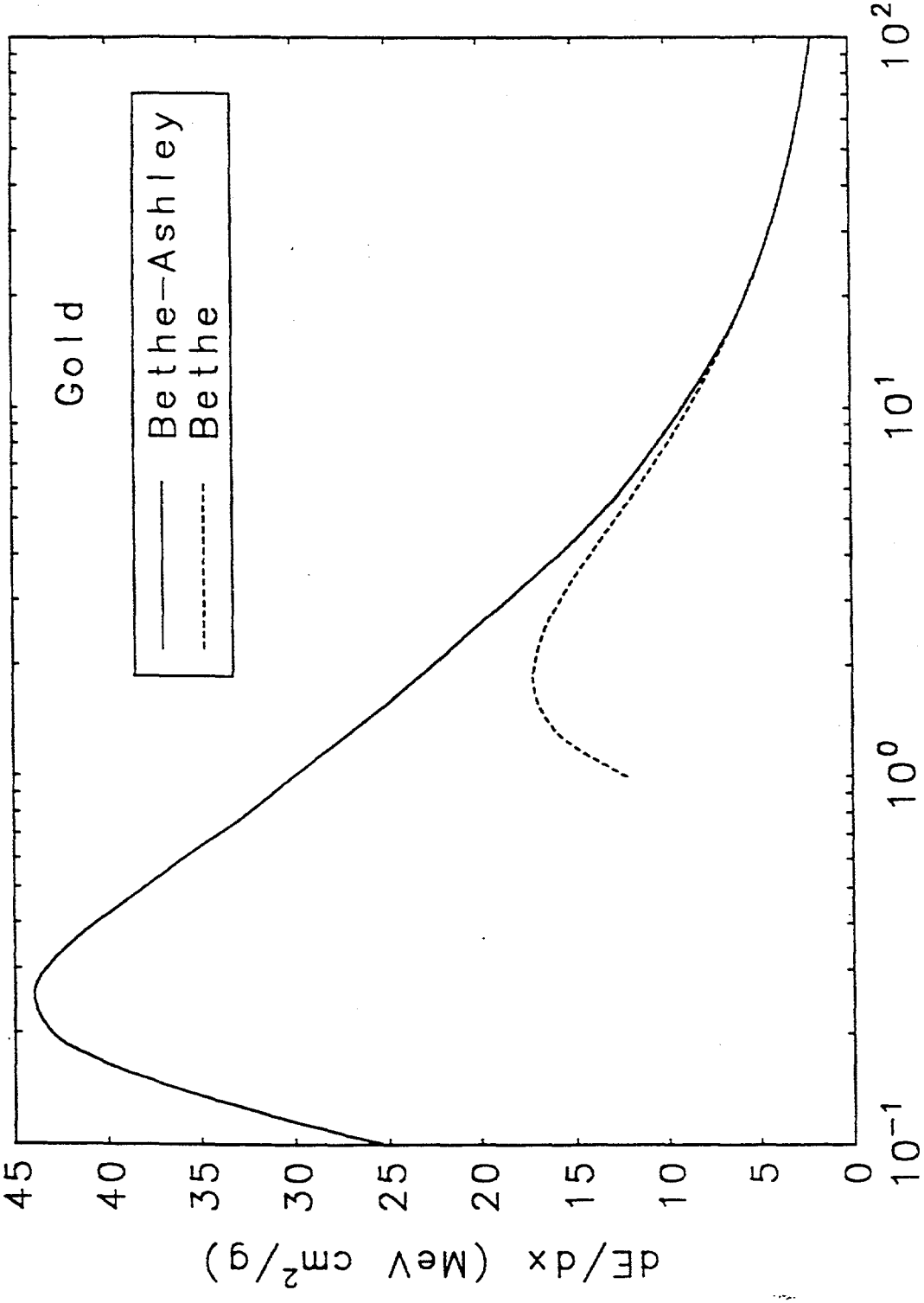
Gold
Bethe–Ashley
Bethe
dE/dx (MeV cm²/g)
T (keV)
0
5
10
15
20
25
30
35
40
45
10⁻¹
10⁰
10¹
10²

Fig.1

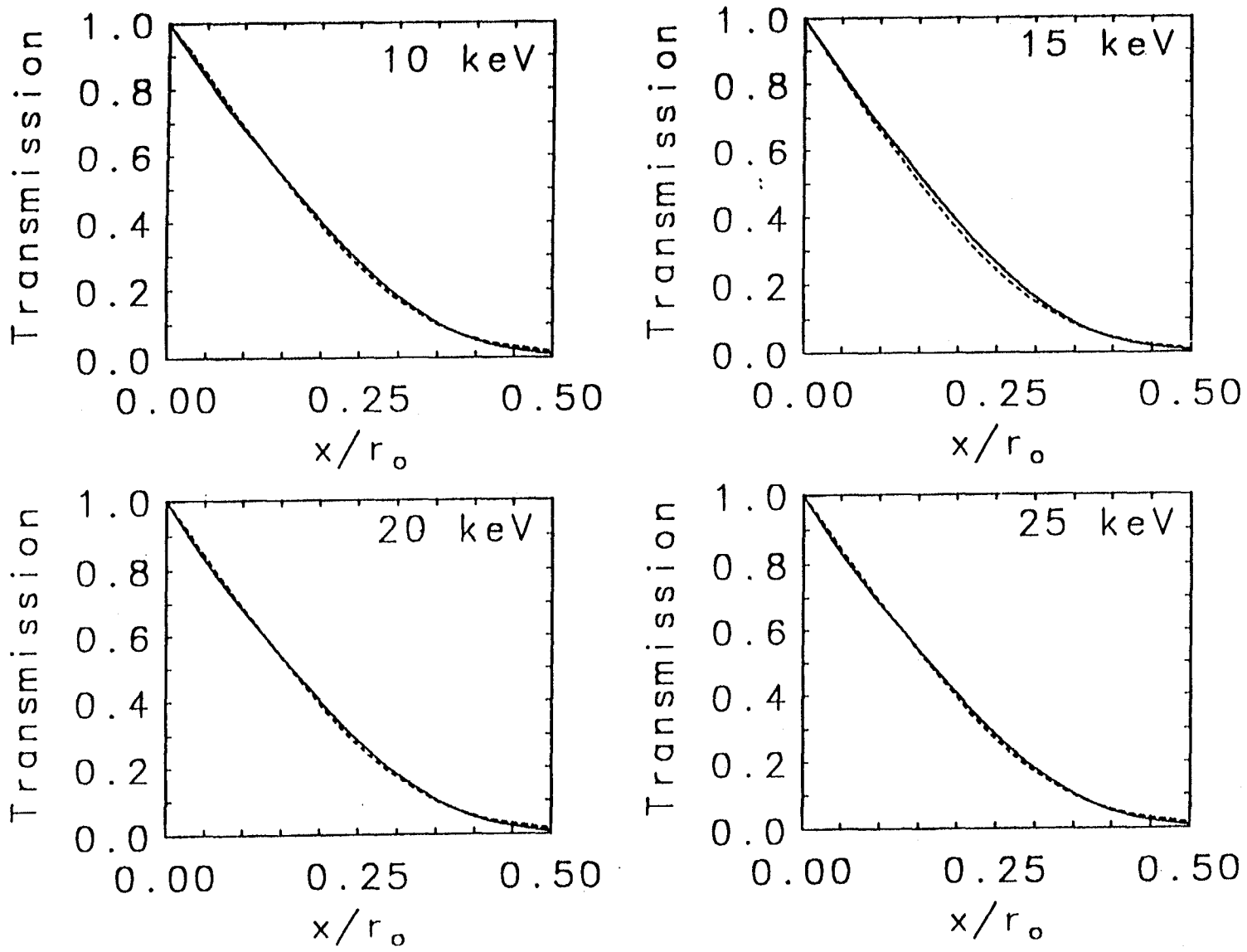
Transmission
1.0
0.8
0.6
0.4
0.2
0.0
10 keV
0.00
0.25
0.50
x/r_o
15 keV
20 keV
25 keV

Fig.2a

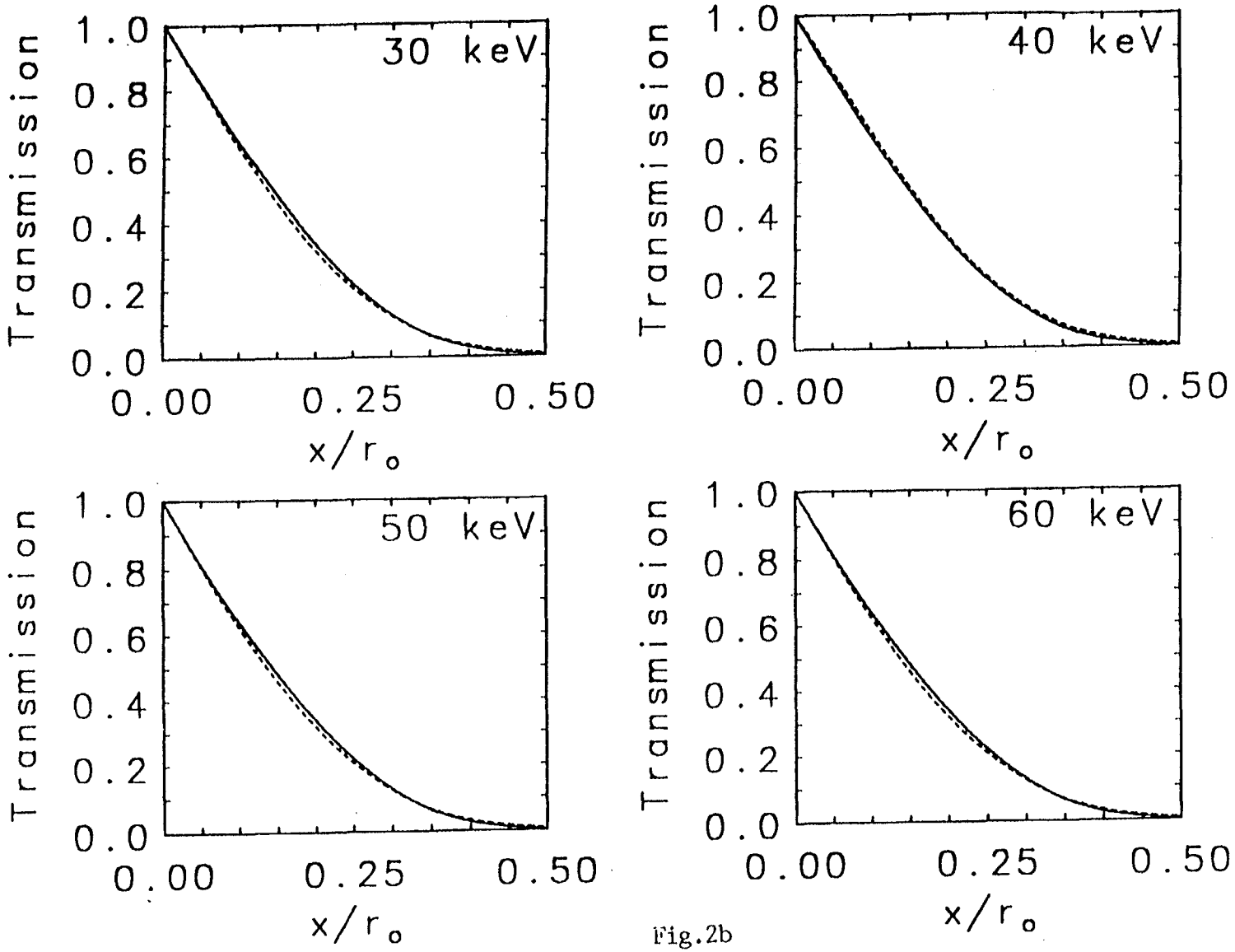
30 keV
40 keV
50 keV
60 keV
Transmission
1.0
0.8
0.6
0.4
0.2
0.0
0.00
0.25
0.50
x/r₀

Fig.2b

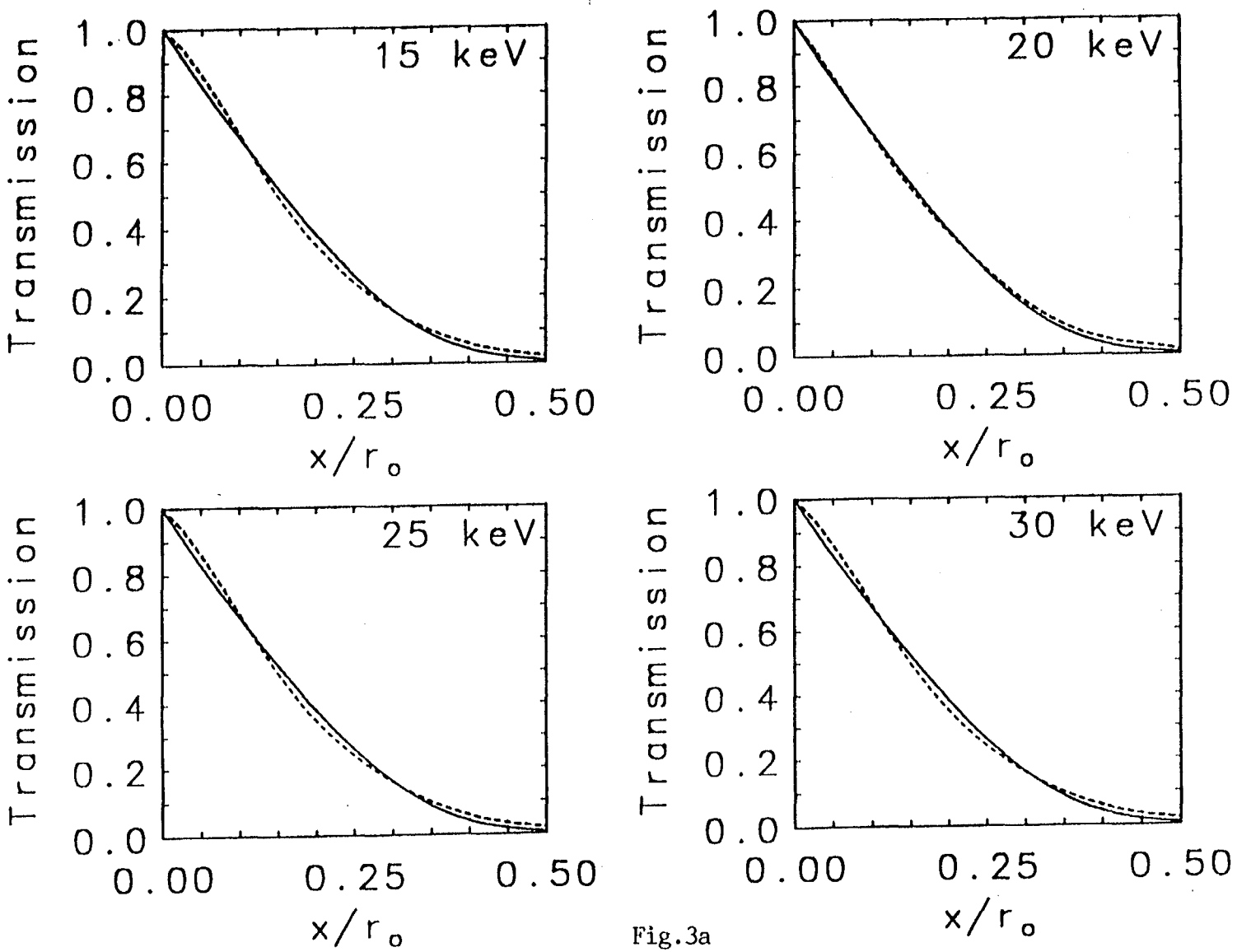
15 keV
20 keV
25 keV
30 keV
Transmission
1.0
0.8
0.6
0.4
0.2
0.0
0.00
0.25
0.50
x/r_o

Fig.3a

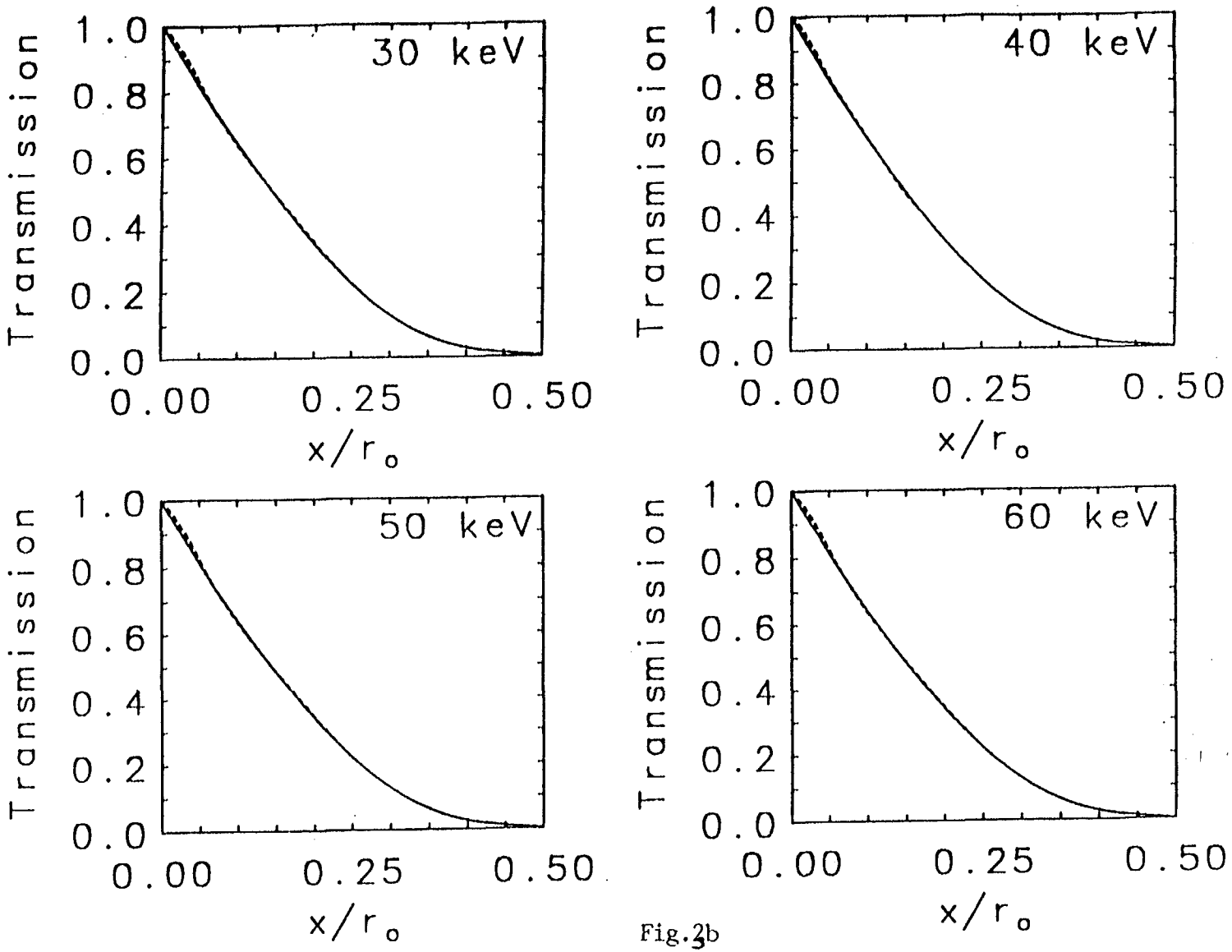
Transmission
1.0
0.8
0.6
0.4
0.2
0.0
30 keV
0.00
0.25
0.50
x/r₀
40 keV
50 keV
60 keV

Fig.2b

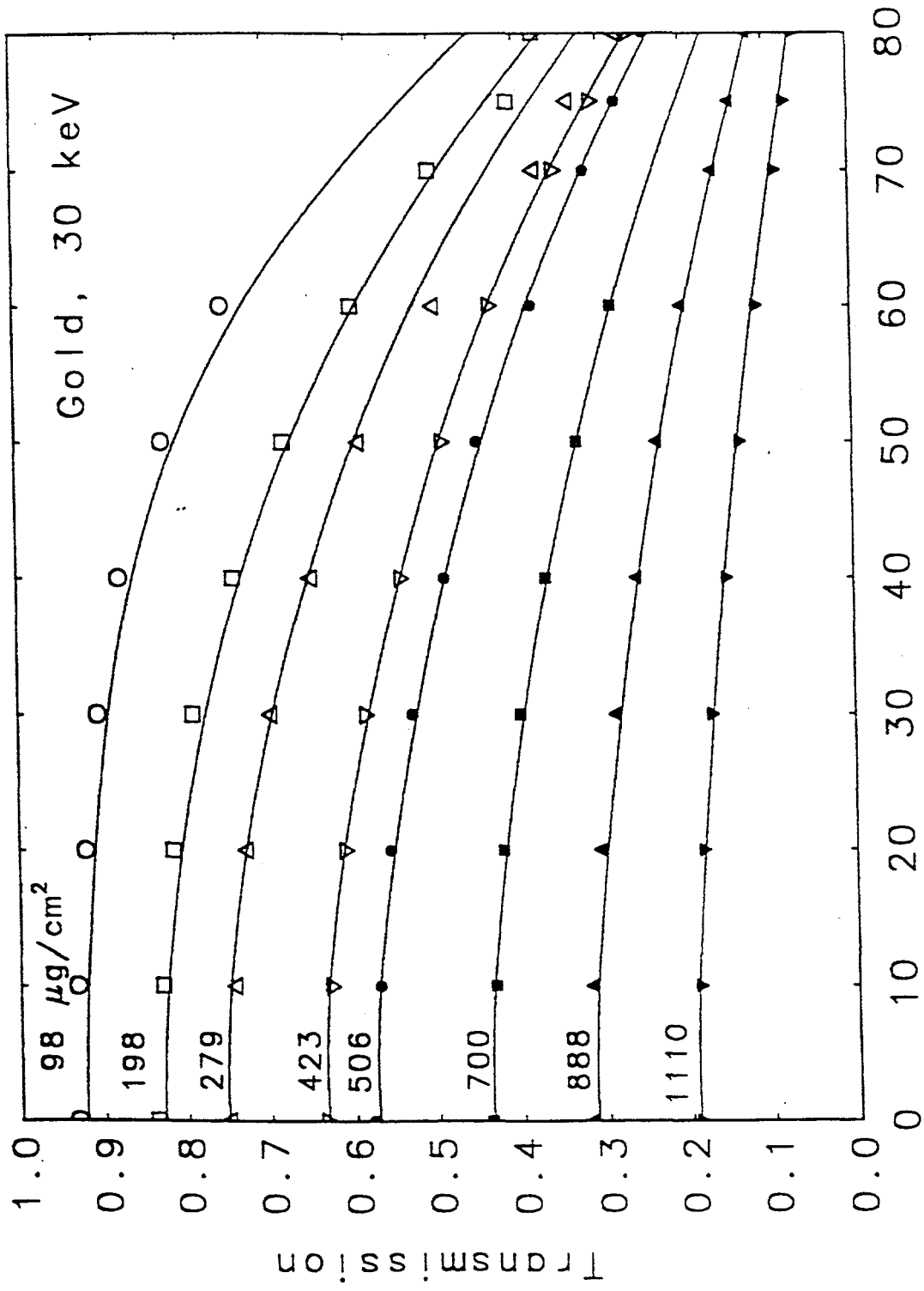
Gold, 30 keV
98 μg/cm²
198
279
423
506
700
888
1110
Transmission
α, deg
0.0
0.1
0.2
0.3
0.4
0.5
0.6
0.7
0.8
0.9
1.0
0
10
20
30
40
50
60
70
80

Fig.4

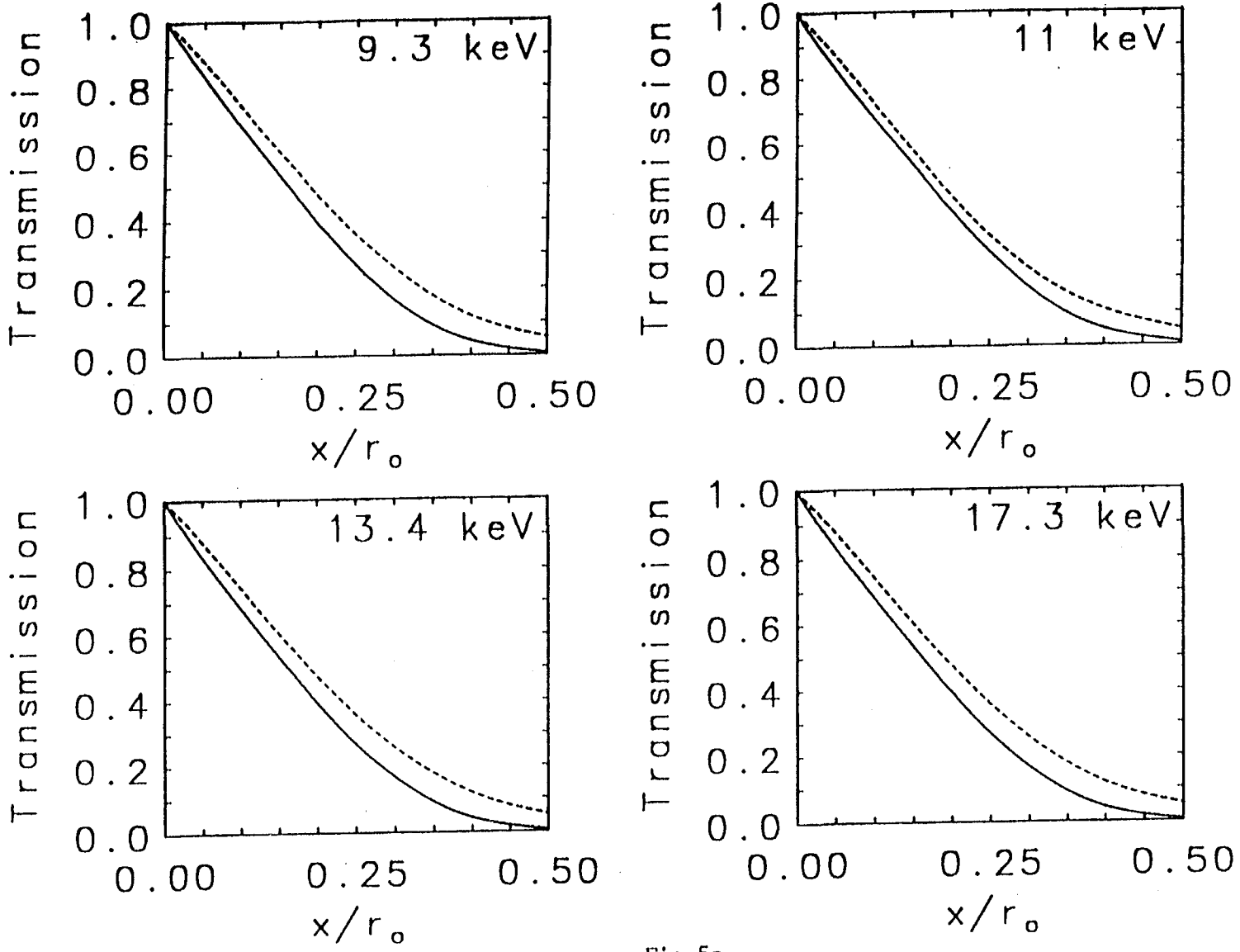
9.3 keV
11 keV
13.4 keV
17.3 keV
Transmission
1.0
0.8
0.6
0.4
0.2
0.0
0.00
0.25
0.50
x/r₀

Fig.5a

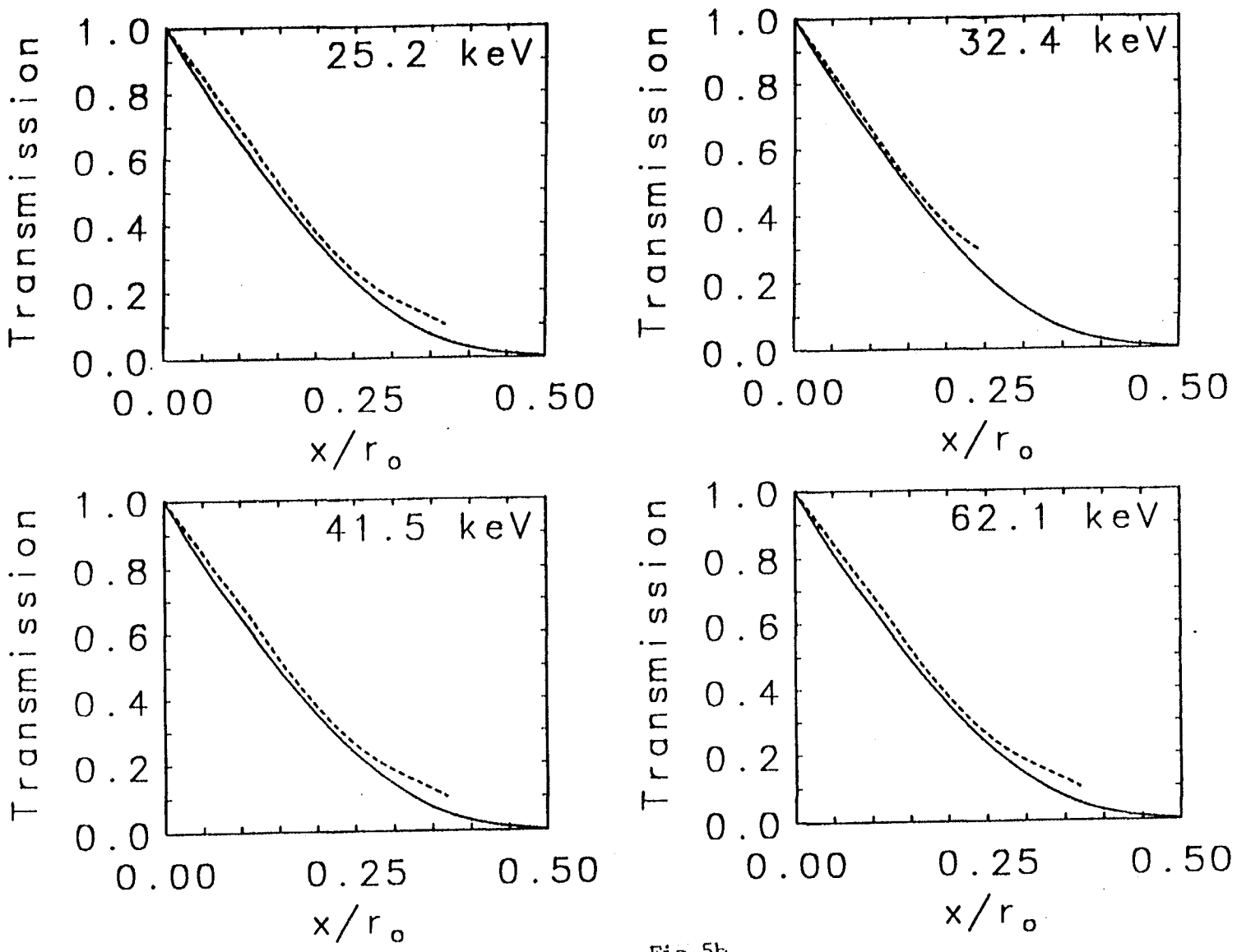
25.2 keV
32.4 keV
41.5 keV
62.1 keV
Transmission
x/r_o
1.0
0.8
0.6
0.4
0.2
0.0
0.00
0.25
0.50

Fig.5b

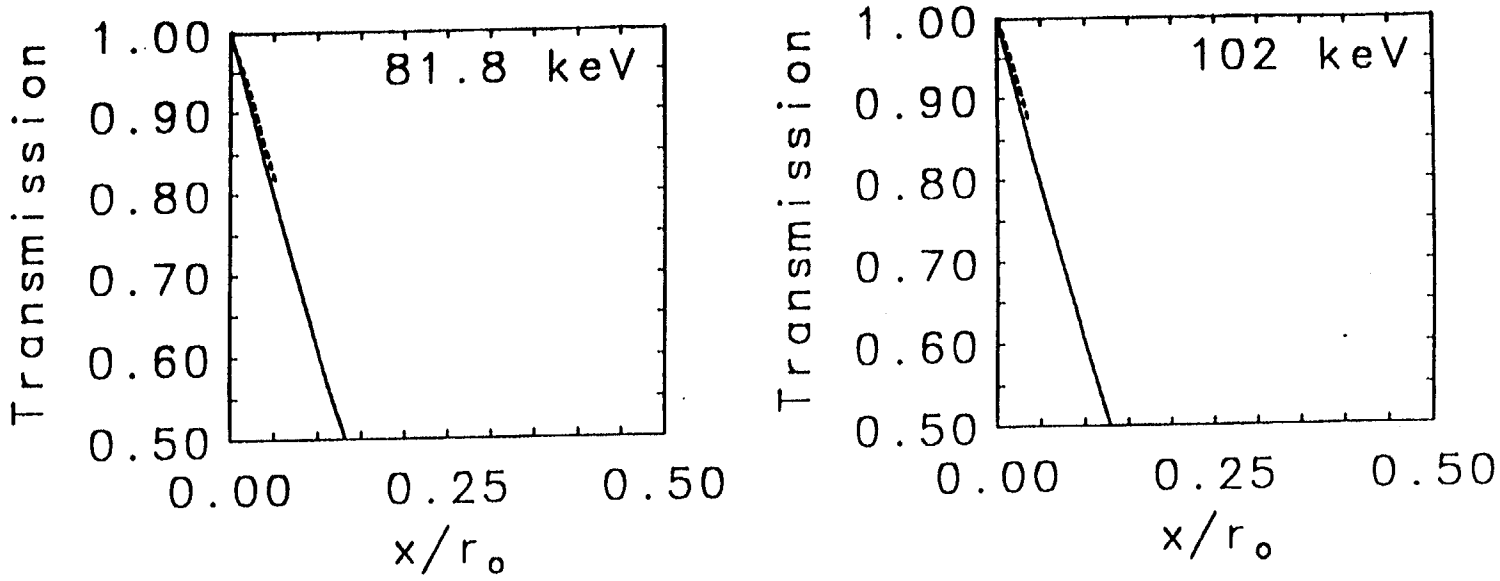
Transmission
1.00
0.90
0.80
0.70
0.60
0.50
81.8 keV
0.00
0.25
0.50
x/r₀
Transmission
1.00
0.90
0.80
0.70
0.60
0.50
102 keV
0.00
0.25
0.50
x/r₀

Fig.5c

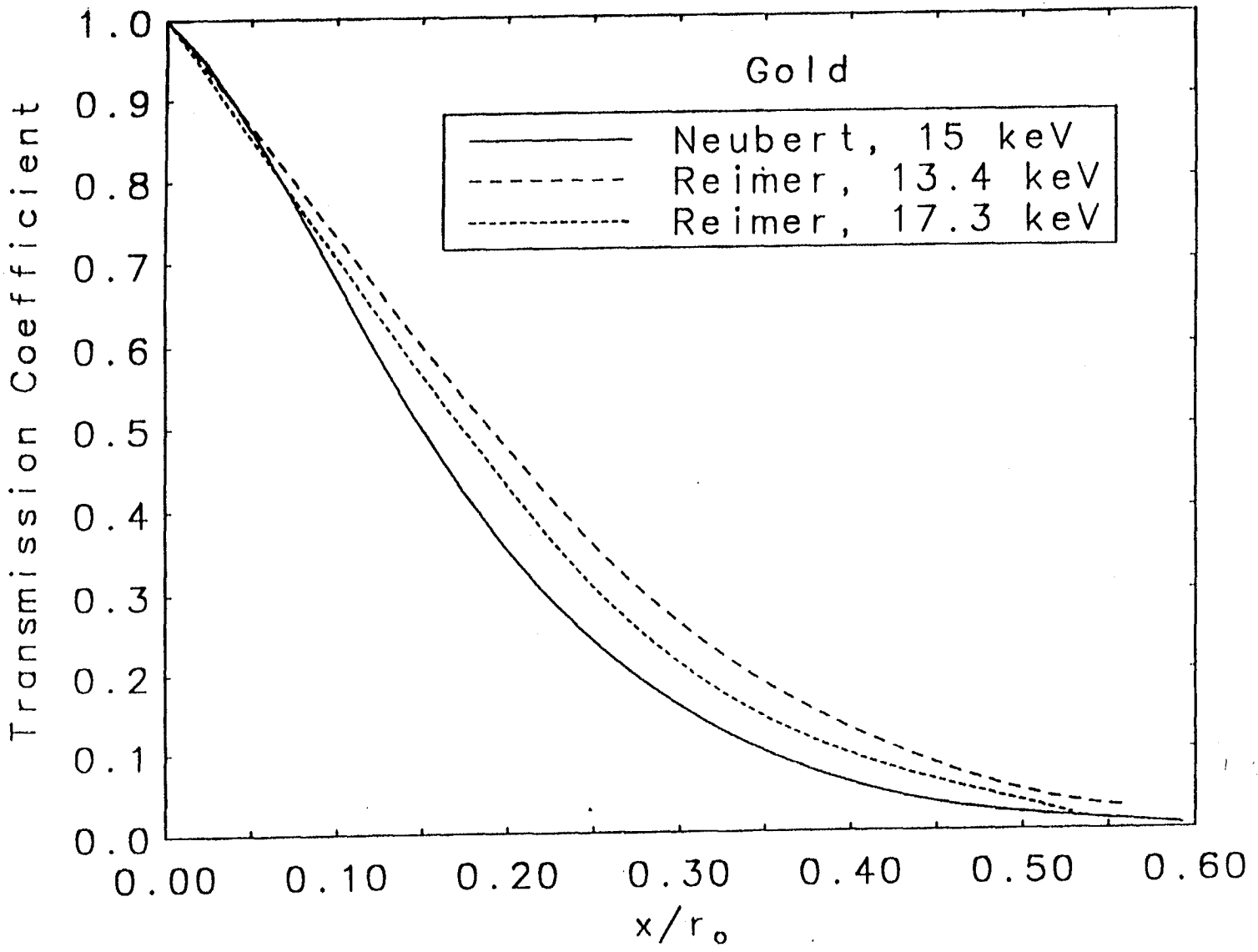
Gold
Neubert, 15 keV
Reimer, 13.4 keV
Reimer, 17.3 keV
Transmission Coefficient
1.0
0.9
0.8
0.7
0.6
0.5
0.4
0.3
0.2
0.1
0.0
0.00
0.10
0.20
0.30
0.40
0.50
0.60
x/r₀

Fig.6

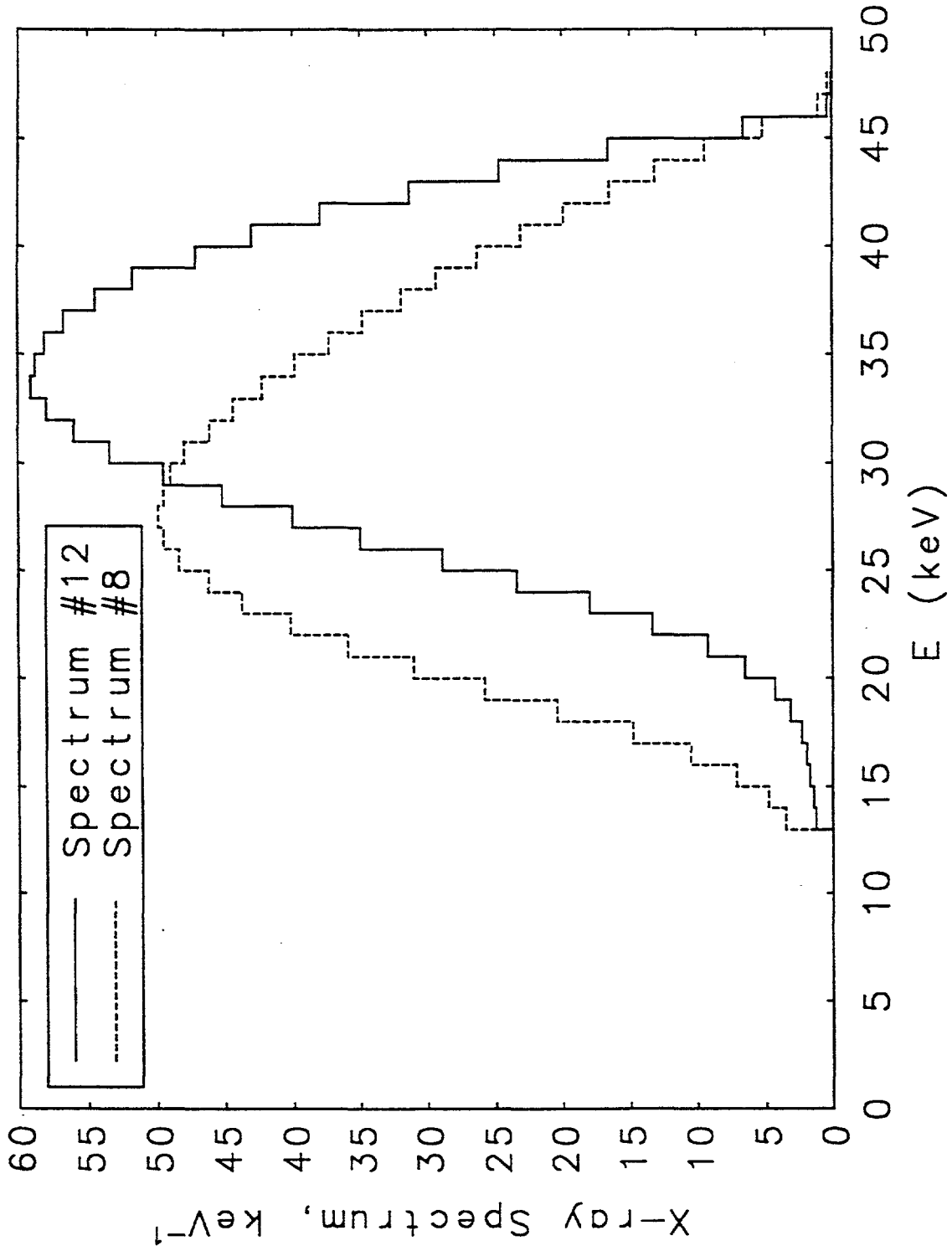
Spectrum #12
Spectrum #8
X-ray Spectrum, keV⁻¹
E (keV)
0
5
10
15
20
25
30
35
40
45
50
55
60

Fig.7a

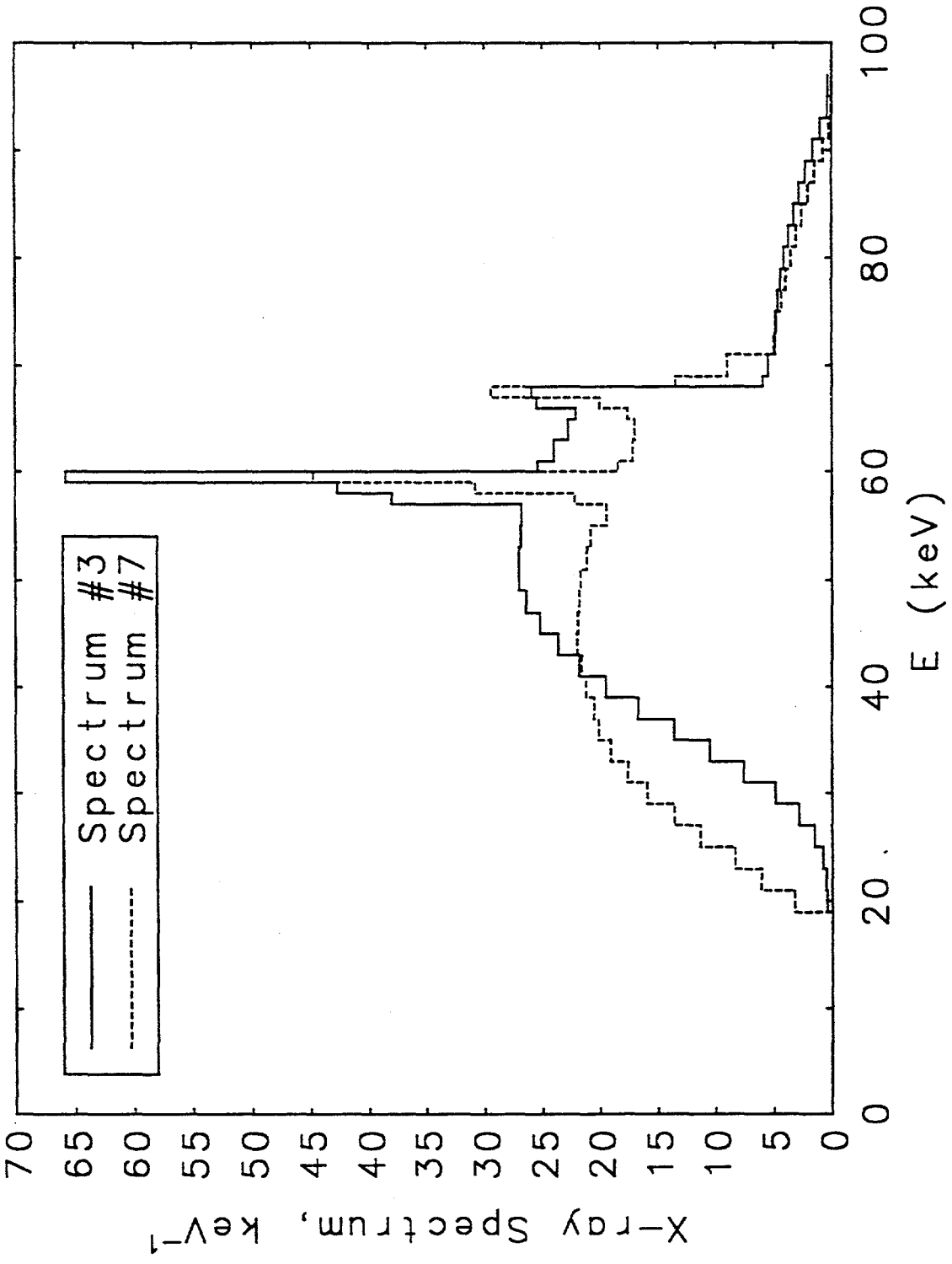
Spectrum #3
Spectrum #7
X-ray Spectrum, keV⁻¹
E (keV)
0
5
10
15
20
25
30
35
40
45
50
55
60
65
70
0
20
40
60
80
100

Fig.7b

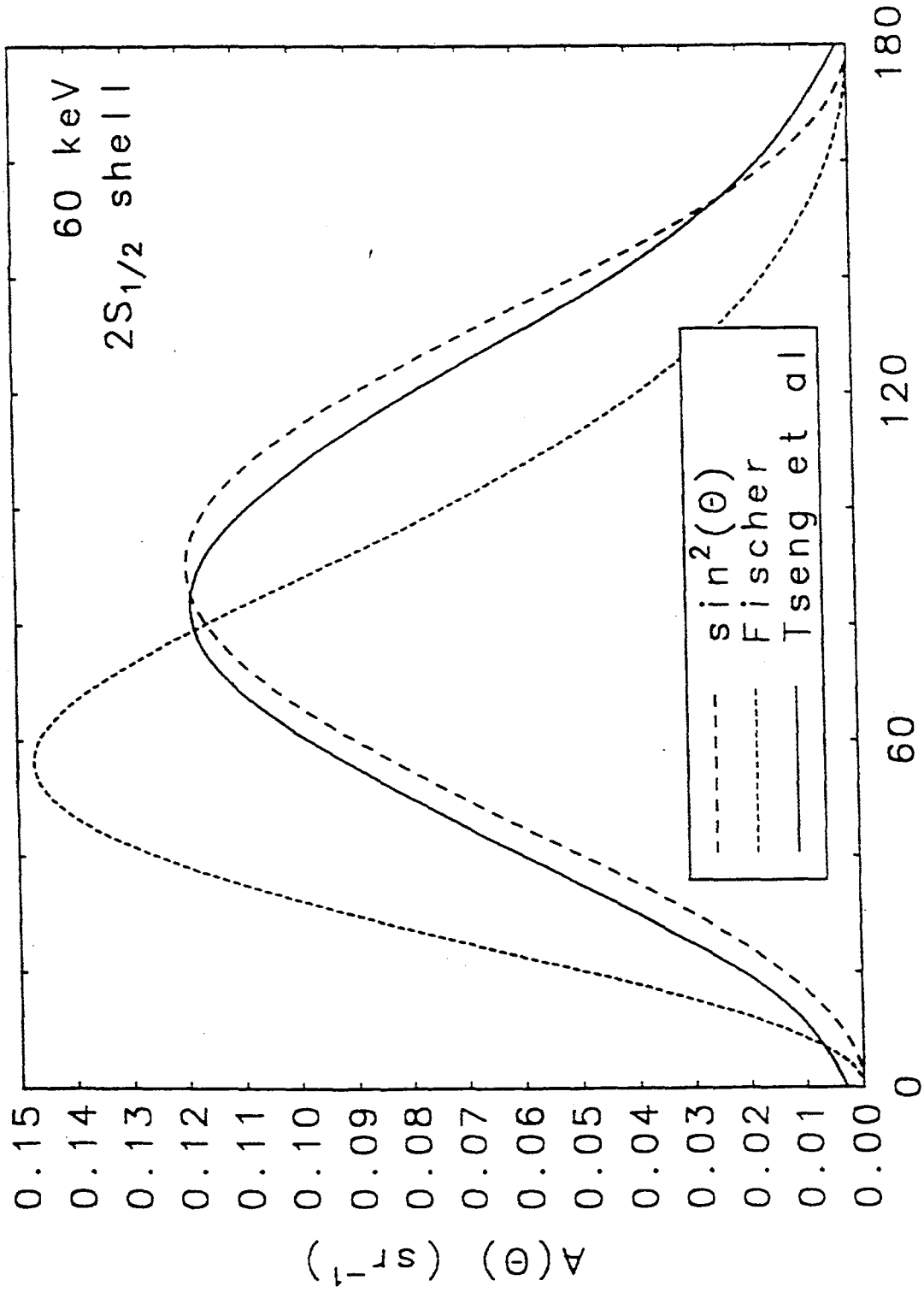
60 keV
2S1/2 shell
sin2(Θ)
Fischer
Tseng et al
A(Θ) (sr-1)
Θ (deg)
0.00
0.01
0.02
0.03
0.04
0.05
0.06
0.07
0.08
0.09
0.10
0.11
0.12
0.13
0.14
0.15
0
60
120
180

Fig.8a

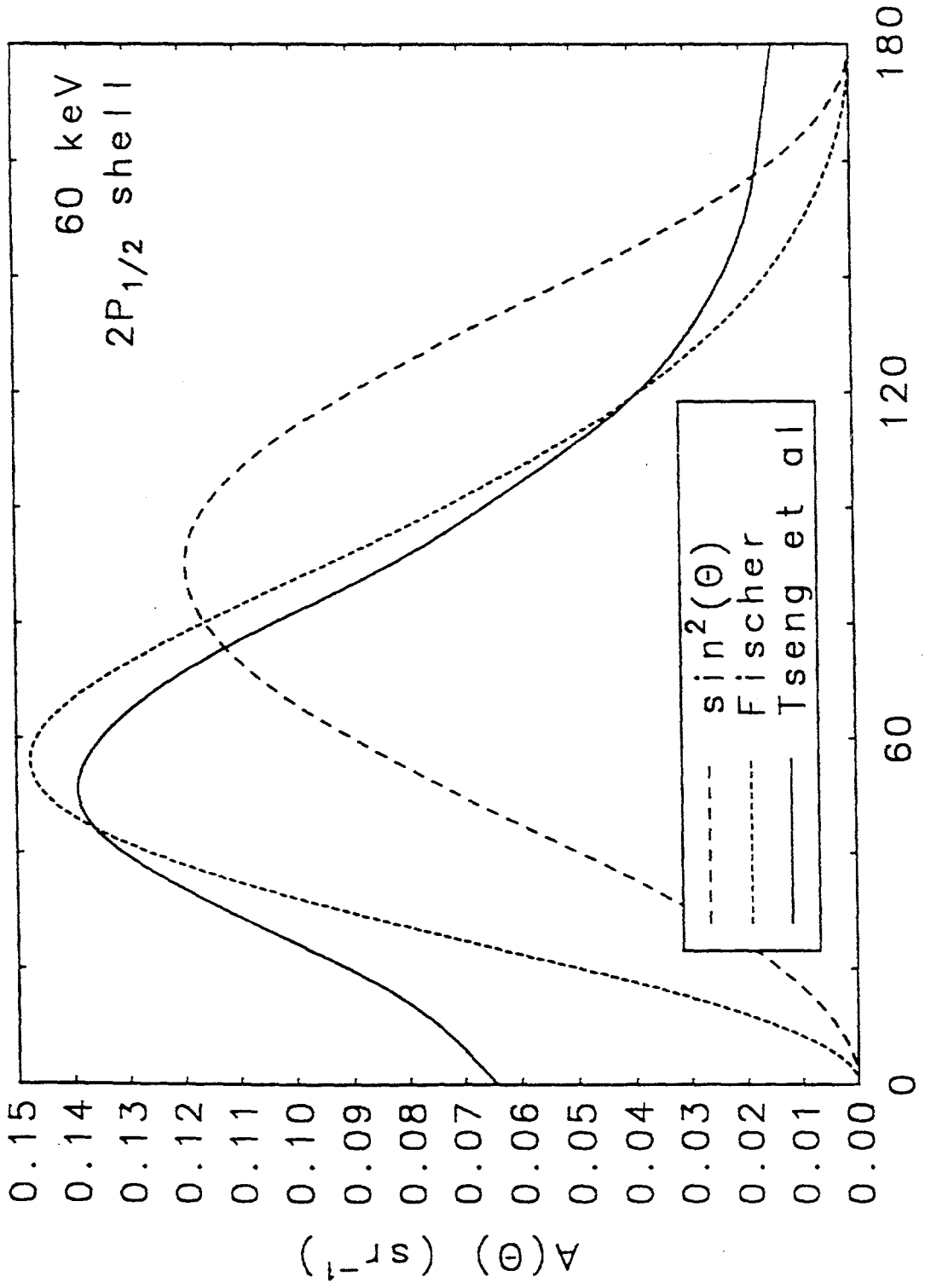
60 keV
2P1/2 shell
sin2(Θ)
Fischer
Tseng et al
A(Θ) (sr-1)
Θ (deg)
0.00
0.01
0.02
0.03
0.04
0.05
0.06
0.07
0.08
0.09
0.10
0.11
0.12
0.13
0.14
0.15
0
60
120
180

Fig.8b

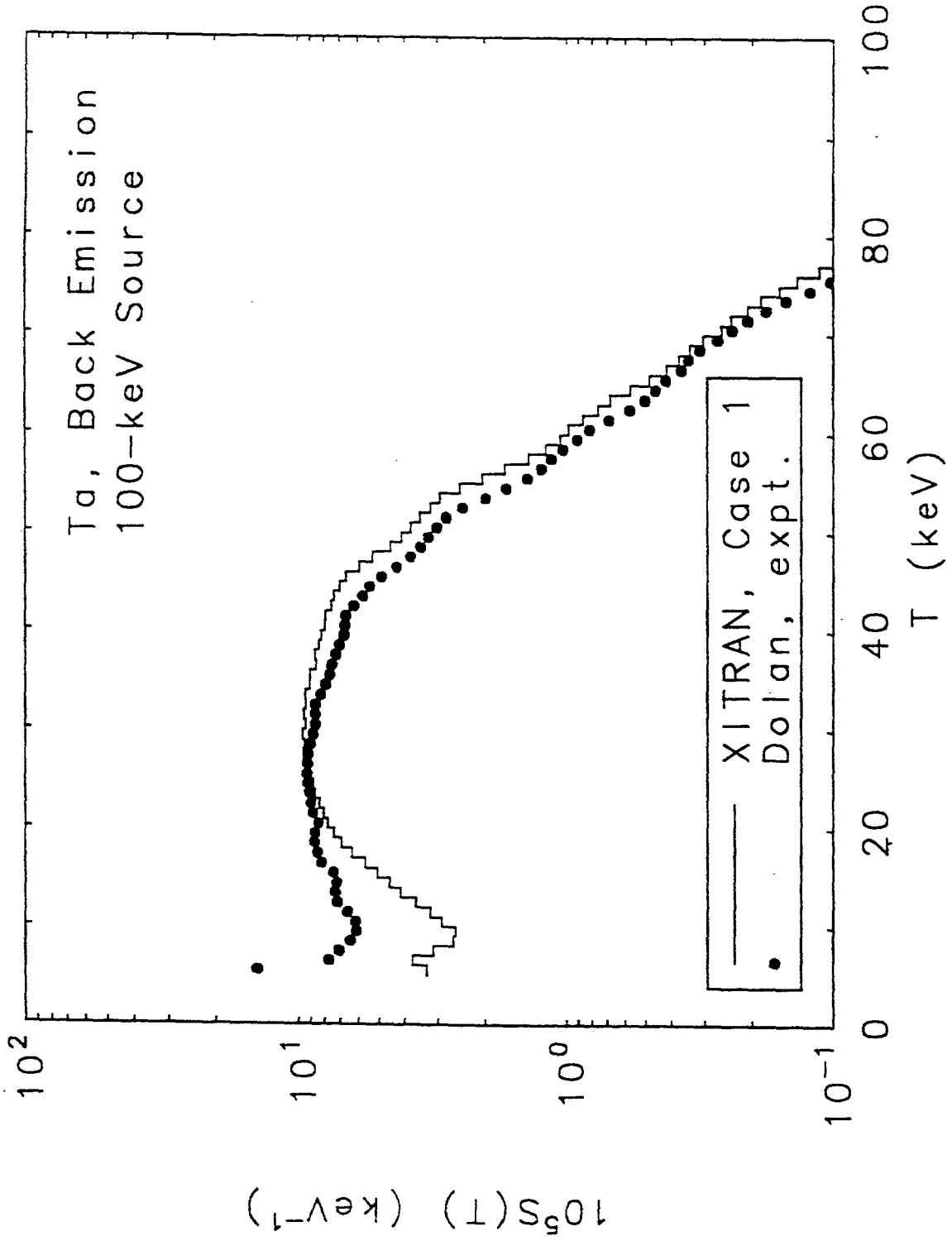
Ta, Back Emission
100-keV Source
XITRAN, Case 1
Dolan, expt.
$10^5 S(T)$ (keV^{-1})
T (keV)
10^2
10^1
10^0
10^{-1}
0
20
40
60
80
100

Fig.9a-1

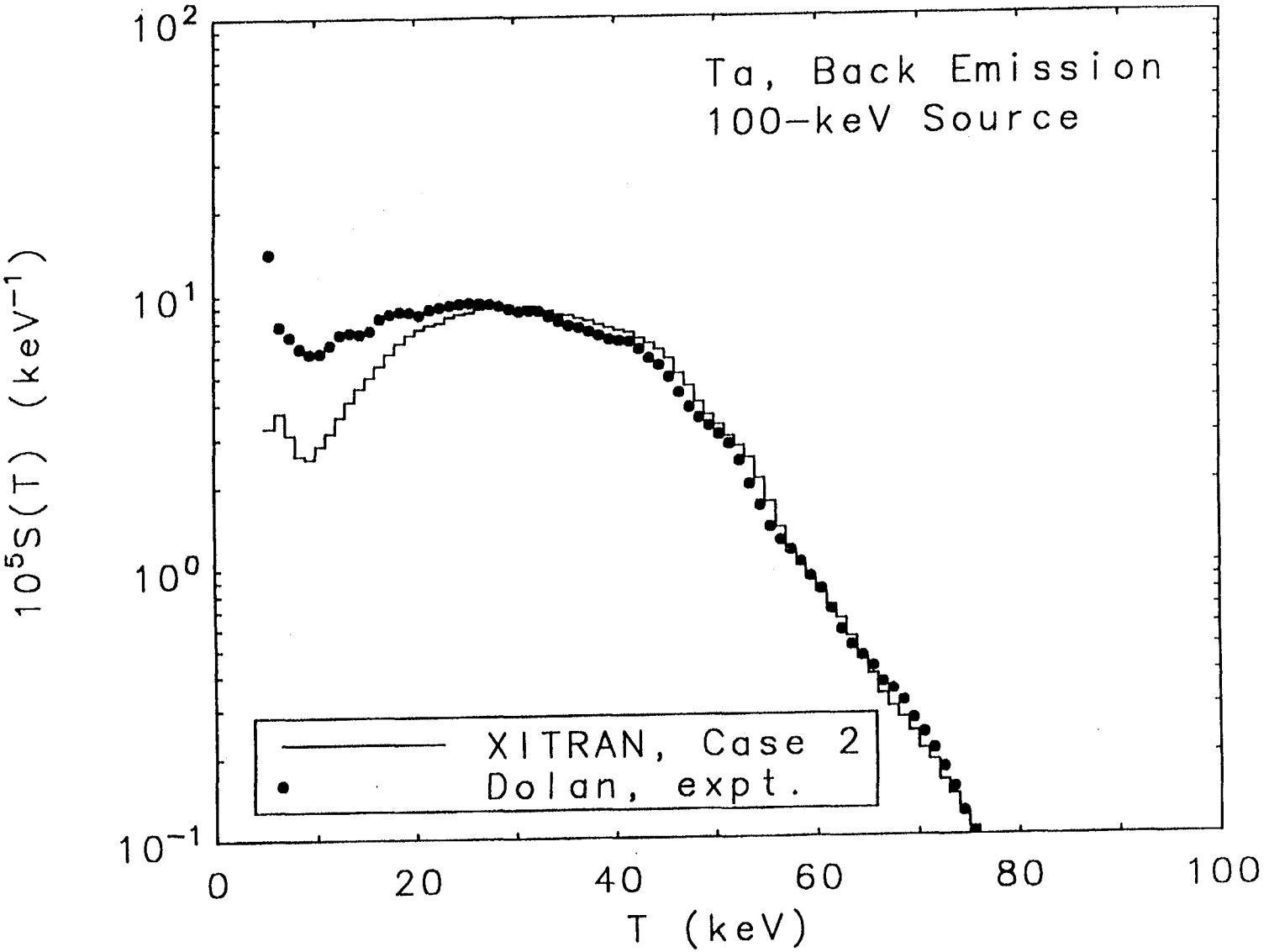
Ta, Back Emission
100-keV Source
XITRAN, Case 2
Dolan, expt.
$10^5 S(T)$ (keV^{-1})
T (keV)
10^2
10^1
10^0
10^{-1}
0
20
40
60
80
100

Fig.9a-2

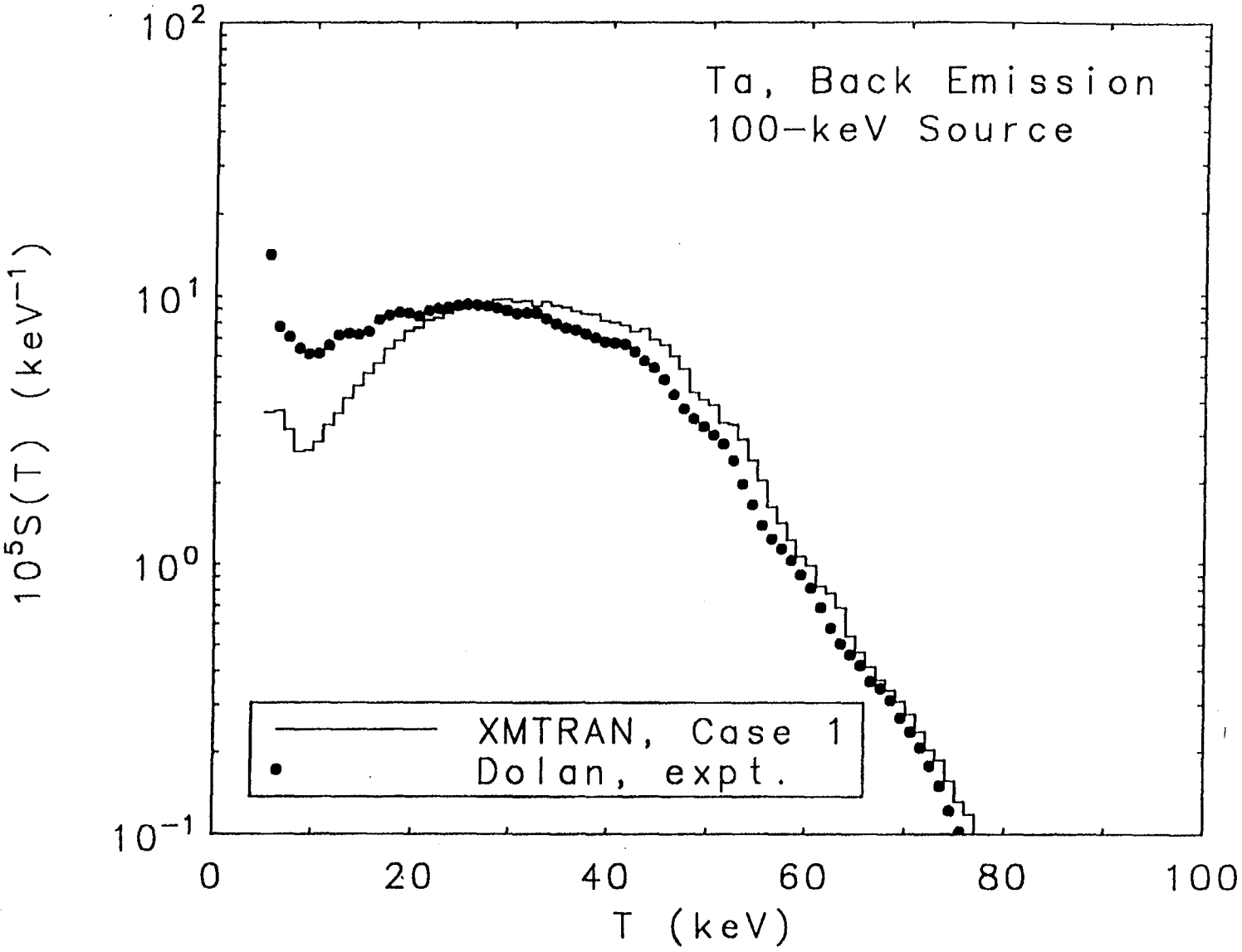
Ta, Back Emission
100-keV Source
XMTRAN, Case 1
Dolan, expt.
$10^5 S(T)$ (keV^{-1})
T (keV)
10^2
10^1
10^0
10^{-1}
0
20
40
60
80
100

Fig.9a-3

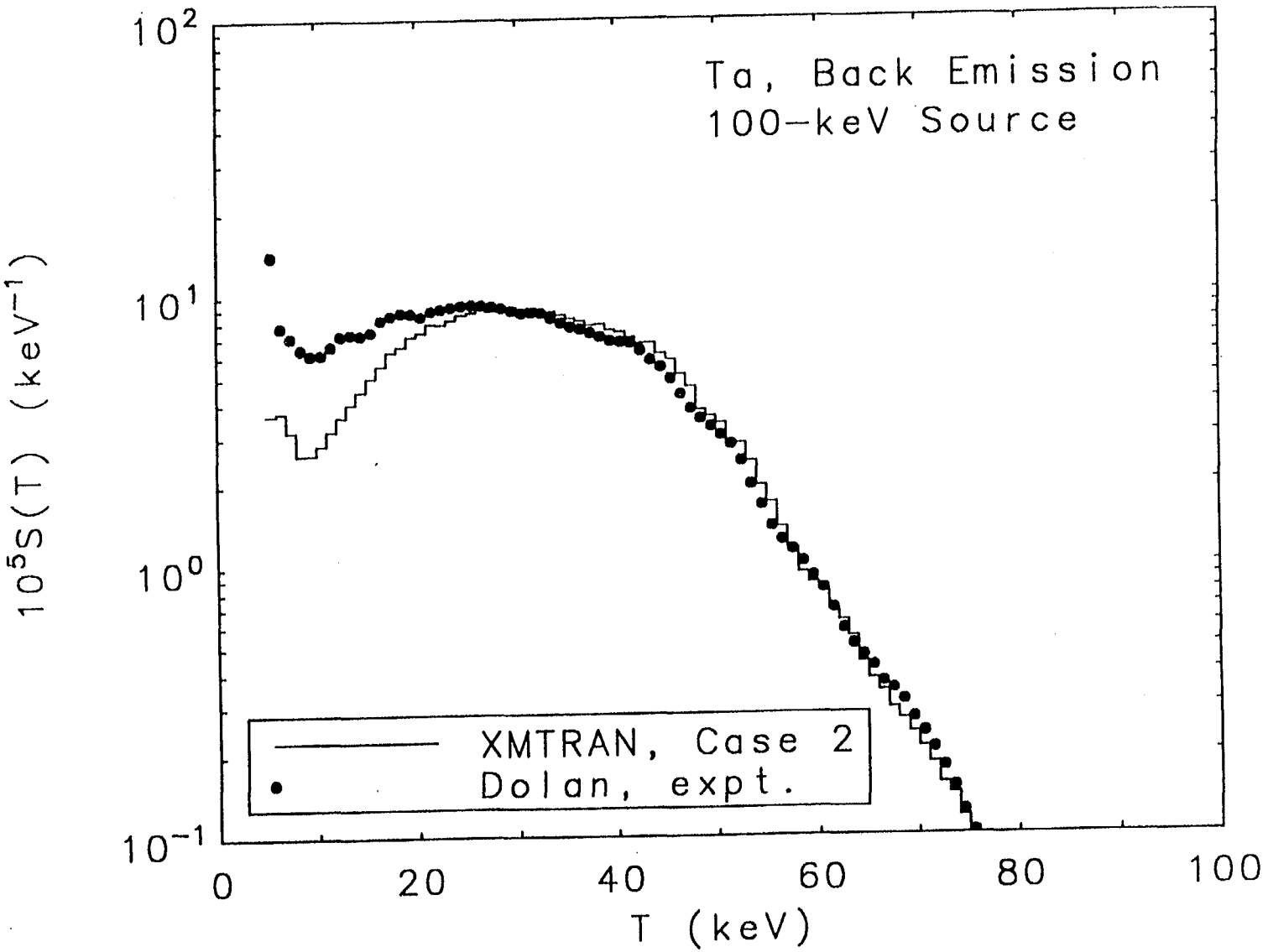
Ta, Back Emission
100-keV Source
XMTRAN, Case 2
Dolan, expt.
$10^5 S(T)$ (keV^{-1})
T (keV)
10^2
10^1
10^0
10^{-1}
0
20
40
60
80
100

Fig.9a-4

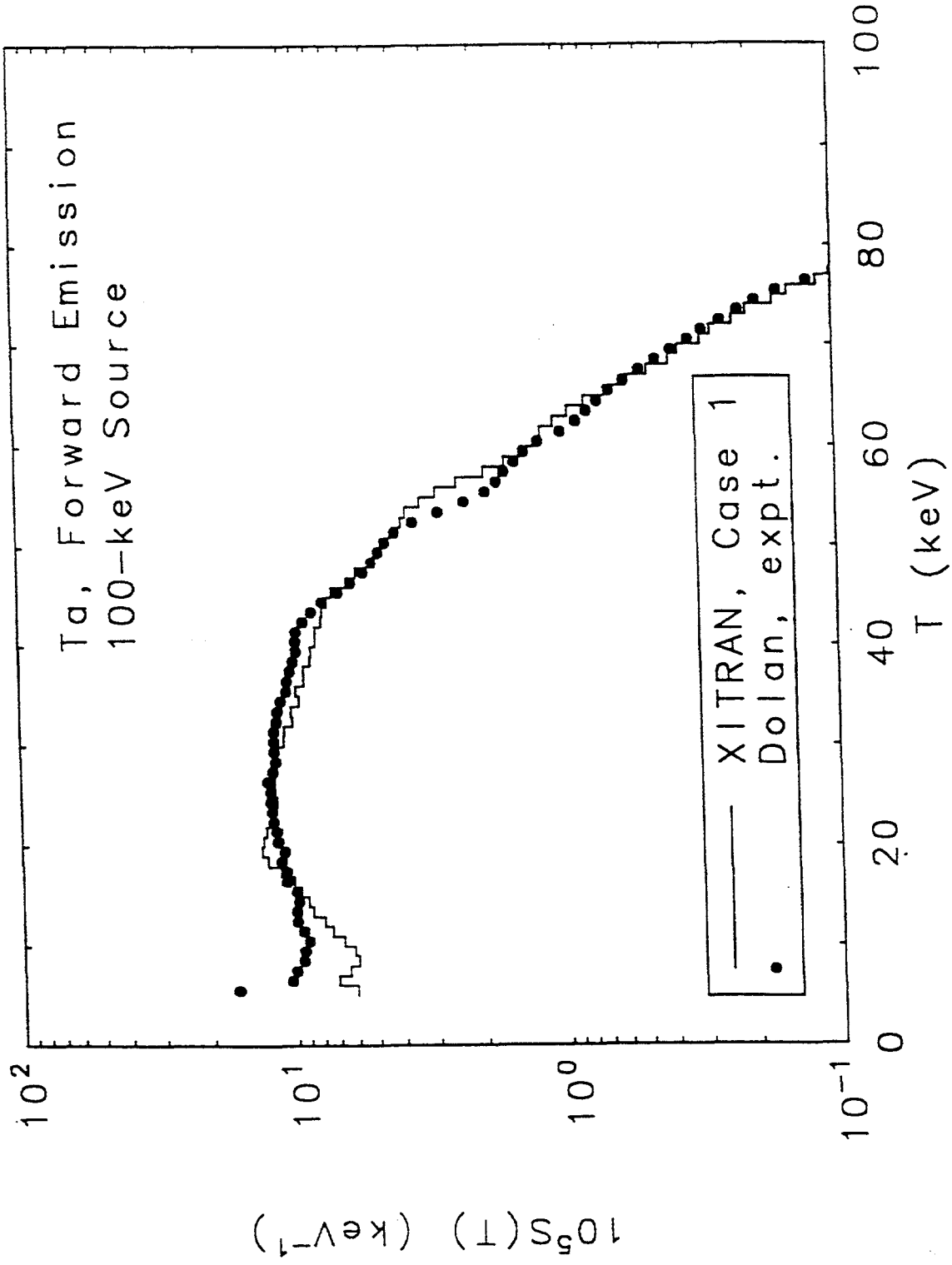
Ta, Forward Emission
100-keV Source
XITRAN, Case 1
Dolan, expt.
$10^5 S(T)$ (keV^{-1})
T (keV)
10^2
10^1
10^0
10^{-1}
0
20
40
60
80
100

Fig.9b-1

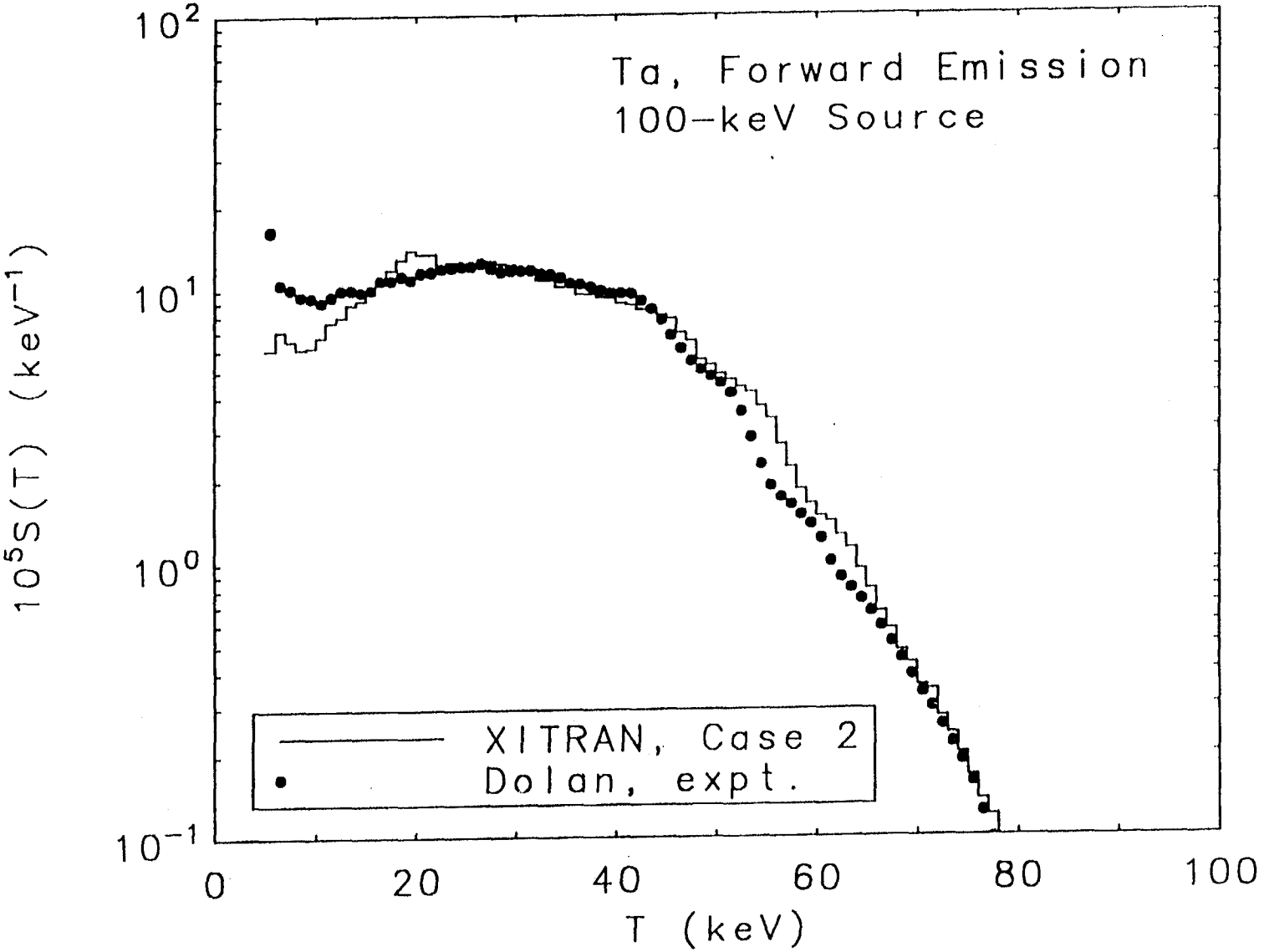
Ta, Forward Emission
100-keV Source
10^2
10^1
10^0
10^{-1}
$10^5S(T)$ (keV^{-1})
0
20
40
60
80
100
T (keV)
XITRAN, Case 2
Dolan, expt.

Fig.9b-2

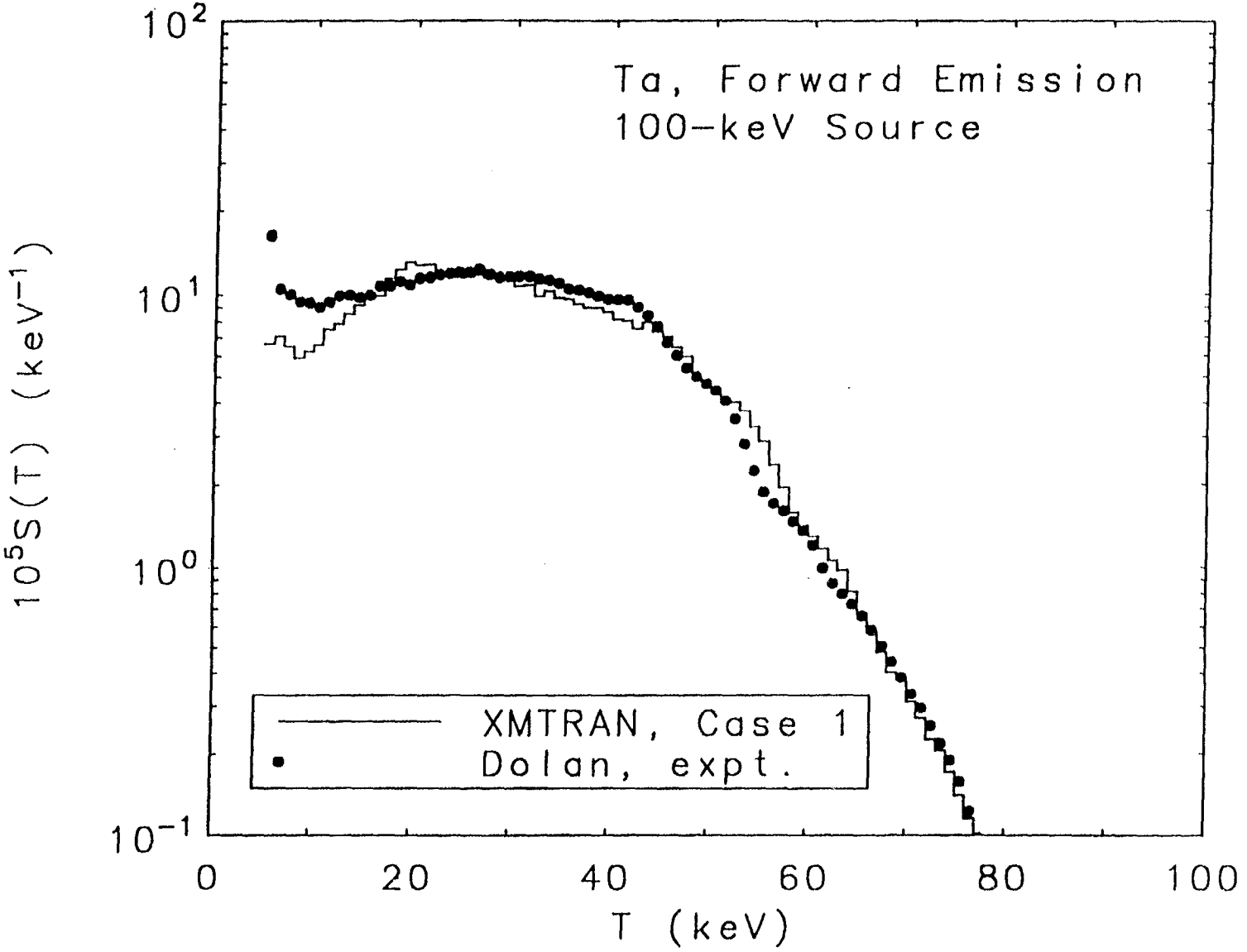
Ta, Forward Emission
100-keV Source
XMTRAN, Case 1
Dolan, expt.
$10^5 S(T)$ (keV^{-1})
T (keV)
10^2
10^1
10^0
10^{-1}
0
20
40
60
80
100

Fig.9b-3

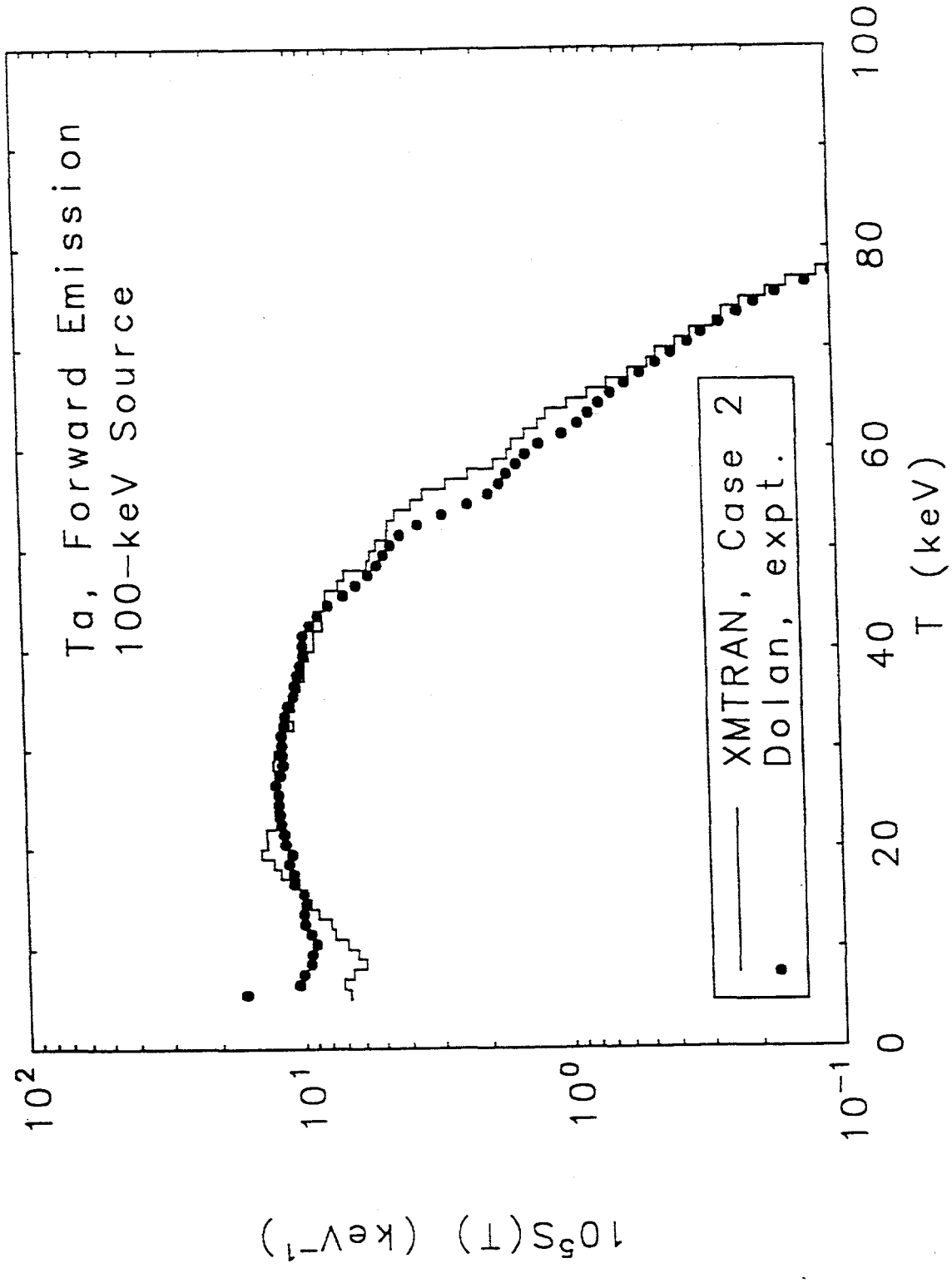
Ta, Forward Emission
100-keV Source
XMTRAN, Case 2
Dolan, expt.
$10^5 S(T)$ (keV^{-1})
T (keV)
10^2
10^1
10^0
10^{-1}
0
20
40
60
80
100

Fig.9b-4

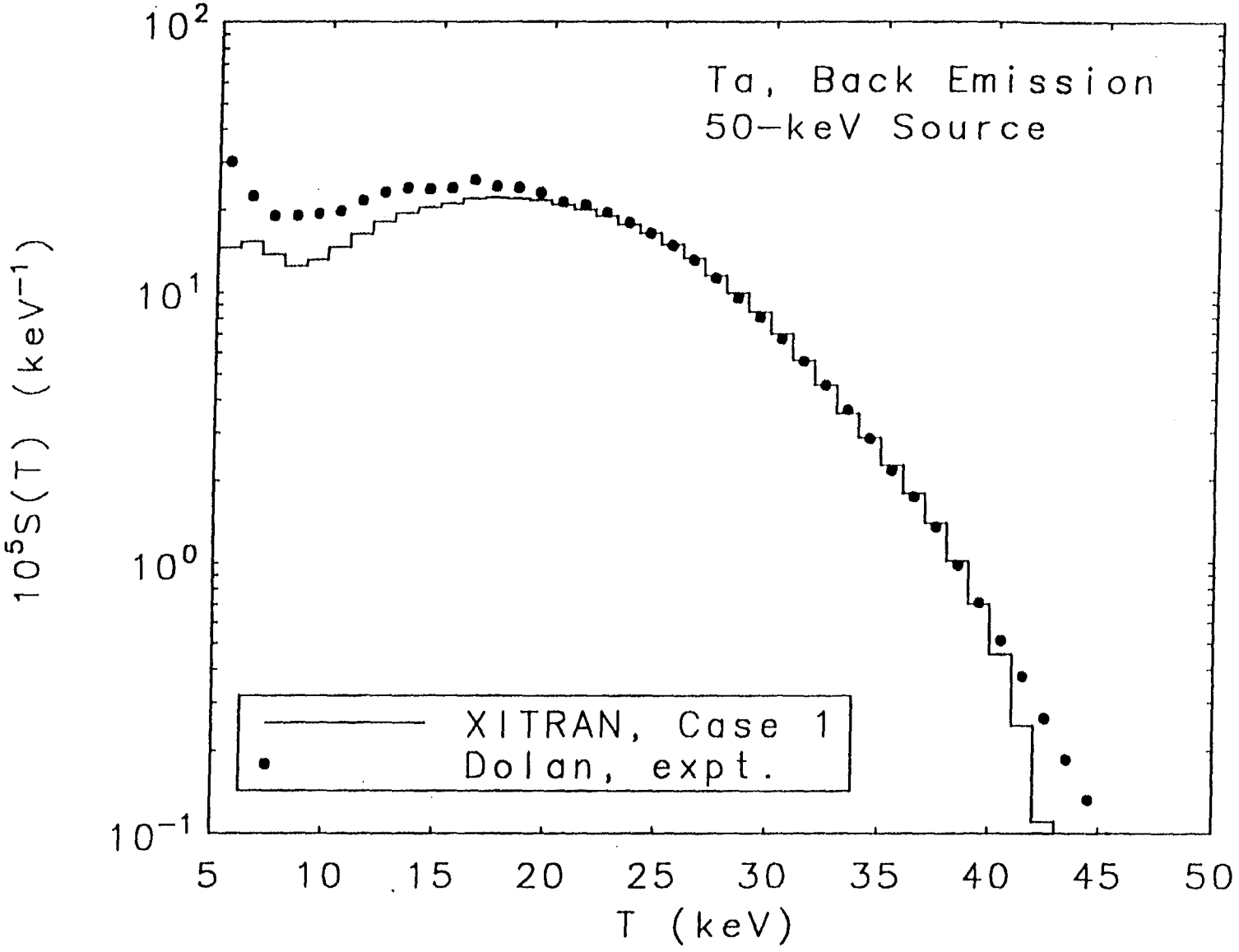
Ta, Back Emission
50-keV Source
XITRAN, Case 1
Dolan, expt.
10^2
10^1
10^0
10^{-1}
$10^5S(T)$ (keV^{-1})
5
10
15
20
25
30
35
40
45
50
T (keV)

Fig.9c-1

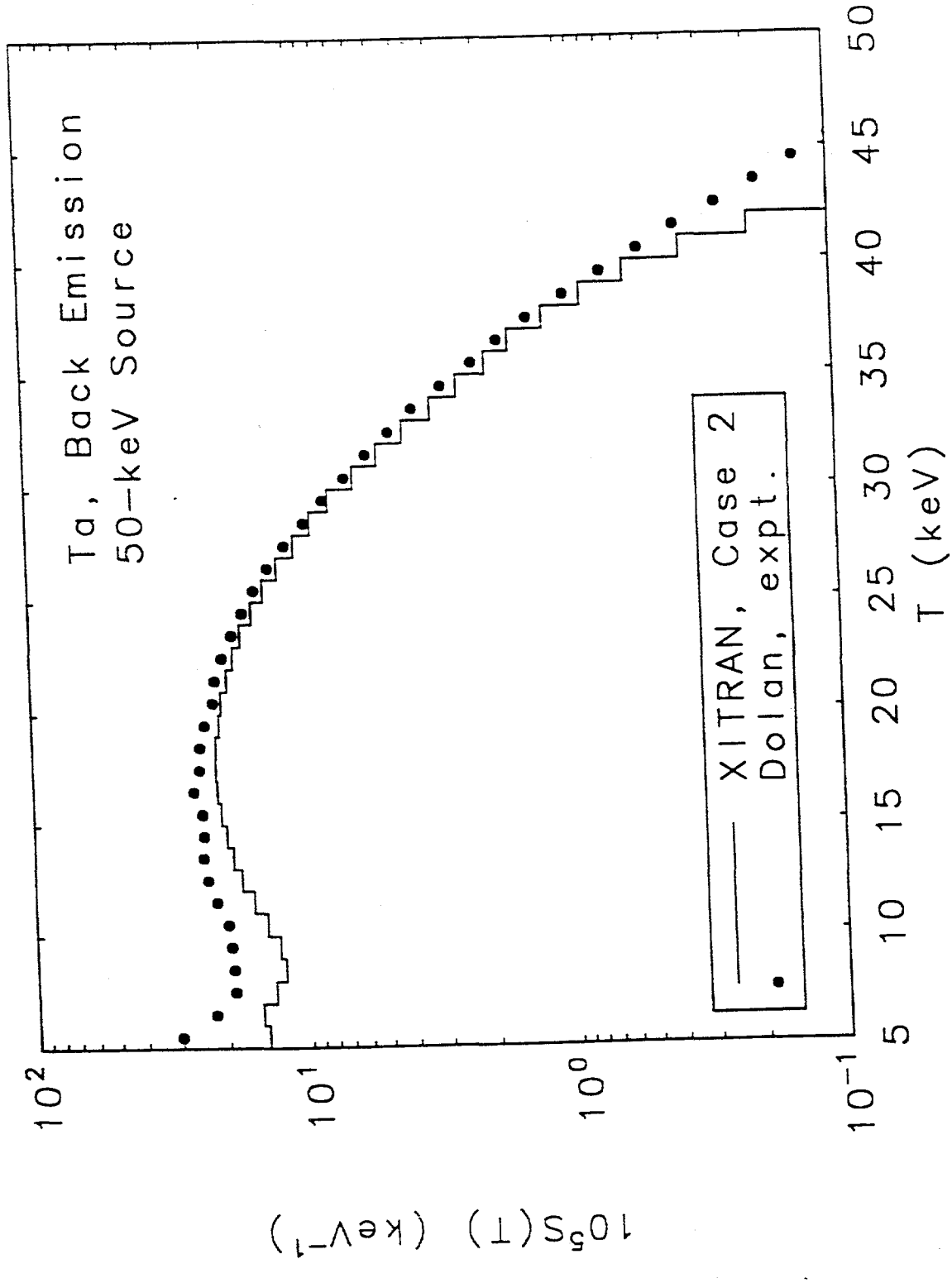
Ta, Back Emission
50-keV Source
XITRAN, Case 2
Dolan, expt.
$10^5 S(T)$ (keV^{-1})
T (keV)
10^2
10^1
10^0
10^{-1}
5
10
15
20
25
30
35
40
45
50

Fig.9c-2

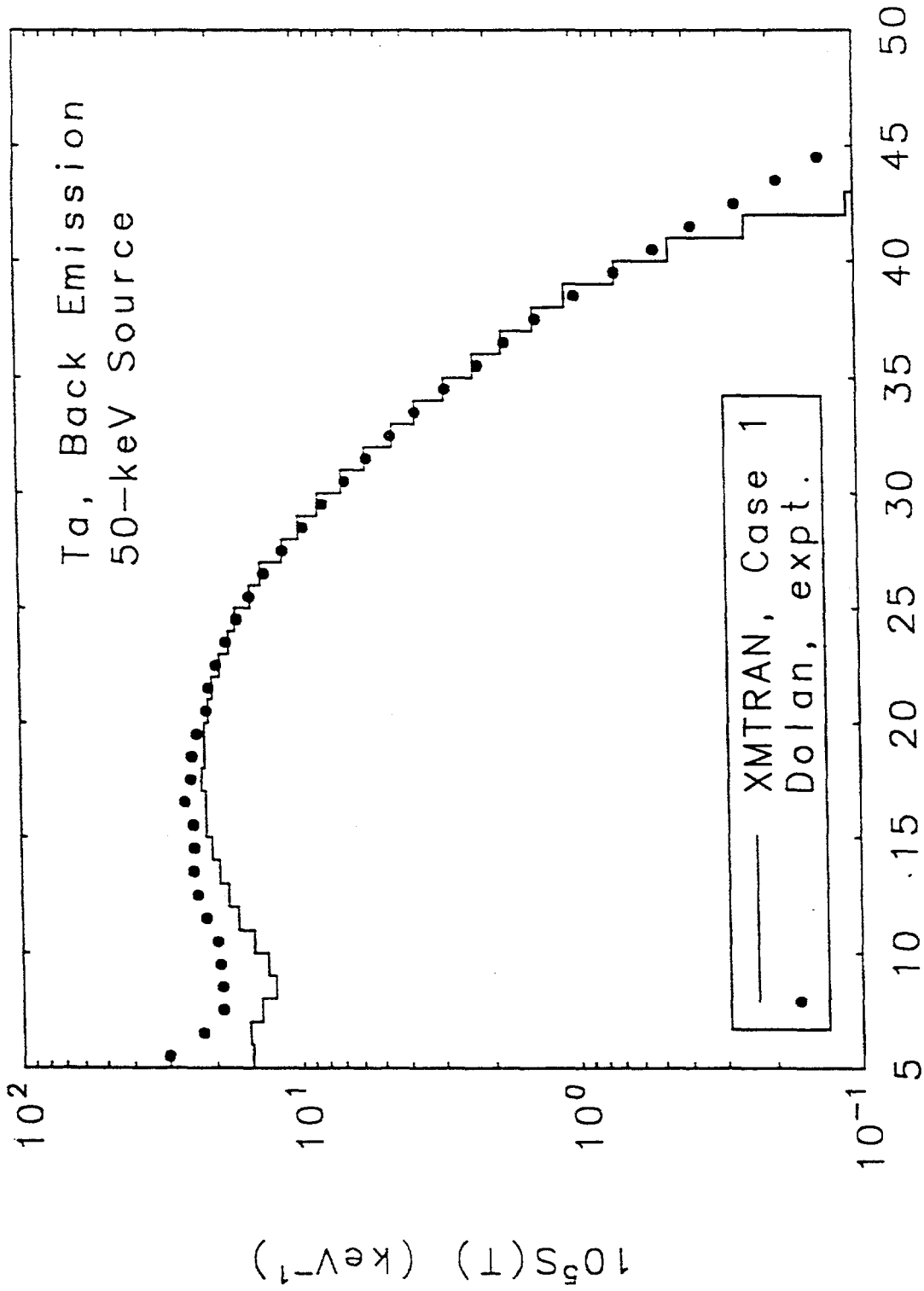
Ta, Back Emission
50-keV Source
XMTRAN, Case 1
Dolan, expt.
$10^5 S(T)$ (keV^{-1})
T (keV)
10^2
10^1
10^0
10^{-1}
5
10
15
20
25
30
35
40
45
50

Fig. 9c-3

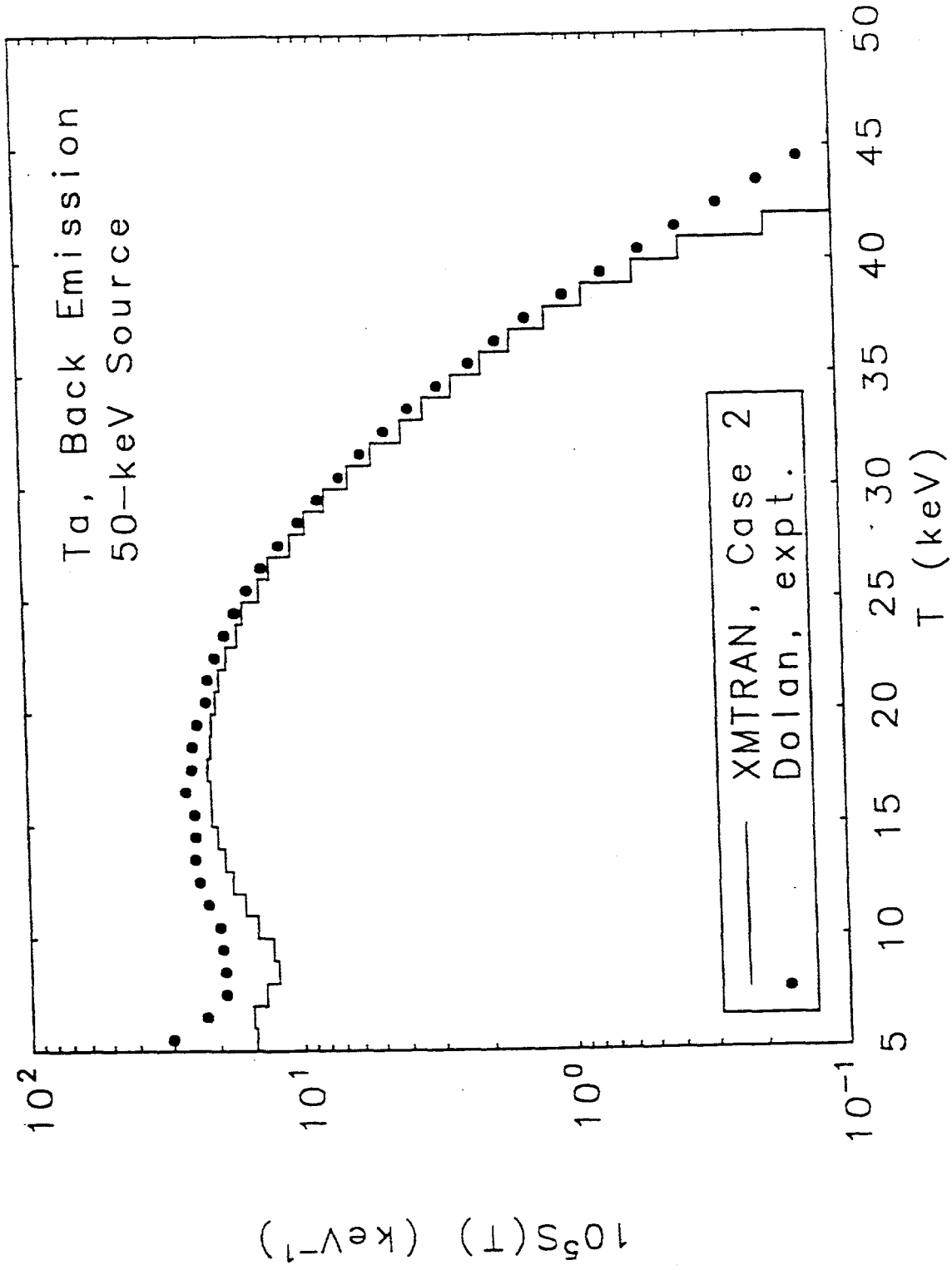
Ta, Back Emission
50-keV Source
XMTRAN, Case 2
Dolan, expt.
$10^5 S(T)$ (keV^{-1})
T (keV)
10^2
10^1
10^0
10^{-1}
5
10
15
20
25
30
35
40
45
50

Fig. 9c-4

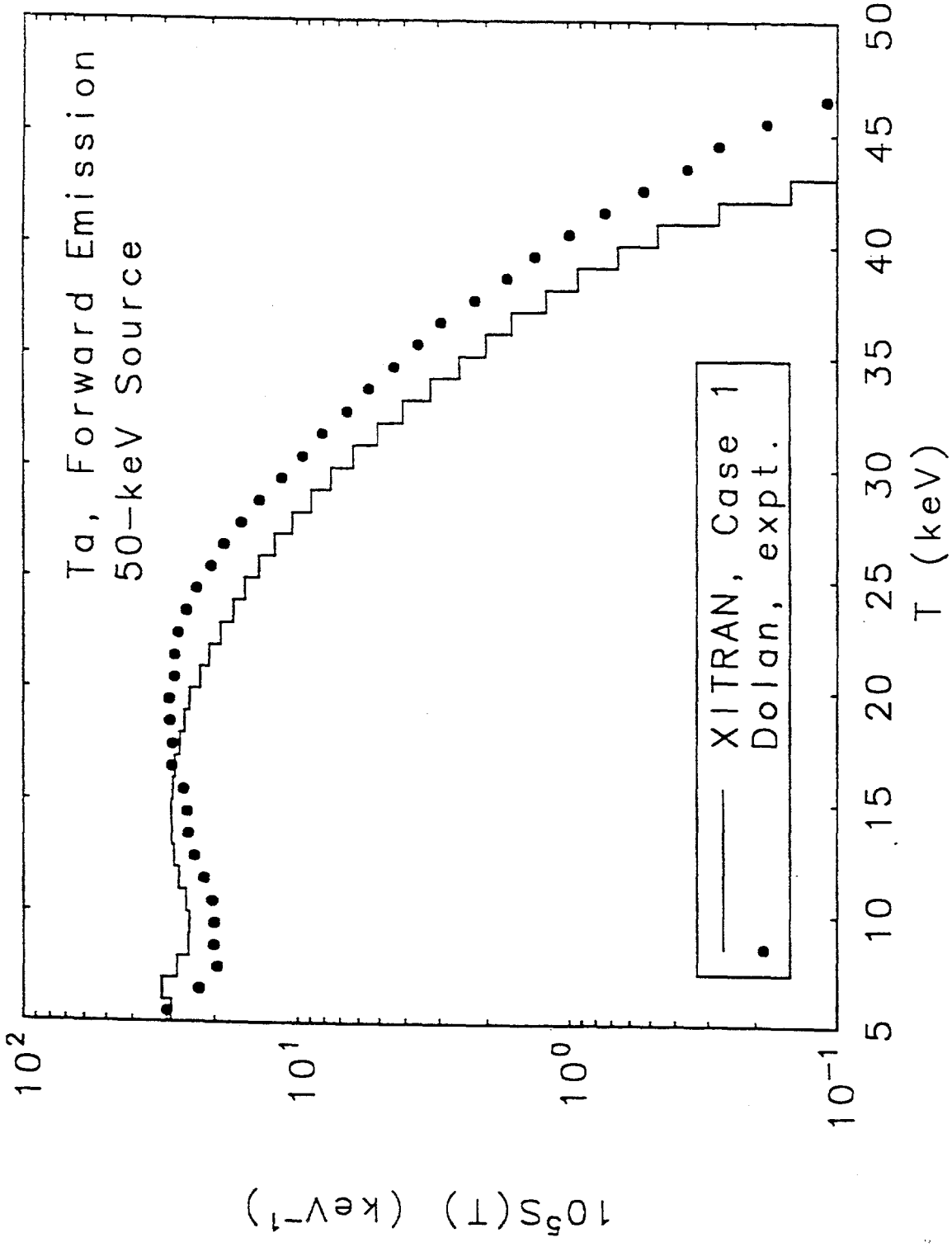
Ta, Forward Emission
50-keV Source
XITRAN, Case 1
Dolan, expt.
$10^5 S(T)$ (keV^{-1})
T (keV)
10^2
10^1
10^0
10^{-1}
5
10
15
20
25
30
35
40
45
50

Fig.9d-1

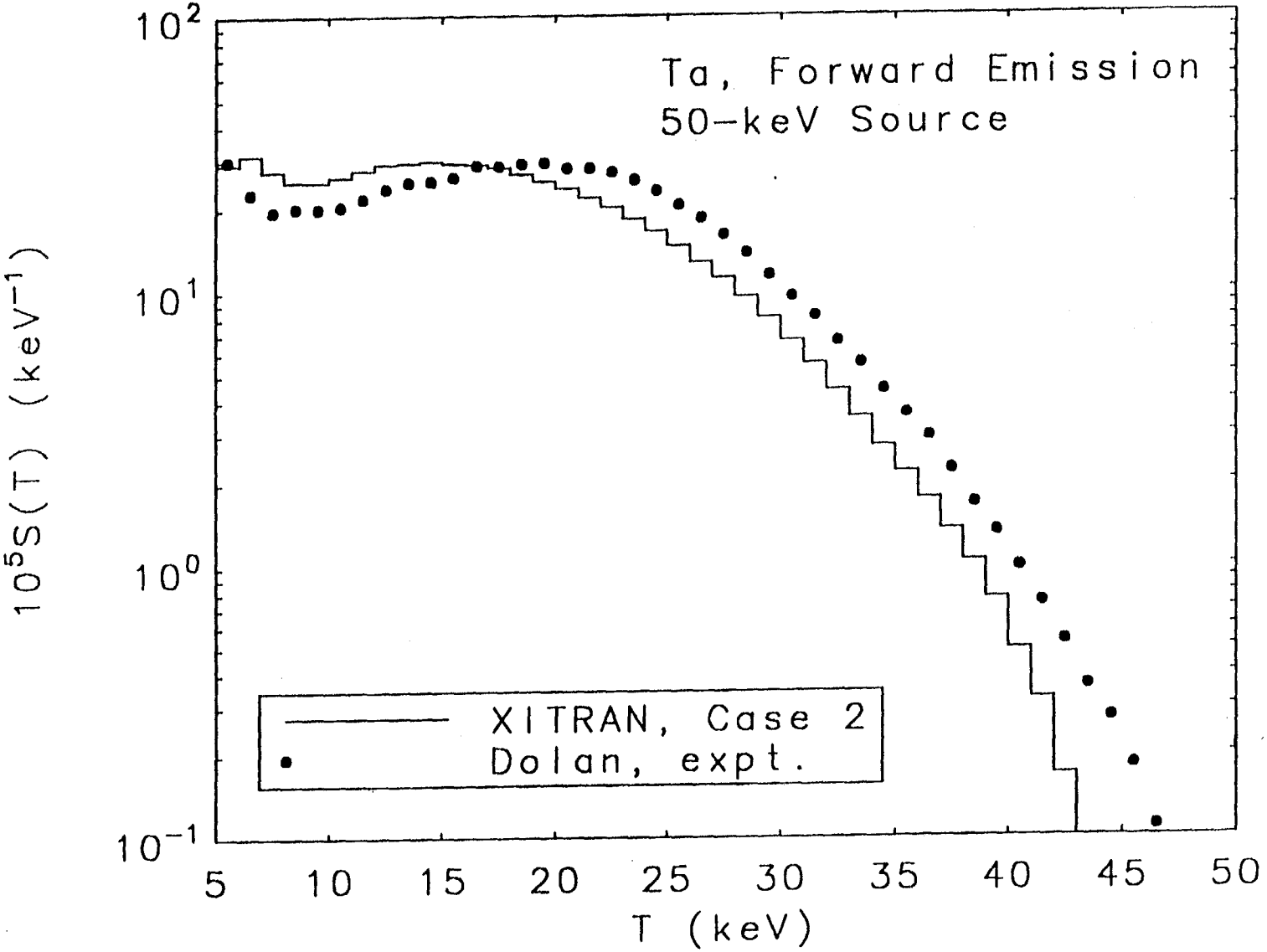
Ta, Forward Emission
50-keV Source
XITRAN, Case 2
Dolan, expt.
$10^5 S(T)$ (keV^{-1})
T (keV)
10^2
10^1
10^0
10^{-1}
5
10
15
20
25
30
35
40
45
50

Fig.9d-2

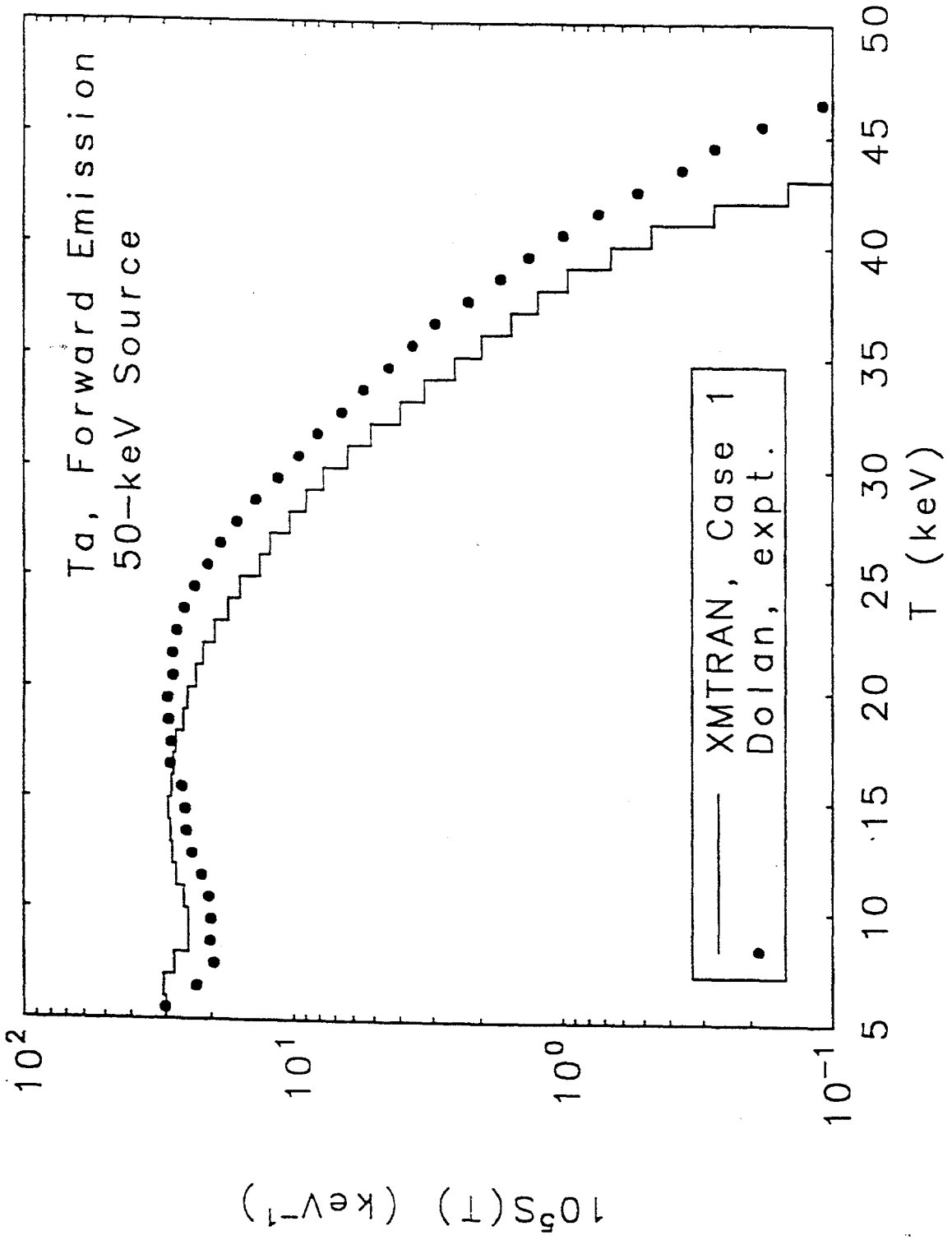
Ta, Forward Emission
50-keV Source
XMTRAN, Case 1
Dolan, expt.
10^2
10^1
10^0
10^{-1}
5
10
15
20
25
30
35
40
45
50
T (keV)
$10^5 S(T)$ (keV^{-1})

Fig. 9d-3

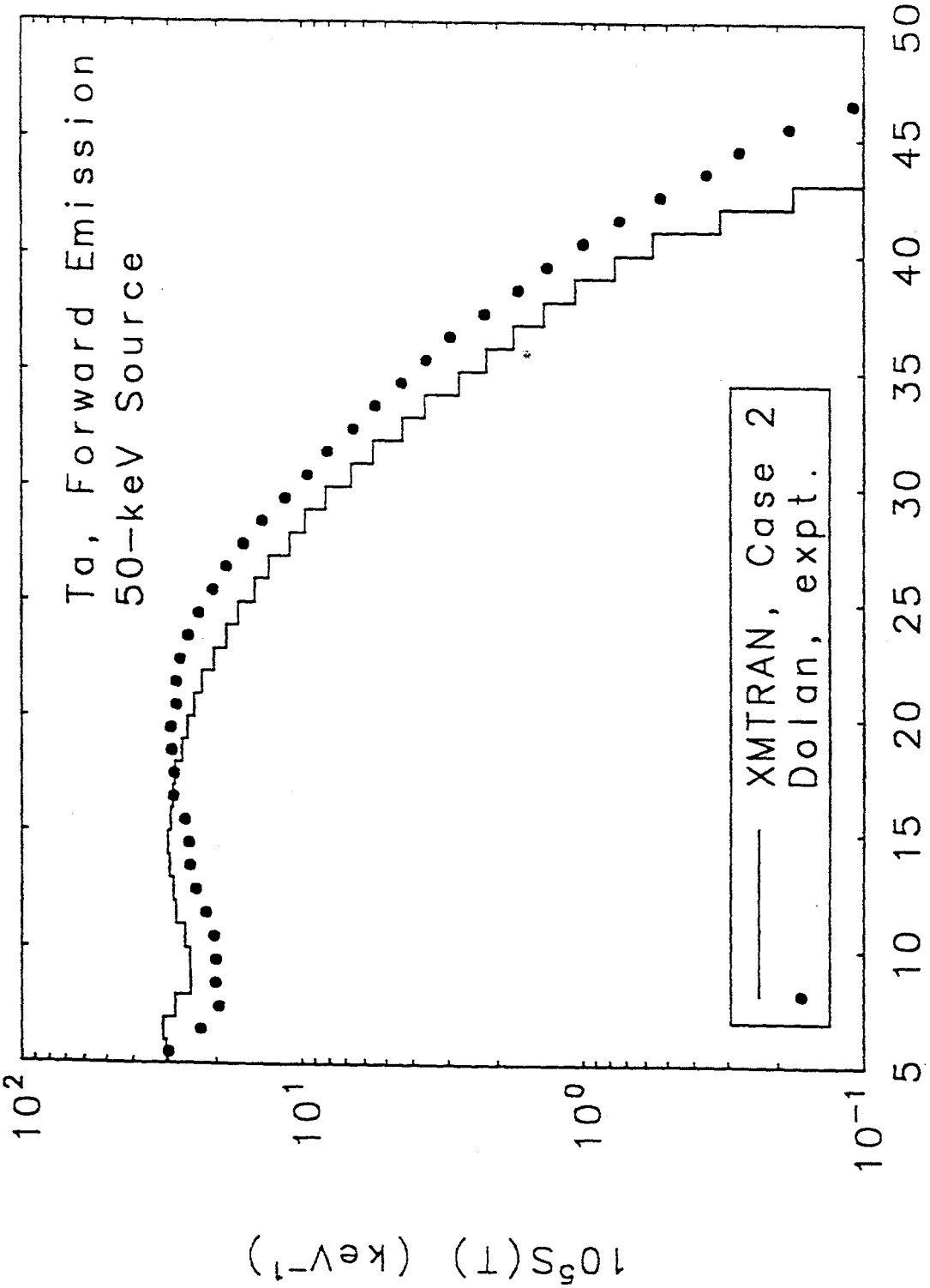
Ta, Forward Emission
50-keV Source
XMTRAN, Case 2
Dolan, expt.
$10^5 S(T)$ (keV^{-1})
T (keV)
10^2
10^1
10^0
10^{-1}
5
10
15
20
25
30
35
40
45
50

Fig.9d-4

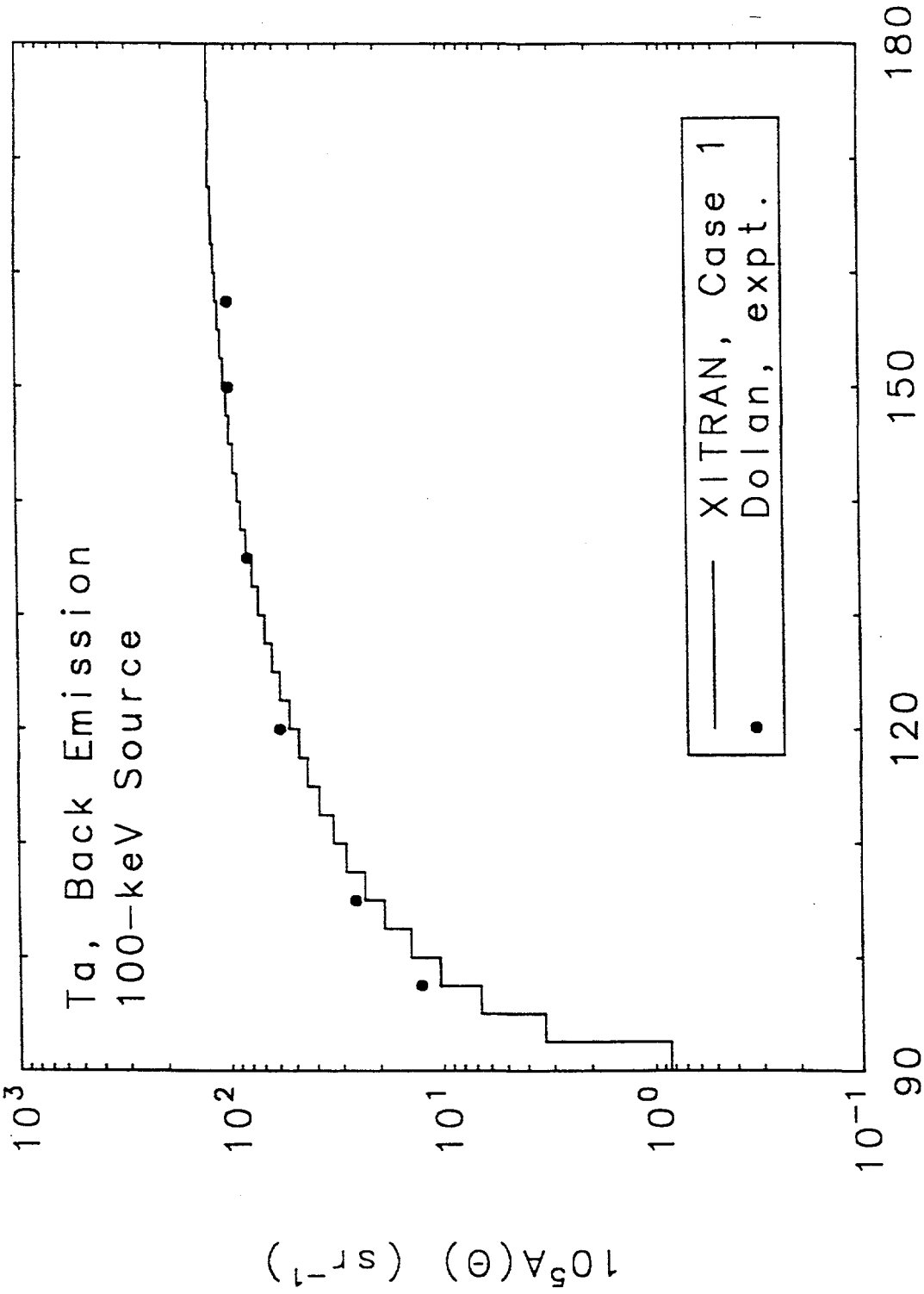
Ta, Back Emission
100-keV Source
XITRAN, Case 1
Dolan, expt.
$10^5 A(\Theta)$ (sr^{-1})
Θ (deg)
10^3
10^2
10^1
10^0
10^{-1}
90
120
150
180

Fig.10a-1

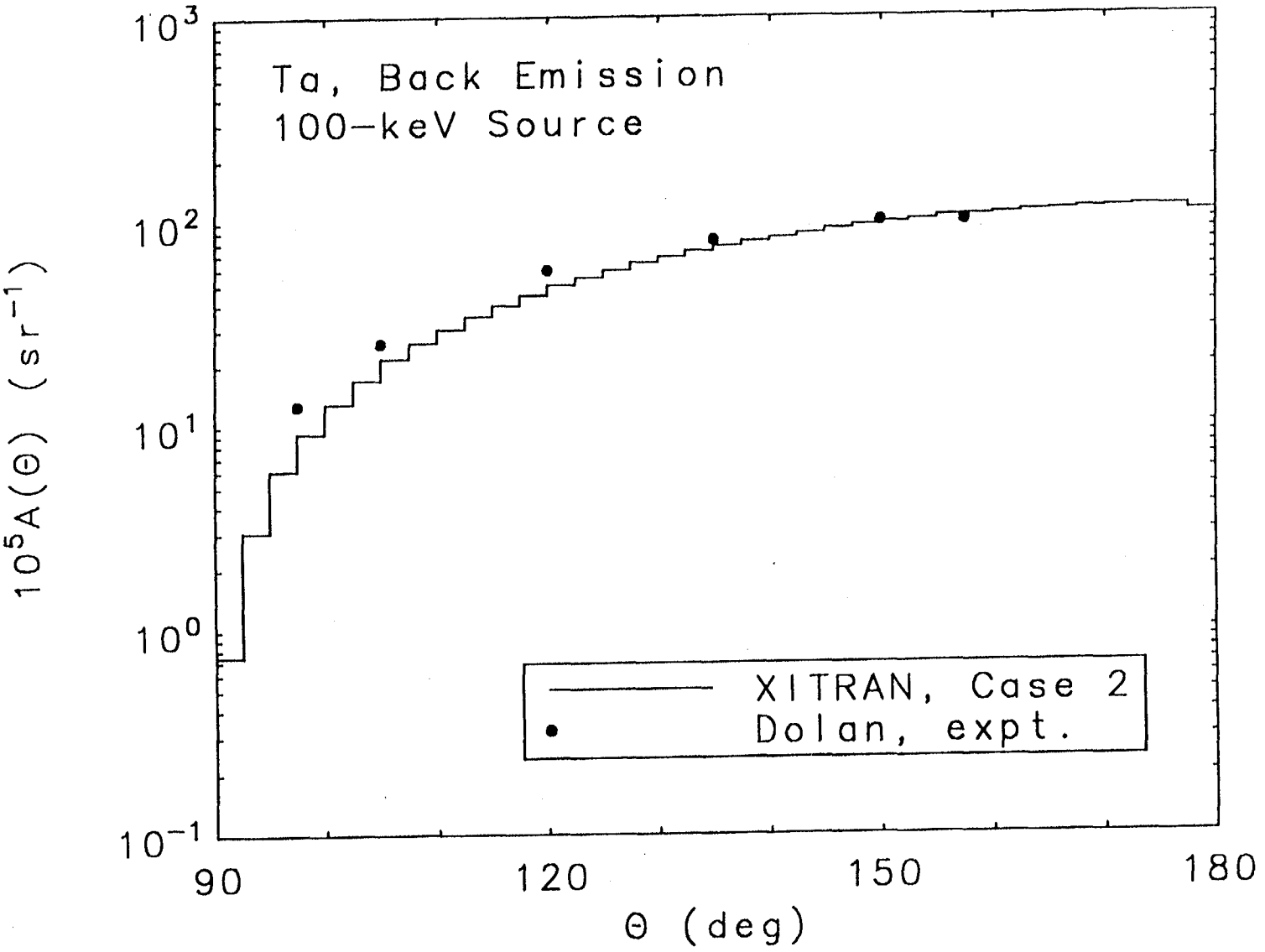
Ta, Back Emission
100-keV Source
10^3
10^2
10^1
10^0
10^{-1}
$10^5A(\Theta)$ (sr^{-1})
90
120
150
180
Θ (deg)
XITRAN, Case 2
Dolan, expt.

Fig.10a-2

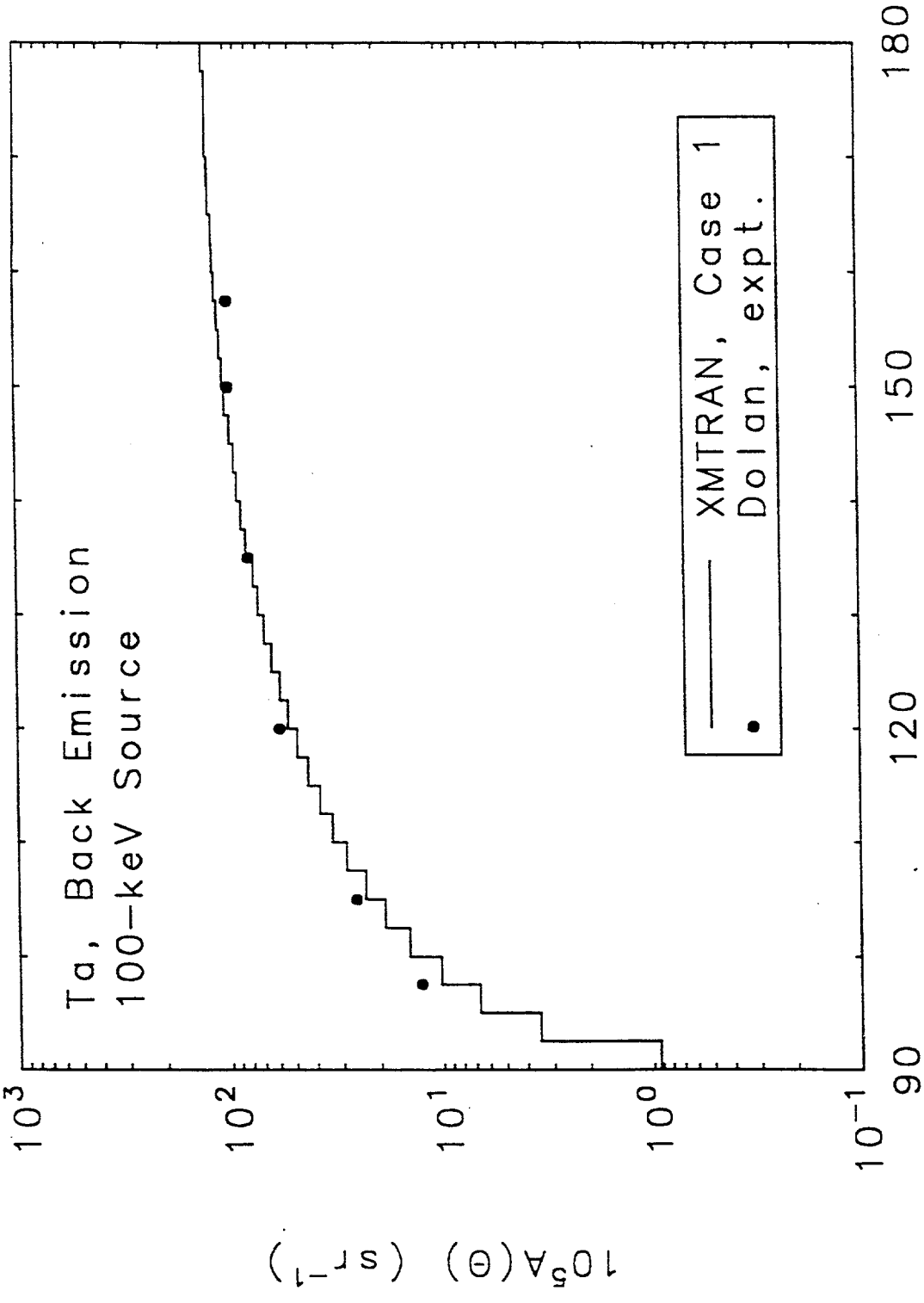
Ta, Back Emission
100-keV Source
XMTRAN, Case 1
Dolan, expt.
$10^5 A(\Theta)$ (sr^{-1})
10^3
10^2
10^1
10^0
10^{-1}
90
120
150
180
Θ (deg)

Fig.10a-3

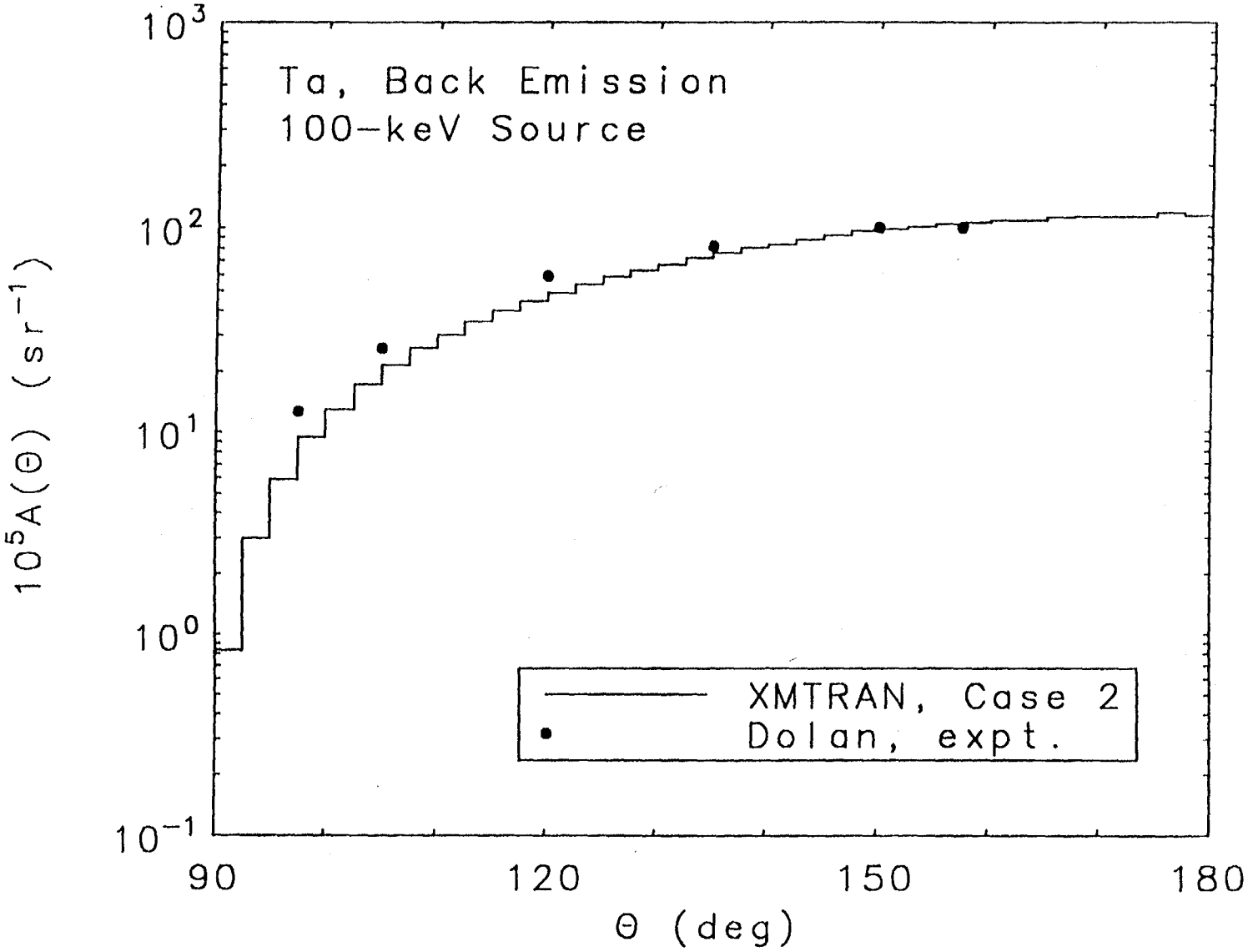
Ta, Back Emission
100-keV Source
XMTRAN, Case 2
Dolan, expt.
$10^5 A(\Theta)$ (sr^{-1})
Θ (deg)
10^3
10^2
10^1
10^0
10^{-1}
90
120
150
180

Fig.10a-4

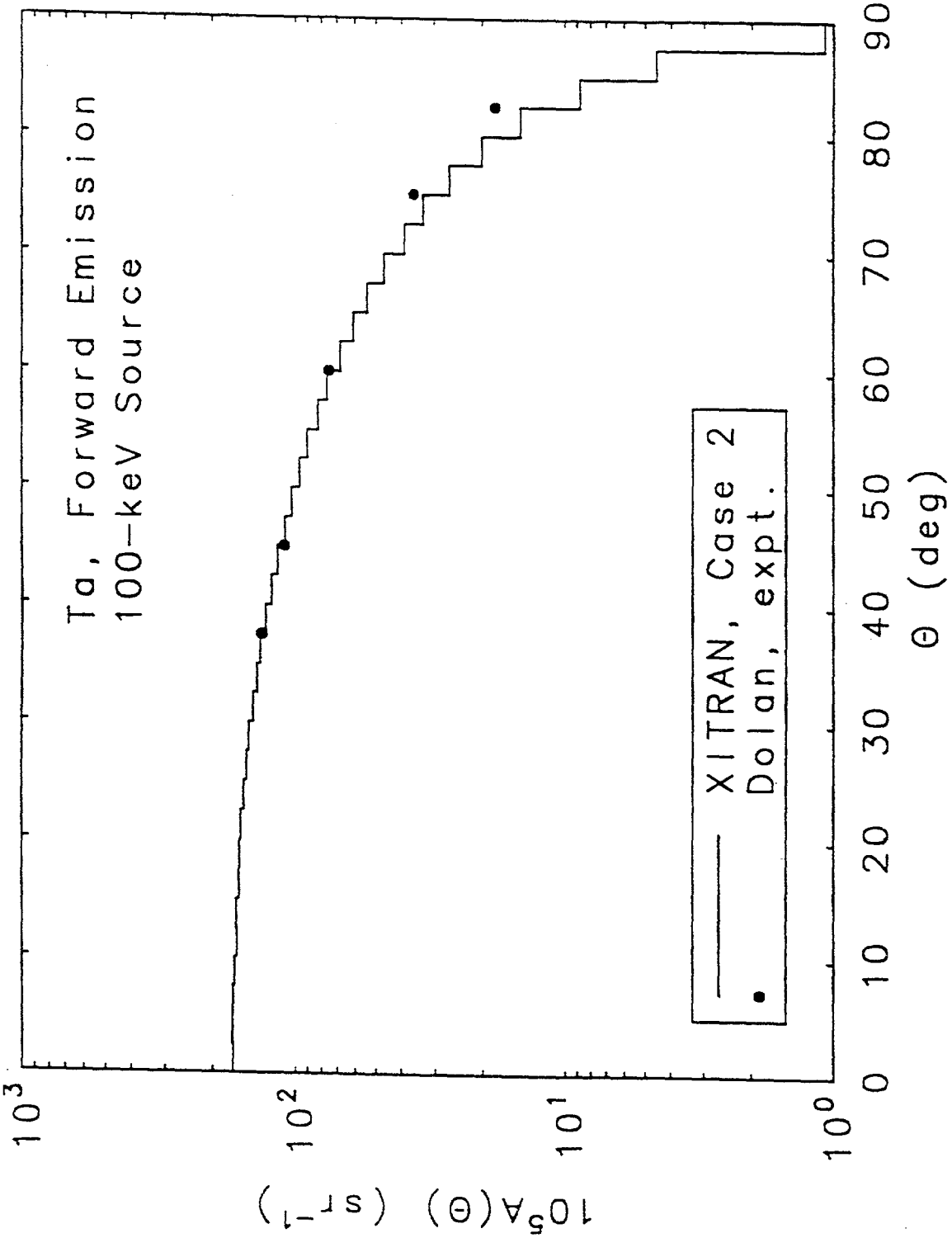
Ta, Forward Emission
100-keV Source
XITRAN, Case 2
Dolan, expt.
$10^5 A(\Theta)$ (sr^{-1})
10^3
10^2
10^1
10^0
0
10
20
30
40
50
60
70
80
90
Θ (deg)

Fig.10b-1

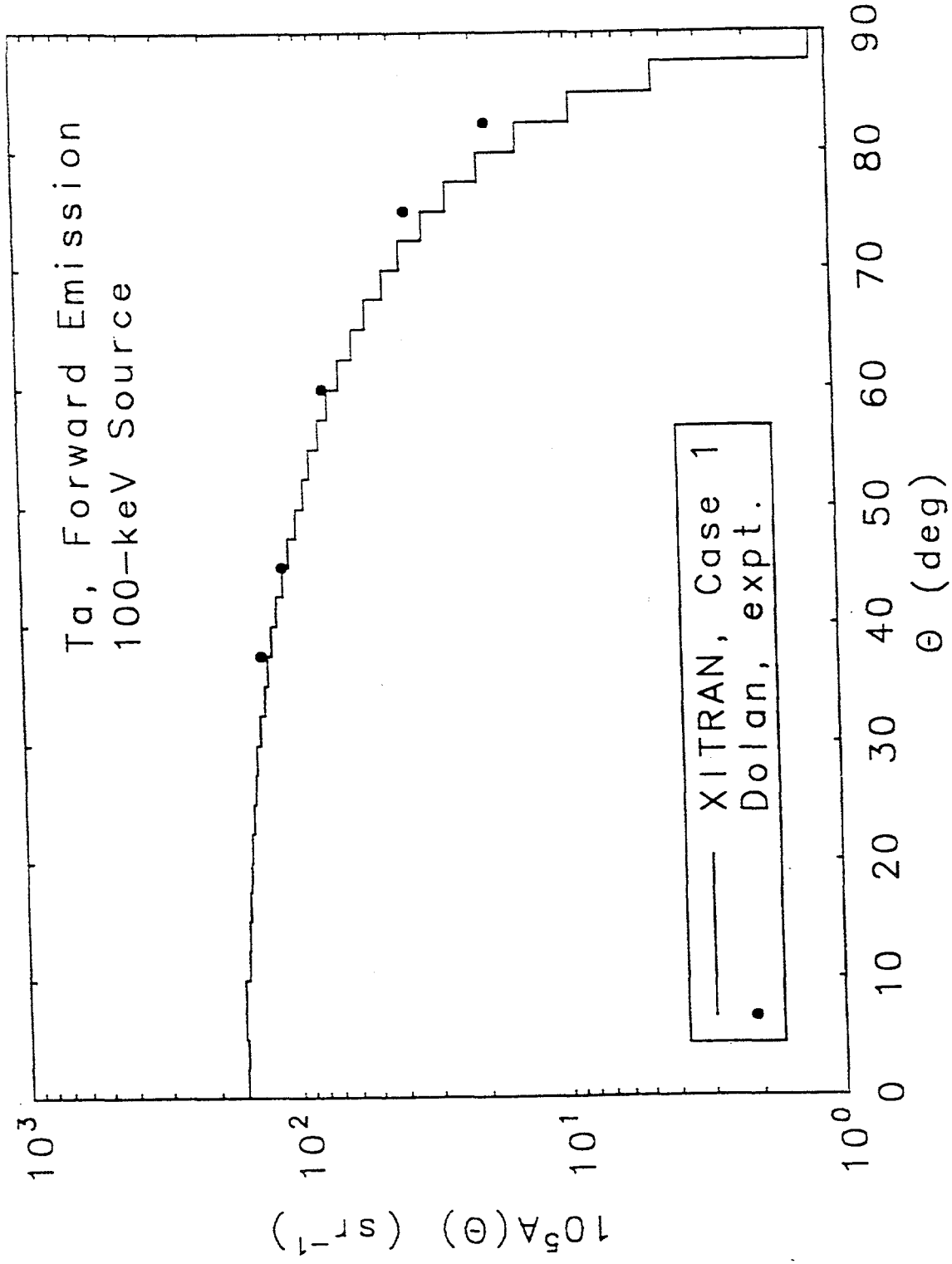
Ta, Forward Emission
100-keV Source
XITRAN, Case 1
Dolan, expt.
$10^5 A(\Theta)$ (sr^{-1})
Θ (deg)
10^0
10^1
10^2
10^3
0
10
20
30
40
50
60
70
80
90

Fig.10b-2

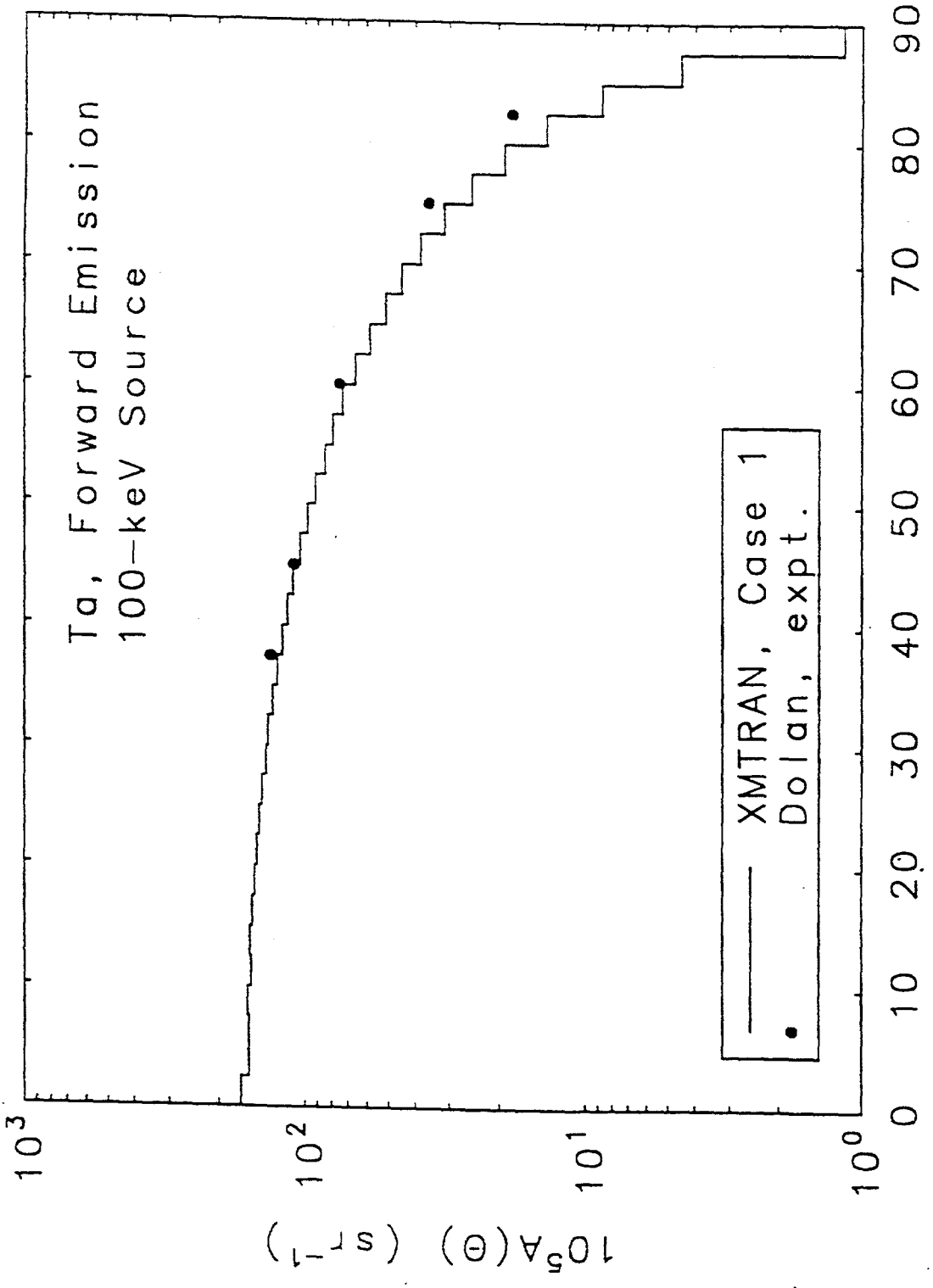
Ta, Forward Emission
100-keV Source
XMTRAN, Case 1
Dolan, expt.
$10^5 A(\Theta)$ (sr^{-1})
Θ (deg)
10^3
10^2
10^1
10^0
0
10
20
30
40
50
60
70
80
90

Fig.10b-3

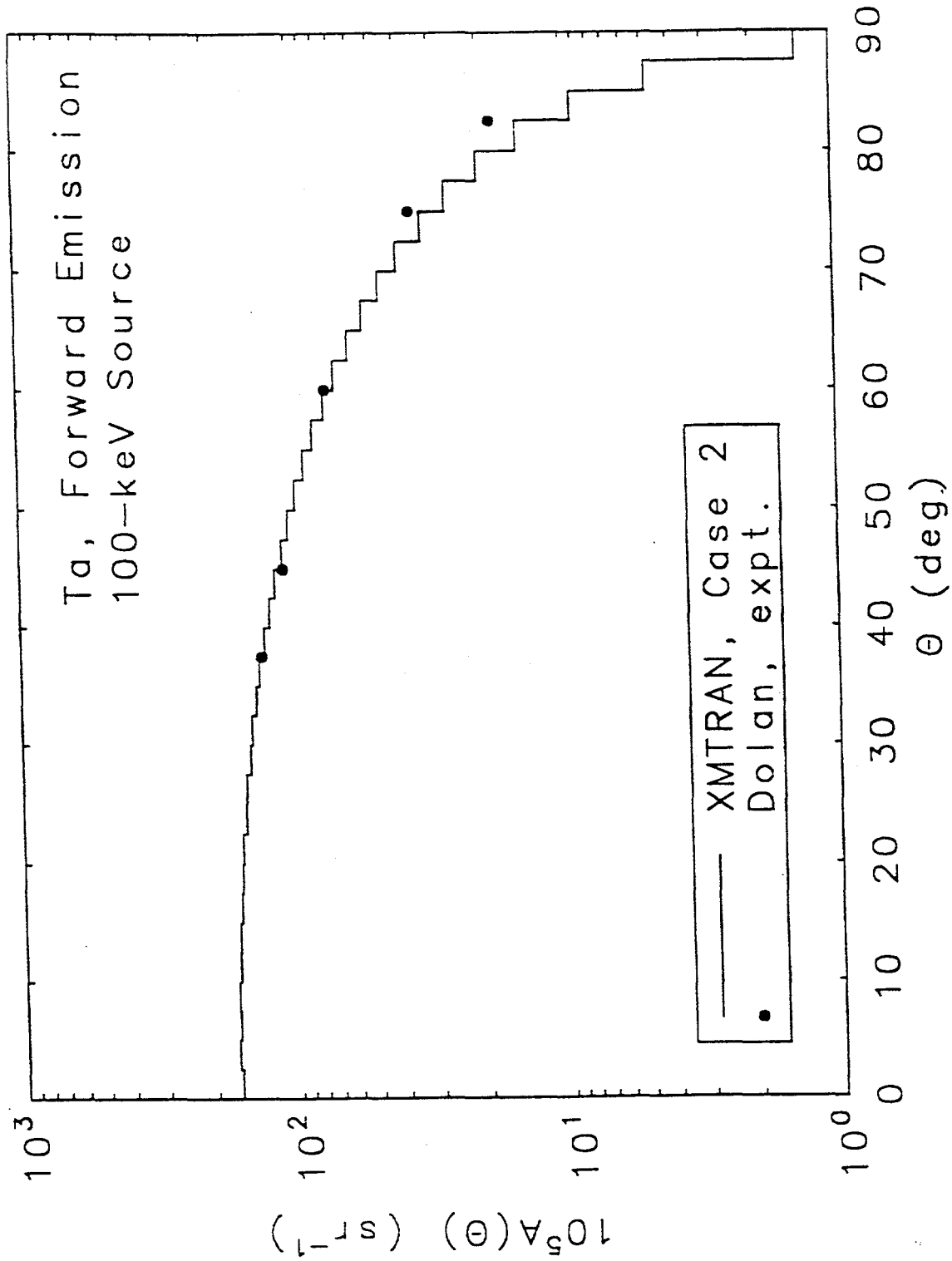
Ta, Forward Emission
100-keV Source
XMTRAN, Case 2
Dolan, expt.
$10^5 A(\Theta)$ (sr^{-1})
Θ (deg.)
10^3
10^2
10^1
10^0
0
10
20
30
40
50
60
70
80
90

Fig.10b-4

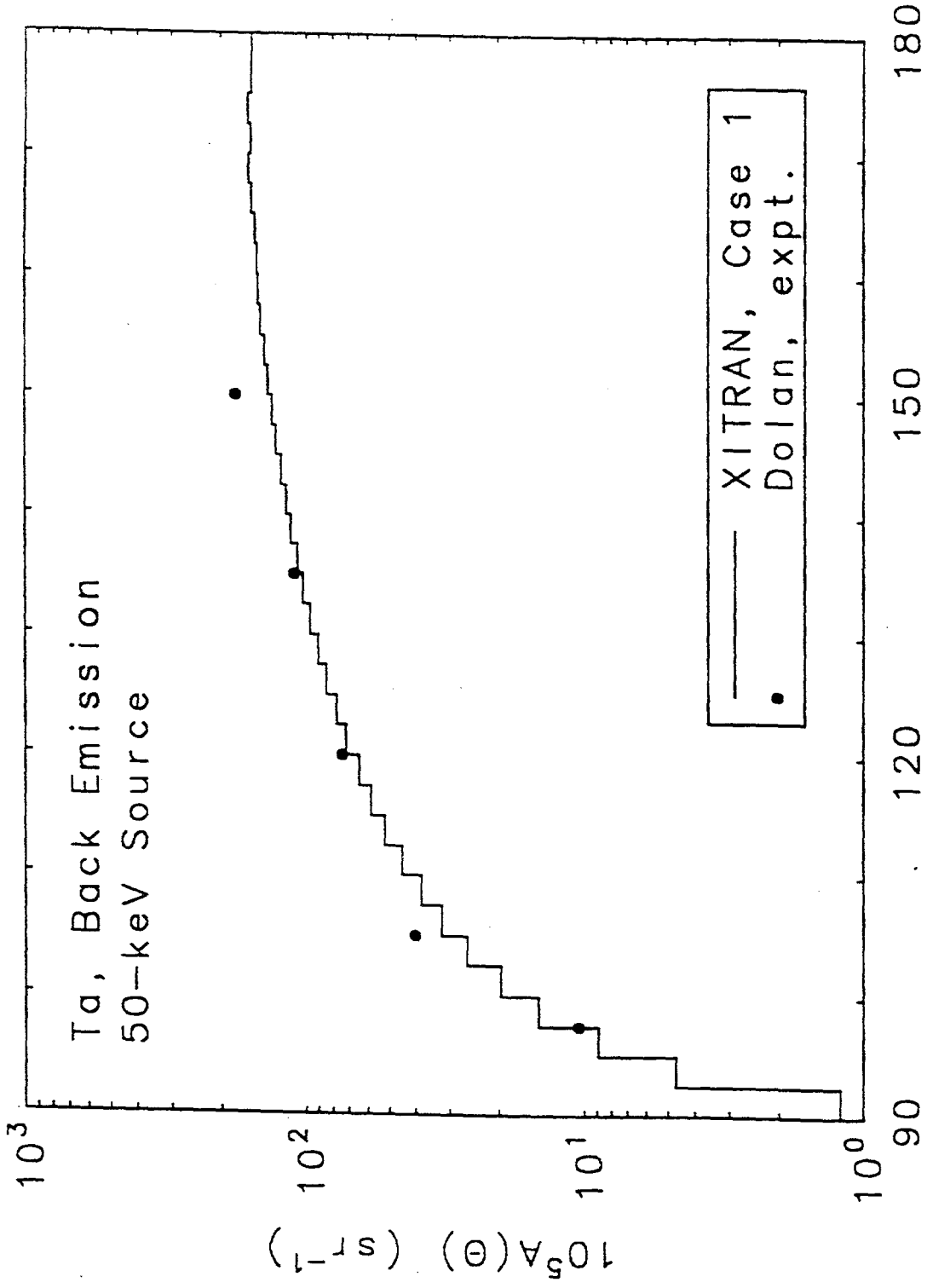
Ta, Back Emission
50-keV Source
XITRAN, Case 1
Dolan, expt.
$10^5 A(\Theta)$ (sr^{-1})
Θ (deg)
10^3
10^2
10^1
10^0
90
120
150
180

Fig.10c-1

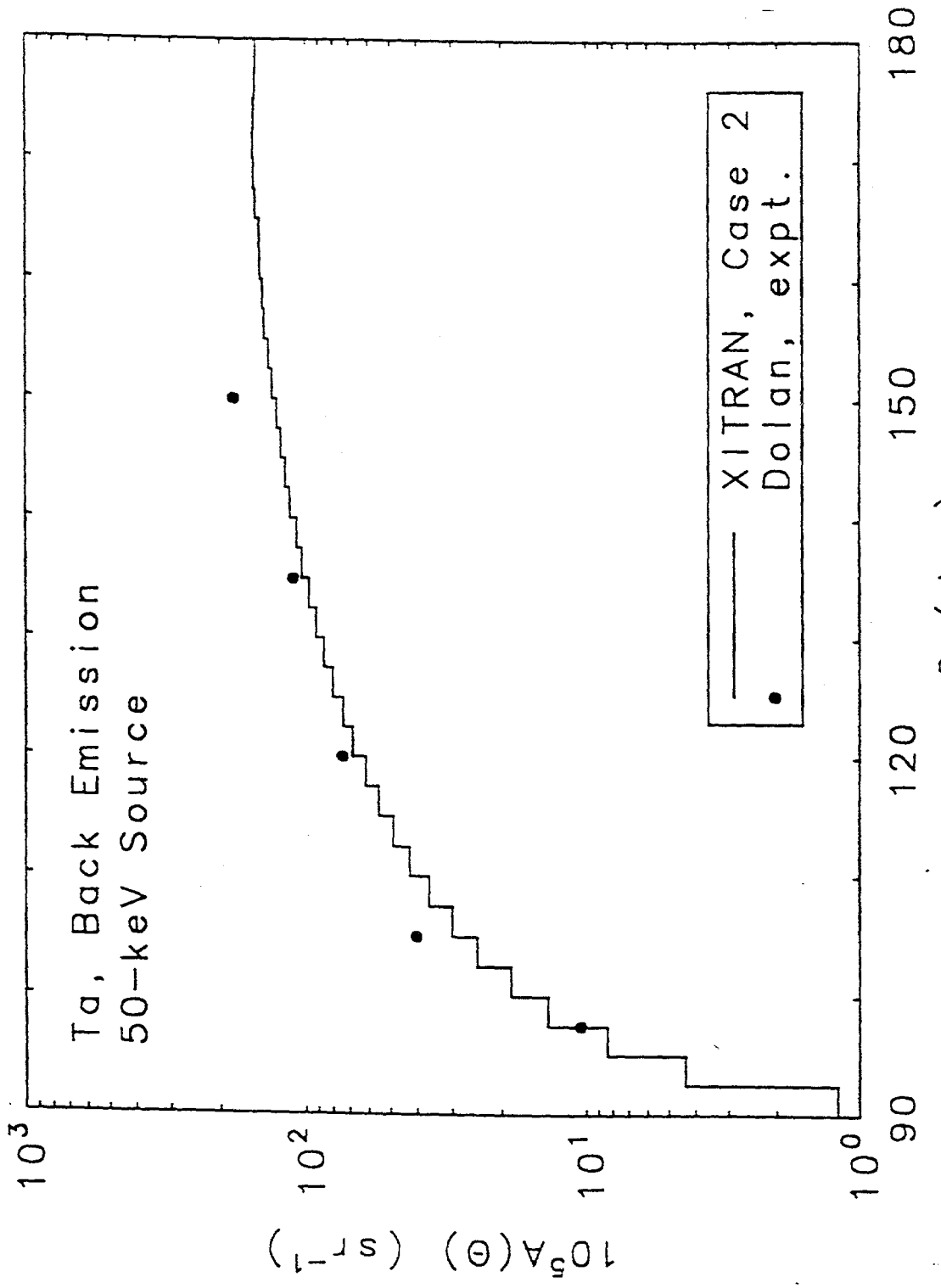
Ta, Back Emission
50-keV Source
XITRAN, Case 2
Dolan, expt.
$10^5 A(\Theta)$ (sr^{-1})
10^3
10^2
10^1
10^0
90
120
150
180
Θ (deg)

Fig.10c-2

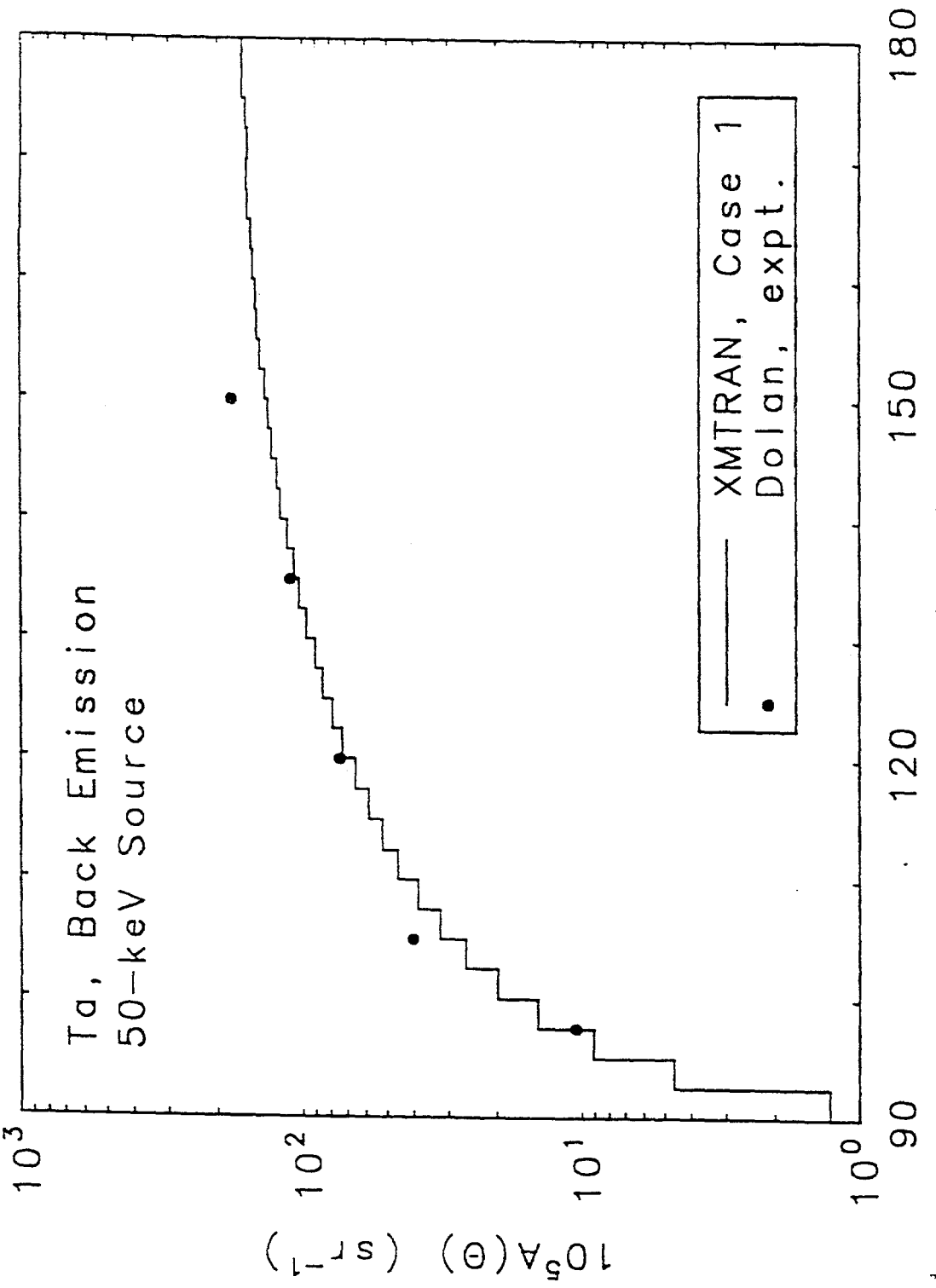
Ta, Back Emission
50-keV Source
XMTRAN, Case 1
Dolan, expt.
$10^5 A(\Theta)$ (sr^{-1})
Θ (deg)
10^3
10^2
10^1
10^0
90
120
150
180

Fig.10c-3

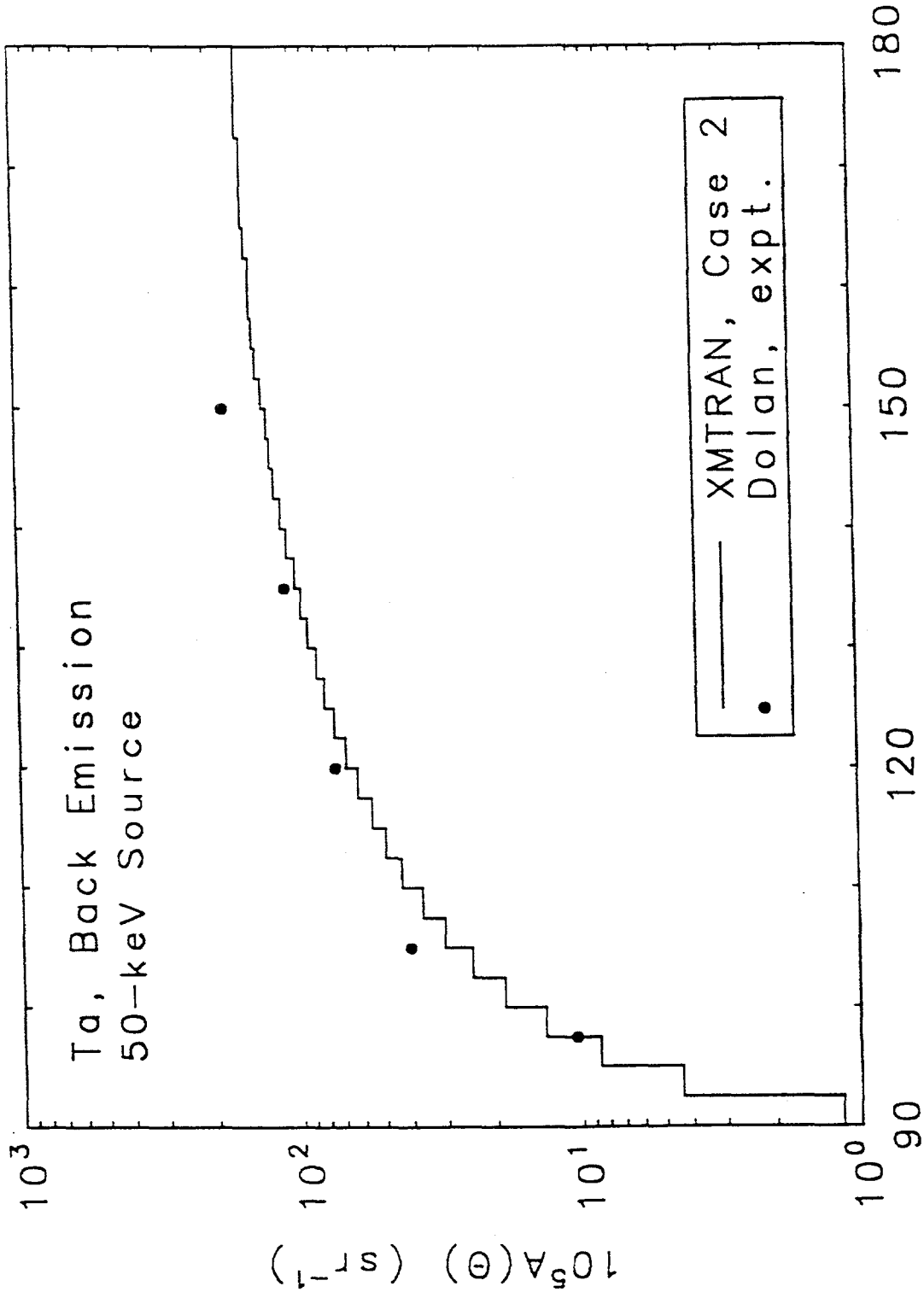
Ta, Back Emission
50-keV Source
XMTRAN, Case 2
Dolan, expt.
$10^5 A(\Theta)$ (sr^{-1})
10^3
10^2
10^1
10^0
90
120
150
180
Θ (deg)

Fig.10c-4

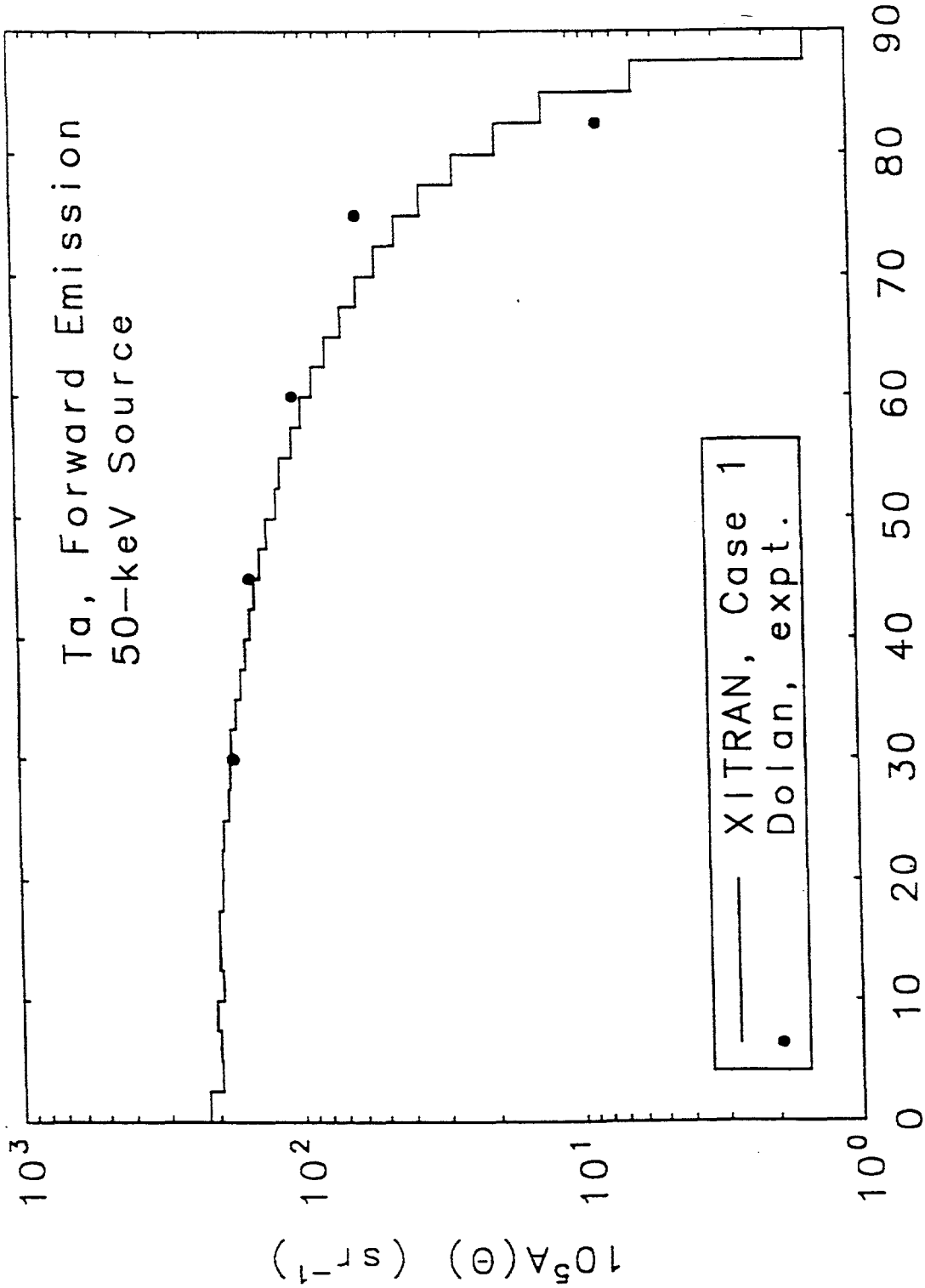
Ta, Forward Emission
50-keV Source
XITRAN, Case 1
Dolan, expt.
$10^5 A(\Theta)$ (sr^{-1})
10^3
10^2
10^1
10^0
0
10
20
30
40
50
60
70
80
90
Θ (deg)

Fig.10d-1

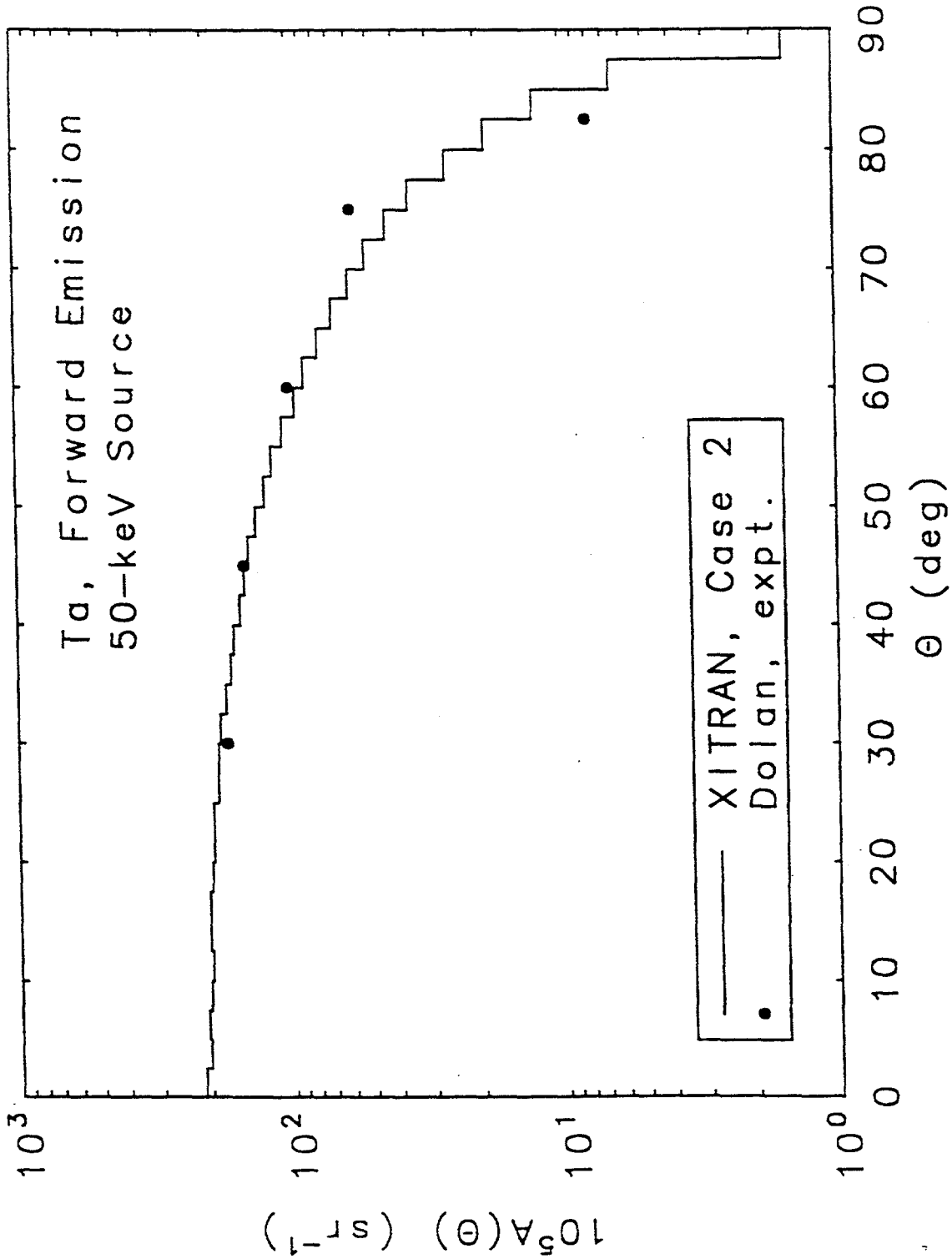
Ta, Forward Emission
50-keV Source
XITRAN, Case 2
Dolan, expt.
$10^5 A(\Theta)$ (sr^{-1})
Θ (deg)
10^3
10^2
10^1
10^0
0
10
20
30
40
50
60
70
80
90

Fig.10d-2

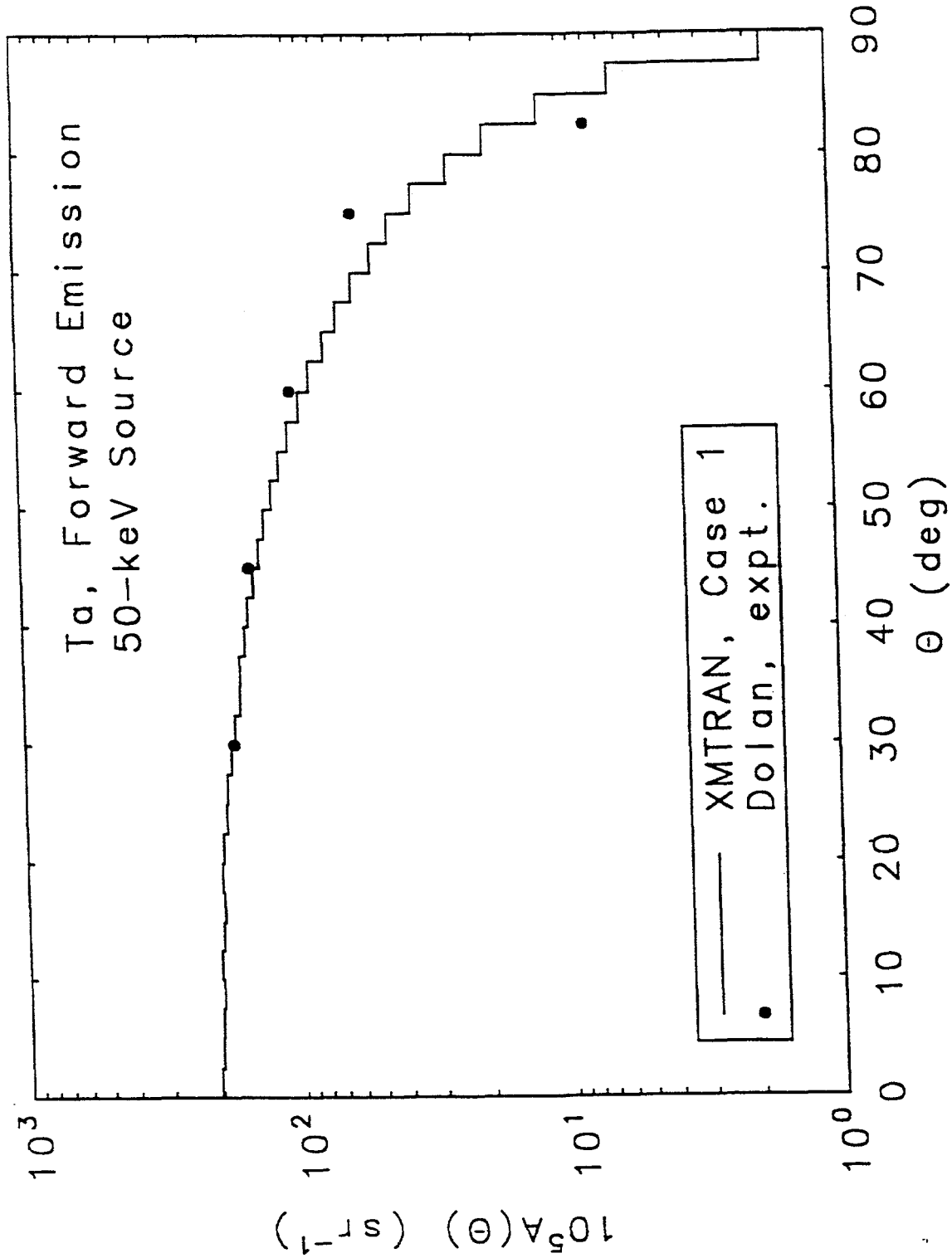
Ta, Forward Emission
50-keV Source
XMTRAN, Case 1
Dolan, expt.
$10^5 A(\Theta)$ (sr^{-1})
Θ (deg)
10^3
10^2
10^1
10^0
0
10
20
30
40
50
60
70
80
90

Fig.10d-3

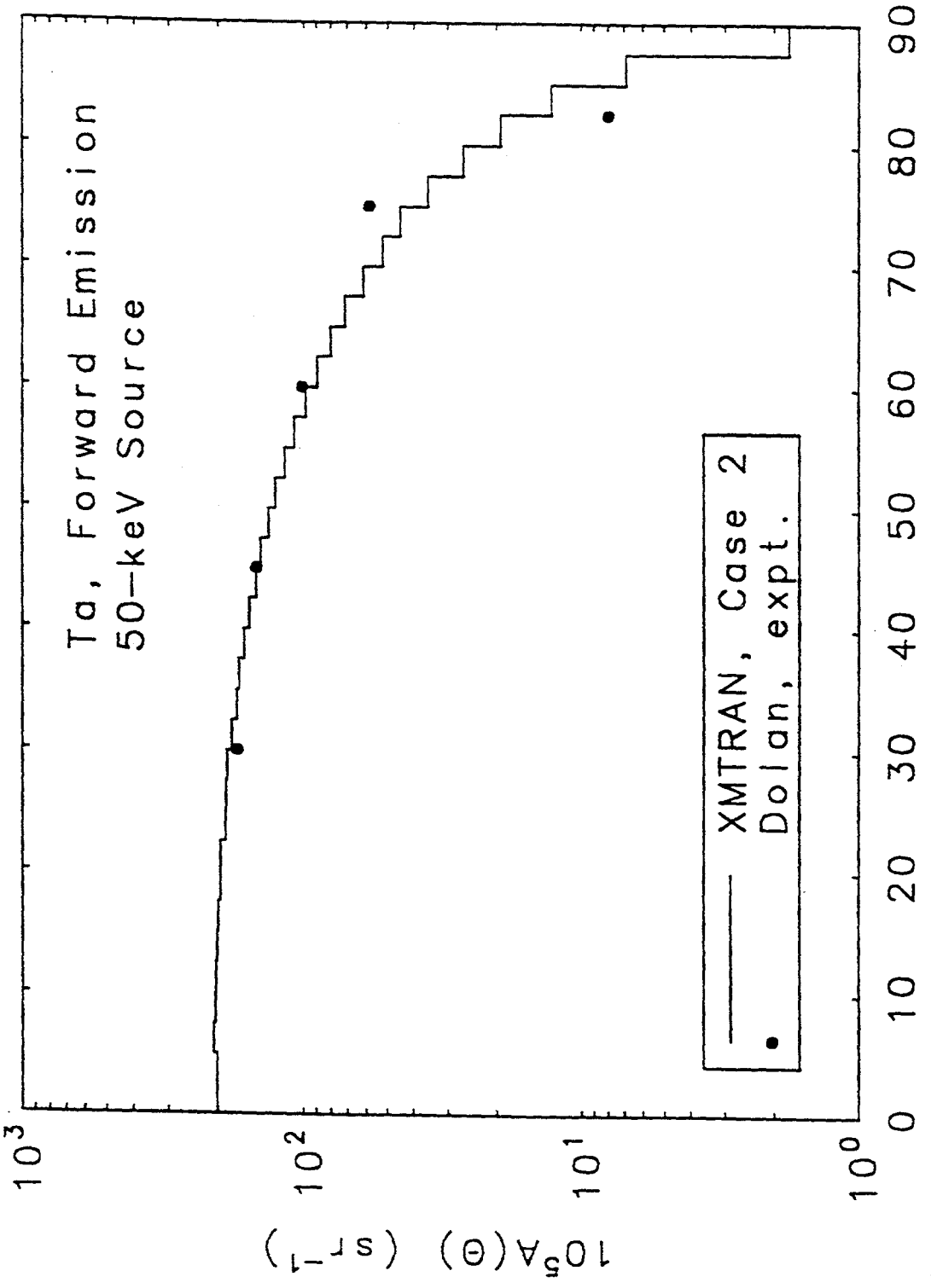
Ta, Forward Emission
50-keV Source
XMTRAN, Case 2
Dolan, expt.
$10^5 A(\Theta)$ (sr^{-1})
10^0
10^1
10^2
10^3
0
10
20
30
40
50
60
70
80
90
Θ (deg)

Fig.10d-4

Distribution:

2 Martin J. Berger
5011 Elm Street
Bethesda, MD 20814

2 Ron Weitz
Science Applications International Corporation
2109 Air Park Rd. SE
Albuquerque, NM 87106

1	MS1155	W. Beezhold, 9303
1	MS1159	W. H. Barrett, 9311
1	MS1159	M. A. Hedemann, 9311
1	MS1166	C. R. Drumm, 9352
1	MS1166	W. C. Fan, 9352
1	MS1166	G. J. Scrivner, 9352
1	MS1167	J. J. Hohlfelder, 9351
9	MS1179	W. P. Ballard, 9341
1	MS1179	D. E. Beutler, 9341
1	MS1179	J. A. Halbleib, 9341
1	MS1179	R. P. Kensek, 9341
1	MS1179	J. R. Lee, 9341
1	MS1179	L. J. Lorence, 9341
1	MS9018	Central Technical Files, 8940-2
2	MS0899	Technical Library, 4916
2	MS0619	Review & Approval Desk, 12690 For DOE/OSTI